Regulation of long non-coding RNA H19 in mesenchymal stromal cells during osteogenic differentiation

Inauguraldissertation

zur Erlangung des Grades eines Doktors der Medizin
des Fachbereichs Medizin der Justus-Liebig-Universität Gießen

vorgelegt von

Dennis Michael Rockenbach

Gießen, 2022

Aus dem Fachbereich Medizin der Justus-Liebig-Universität Gießen

Campus Kerckhoff, Bad Nauheim
Abteilung für Rheumatologie und Klinische Immunologie

Betreuer/in:	Herr Prof. Dr. Müller-Ladner, Ulf
Gutachter/in:	Herr Prof. Dr. Samakovlis, Christos
Prüfungsvorsitz:	Frau Prof. Dr. Rohrbach, Susanne
Prüfungsmitglied:	Frau Prof. Dr. Schänzer, Anne

Tag der Disputation: 12.02.2024

Contents

1 Summary

Healthy bone is a vital, constantly remodeling system. This process is balanced between bone formation by osteoblasts and resorption by osteoclasts. Osteoblasts originate from mesenchymal stem cells which inherit the pluripotency to differentiate into various phenotypes within connective tissues.

In rheumatic diseases like osteoarthritis (OA), rheumatoid arthritis (RA) as well as osteoporosis, inflammatory factors and other cell-targeting mediators influence the differentiation of mesenchymal stromal cells (MSC). Preliminary studies by Tsiklauri et al. showed a higher expression of the adipokine visfatin in osteoporotic bone. Adipokines are adipose tissue derived proteins involved in the regulation of metabolic processes and inflammatory conditions. Visfatin stimulation of MSCs altered the expression of matrix metalloproteinases and inflammation mediators as well as in-vitro matrix composition during osteogenic and adipogenic differentiation.

Long non-coding (lnc-)RNAs are RNA polymerase II transcribed, processed RNA molecules of more than 200 bases in length. Although they are formed like classic messenger RNA, they do not share the same fate and are not translated into proteins but act as RNA molecules to regulate gene expression, RNA-protein interaction and other metabolic processes. lncRNA H19 was found to be up-regulated over the course of osteogenic differentiation of MSCs, suggesting H19 to be involved in its regulation.

By investigating the role of adipokines in the bone metabolism of rheumatic diseases, it could be demonstrated that visfatin but not other adipokines, such as resistin or leptin reduced the up-regulation of H19. Therefore, the aim of this thesis was to further explore the effects of visfatin on lncRNA expression and the downstream mechanisms of the target lncRNA H19.

This reduction of lncRNA H19 could be replicated with primary human MSCs of different origin (hip and knee) from OA patients as well as with commercially obtained MSCs from healthy donors over the course of osteogenic differentiation. A similar, but lesser reduction of H19 could be observed during adipogenic differentiation.

Visfatin enhanced matrix mineralization and increased Interleukin (IL)-6 expression

of differentiating MSCs during OD. To distinguish a visfatin specific effect from a general response to inflammation, visfatin co-stimulation was compared to TNFα stimulation of MSCs. TNFα, however, did not down-regulate lncRNA H19 expression and likewise did not induce matrix mineralization.

To investigate potential downstream mechanisms of H19, the TGFβ1 and WNT signaling pathways were investigated. In phMSCs, a time-dependent down-regulation of secreted TGFβ1 could be observed, an effect which was not present in hMSC cultures. An attempt was made to substantiate these results by inhibition experiments, but no differences could be observed in comparison to the solvent control. However, due to strong side effects of the solvent used for these experiments, further evaluations are required.

Different downstream mechanisms of H19 are discussed in current literature. One potential pathway involves its two inherent micro RNAs 675-3p and -5p, which are encoded within H19s nucleotide sequence. With the support of our cooperation partner, these micro-RNAs could also be analyzed using the TaqMan Assay. Here, a differential regulation of both miRNAs was identified, with miRNA 675-5p increasing continuously over the course of the differentiation in a similar way to H19. miRNA 675-3p, on the other hand, decreased continuously during the entire 14-day differentiation. These observed (dys-)regulations of the different miRNAs were attenuated upon stimulation with visfatin.

In addition, the comparison of the visfatin-stimulated samples with unstimulated controls showed a continuous down-regulation of H19 and miRNA 675-5p, and an induction of miRNA675-3p.

In summary, a hither to unknown of the cytokine visfatin, which is secreted by adipose tissue, on the expression of lncRNA H19 could be observed. This effect appears to be solely mediated by visfatin, but not by other key adipokines, such as resistin and leptin. Likewise, the effect could not be triggered by other pro-inflammatory stimuli (TNFα), which supports the hypothesis of a visfatin-specific effect.

Potential effects of H19 on intracellular signaling pathways (TGFβ1 and WNT) could not be experimentally confirmed. However, a differential regulation of the endogenous

microRNAs 675-3p and -5p, which can be formed by alternative splicing of the lncRNA H19, could be shown. The modulation of this process by visfatin may represent an effector mechanism of the alterations in the osteogenic differentiation of MSCs under the influence of visfatin.

2 Zusammenfassung

Gesunder Knochen ist ein dynamisches, in ständigem Umbau befindliches System. Er befindet sich im Gleichgewicht zwischen Knochenaufbau durch Osteoblasten und Knochenabbau durch Osteoklasten. Osteoblasten entstammen pluripotenten mesenchymalen Stammzellen (MSC), welche in verschiedene Zelllinien des Bindegewebes ausdifferenzieren können.

Bei rheumatischen Erkrankungen wie der Arthrose (engl.: Osteoarthritis, OA), der rheumatoiden Arthritis (RA) und der Osteoporose beeinflussen Entzündungsfaktoren und andere Mediatoren die Differenzierung von MSCs. Adipokine sind Proteine, die im Fettgewebe exprimiert werden und an der Regulation von Stoffwechselvorgängen und Entzündungsprozessen beteiligt sind. Voruntersuchungen von Frau Dr. Tsiklauri in unserem Labor zeigten eine gesteigerte Expression des Adipokins Visfatins im osteoporotischem Knochen. Ihre Arbeit konnte nachweisen, wie die Stimulation von MSCs mit Visfatin die Expression von Matrix-Metalloproteinasen und Entzündungsmediatoren sowie der in-vitro Matrixmineralisierung während der osteogenen (OD) und adipogenen Differenzierung verändert.

Long non-coding (lnc-)RNAs sind RNA Moleküle mit über 200 Nukleotiden Länge. Sie werden durch die RNA Polymerase II transkribiert und analog zu messenger-RNA (mRNA) prozessiert. Obwohl diese wie “klassische” mRNAs gebildet werden, werden sie nicht in Proteine translatiert, sondern agieren als RNA-Moleküle und regulieren die Genexpression, die RNA-Protein-Interaktion und andere Stoffwechselprozesse. Von besonderem Interesse ist die lncRNA H19. Sie wird im Laufe der osteogischen Differenzierung von MSCs vermehrt exprimiert und wirkt regulatorisch auf diese ein. In dieser Studie wurden die Einflüsse von Visfatin auf die Expression der lncRNA H19 im Rahmen der

OD sowie deren mögliche Wirkmechanismen auf differenzierende MSCs untersucht.

Bei der Untersuchung der Rolle von Adipokinen im Knochenstoffwechsel bei rheumatischen Erkrankungen konnte gezeigt werden, dass Visfatin, anders als andere getesteten Adipokine Resistin oder Leptin, zu einer verminderten Expression von H19 führte. Diese Reduktion könnte sowohl mit primären humanen MSCs aus unterschiedlichen Gelenke (Hüfte und Knie) von OA-Patienten (phMSC) als auch mit kommerziell erworbenen MSCs von gesunden Spendern (hMSC) im Zuge der OD nachgewiesen werden. Eine ähnliche Reduktion von H19 wurde in geringerem Maße bei der adipogenen Differenzierung beobachtet.

Visfatin verstärkte die Matrixmineralisierung und steigerte die Expression von IL-6 in differenzierenden MSCs. Um einen visfatinspezifischen Effekt von einer allgemeinen Reaktion auf Entzündungen zu unterscheiden, wurde die Visfatin Stimulation mit der TNFα Stimulation von MSCs verglichen. Die Stimulation mit TNFα ergab dabei keine vergleichbare Herabregulation der lncRNA H19 Expression und keine Induktion der Matrix-Mineralisierung.

Um mögliche Effektormechanismen von H19 zu untersuchen, wurden die Signalwege TGFβ1 und WNT untersucht. In phMSCs konnte eine Herabregulation von sezerniertem TGFβ1 beobachtet werden, die jedoch in hMSC-Kulturen nicht nachweisbar war. Es wurde versucht, diese Ergebnisse durch Hemmung der Signalwege zu verifizieren, die jedoch aufgrund zu ausgeprägter Effekte des für diese Experimente verwendeten Lösungsmittels nicht auswertbar waren.

In der aktuellen Literatur werden unterschiedliche Effektormechanismen von H19 diskutiert. Ein möglicher Signalweg beinhaltet die micro (mi-)RNAs 675-3p und -5p, welche Bestandteile der Nukleotidsequenz des RNA-Moleküls H19 sind.

Mit der Unterstützung unserer Kooperationspartnerin Prof. Dr. Caroline Ospelt in Zürich konnten diese miRNAs mittels TaqMan Assay in den OD-Proben quantifiziert werden. Hier zeigte sich eine Regulation beider miRNAs, wobei miRNA 675-5p in ähnlicher Weise wie H19 über den Verlauf der Differenzierung herabreguliert wurde, die Expression der miRNA 675-3p hingegen stieg während der gesamten 14tägigen Differenzierung

kontinuierlich an. Alle gezeigten Regulationen, die gesteigerte Expression von H19 und miRNA 675-5p und die Reduktion von miRNA675-3p, wurden unter Stimulation mit Visfatin abgeschwächt. Beim Vergleich der Visfatin-stimulierten Proben mit unstimulierten Kontrollen zeigte sich jeweils eine kontinuierliche Herabregulation durch Visfatin von H19 und miRNA 675-5p sowie eine Induktion von miRNA675-3p.

Zusammenfassend wurde ein bisher nicht bekannter Einfluss des von Fettgewebe sekretierten Zytokins Visfatin auf die Expression von lncRNA H19 nachgewiesen. Dieser Effekt wird durch Visfatin, nicht aber durch andere Adipokine (Resistin, Leptin) vermittelt. Ebenso ist der Effekt nicht durch andere proinflammatorische Reize (TNFα) auslösbar, was die These eines Visfatin-spezifischen Effektes untermauert.

Mögliche Einflüsse von H19 auf intrazelluläre Signalwege (TGFβ1 und WNT) konnten nicht experimentell bestätigt werden. Jedoch zeigte sich eine differenzielle Regulation der Mikro-RNAs 675-3p und -5p, die durch Splicing der lncRNA H19 gebildet werden können. Die Modulation dieses Prozesses durch Visfatin kann ein möglicher Effektormechanismus der hier gezeigten Veränderungen der osteogenen Differenzierung von MSCs unter dem Einfluss von Visfatin sein.

Part I. Background

3 Clinical problem

Destructive joint diseases like osteoarthritis, rheumatoid arthritis and osteoporosis are amongst the most common age-related diseases leading to chronic pain and disability [1]. The progressive destruction of the affected joints is usually irreversible and leads to substantial impairment of quality of life, functional limitations, severe disabilities and premature mortality [2, 3]. Currently available treatment options are still afflicted with side effects. They can ease or delay, but are not curative and cannot stop progression of these diseases. Clinical features are described in comparison, chapter four focuses on osteoarthritis in more detail.

Osteoarthritis (dt.: 'Arthrose', OA) is a degenerative 'wear and tear' related joint disease with systemic and metabolic effects leading to an imbalance between joint degeneration and insufficient repair processes [4]. With the progression of the disease, joint cartilage and underlying bone are destroyed irreversibly. The formation of osteophytes is an attempt to (re-)stabilize the damaged joint [5]. These processes cause joint pain and stiffness and often lead to the inevitable consequence of joint replacement surgery. Common risk factors for OA are an excess of stress to the joint most often caused by increased body weight as well as congenital disorders (e.g. hip dysplasia), trauma leading to malpositioning of the joint or deformations caused by bone diseases such as osteoporosis. Obesity is a shared risk factor for practically all rheumatic and inflammatory diseases. Excess body fat contributes to a state of chronic low-grade systemic inflammation with pro-inflammatory adipokines impairing joint cartilage homeostasis.

Osteoarthritis can also occur as a result of other diseases (secondary OA) such as connective tissue disorders (Ehlers-Danlos sydrome, Marfan syndrome), metabolic disorders (diabetes, hemochromatosis, Wilsons's disease, gout), joint infections or inflammatory diseases (Perthes' disease, lyme borreliosis and chronic arthritis) or as a result of overuse (secondary inflammatory reaction, activated OA).

Osteoporosis is, similar to OA, a common age-related disease of the bone resulting in thinner and more porous bone structures with higher levels of adipose tissue in the bone marrow and a shift from osteogenic towards adipogenic differentiation of mesenchymal stem cells, often associated with calcium deficiency. The reduced osteogenic potency of stem cells of the connective tissues in age-related osteoporosis can therefore lead to an increase in adipogenic differentiation and decreased bone density, resulting in more fragile bones and higher fracture rates [6–8]. Most common are vertebral collapse ("compression fractures") and proximal femoral fractures.

Besides age-related OP, the disease is often induced and perpetuated iatrogenically, in particular due to the predominant use of corticoids in clinical application, including in rheumatology.

Fig. 1: Clinical presentation of osteoporosis (OP). Left: 50 year old female patient with postmenopausal osteoporosis and a decrease in size of 5 cm due to fractures of the thoracic vertebrae 6, 8, 11, 12 and the lumbar vertebra 3. Center: Magnetic resonance imaging (MRI) image of an OP patient with new (light, higher intensity) and old (dark, lower intensity) compression fractures and codfish vertebrae. Right: Anatomical preparation of an OP-affected spinal column with codfish vertebrae formation.
Pictures used with the kind permission of Prof. Dr. Uwe Lange, Dept. of Rheumatology and Clinical Immunology, Campus Kerckhoff, Justus-Liebig University Giessen.

Chronic inflammatory arthritis and rheumatoid arthritis: Apart from secondary or primary osteoarthritis and osteoporosis, chronic inflammatory disease like rheumatoid arthritis (RA) are another major cause for joint pain and impairment and may result in a

similar clinical presentation.

RA is a chronic inflammatory auto-immune disease affecting ~1% of the global population with a higher incidence in females. Affected joints characteristically show symptoms of local inflammation (warm, swollen, painful joints), synovitis and destruction of cartilage and bone tissue [9, 10]. The onset of the disease is often insidious, starting with pain in the small finger or toe joints. Other joints can be affected as well, especially the hand, knee, shoulder, foot and hip joints. In most cases, the disease progresses intermittently, with an episode typically lasting between several weeks to months. Systemic affections include non-specific symptoms such as fever, fatigue and loss of appetite. Like in OA, treatment options include pain control and physical activity, but also extend to corticoids and 'disease modifying' drugs like methotrexate (MTX) and biologicals.

Fig. 2: Clinical presentation of rheumatoid arthritis (RA) Top: Hands of an advanced stage RA patient (x-ray and photograph) with prominent ulnar deviation in all MCPs.
Bottom: X-ray images over the course of RA. Left: Early inflammation in the carpus, luxation of the metacarpophalangeal (MCP) joints; Middle: Luxation, inflammation and destructive changes at all MCPs and formation of an os carpale; Right: advanced inflammatory destructive manifestations.
Pictures used with the kind permission of Prof. Dr. Uwe Lange, Dept. of Rheumatology and Clinical Immunology, Campus Kerckhoff, Justus-Liebig University Giessen.

Obesity The prevalence of individuals who are overweight or obese is rising worldwide and is expected to continue to increase [11]. Many chronic metabolic and autoimmune-related conditions such as diabetes mellitus and cardiovascular disease [12], osteoarthritis [13, 14] and a variety of malignancies [15] are associated with obesity and/or high body mass index (BMI).

One important health implication in obese individuals is a state of chronic low-grade inflammation [16, 17]. The increasing amount of adipose tissue leads to a higher release of pro-inflammatory adipose tissue-derived factors (adipokines). This effect is further increased by a down-regulation of the primarily anti-inflammatory adipokine adiponectin [18]. Adipose tissue in obese individuals was shown to chemoattract immuno-active macrophages, which also contribute to local and low level systemic inflammation leading to the systematic complications of obesity [19].

Obesity is not only a prominent cause of disease and hence health system expenditure, it remains primarily a lifestyle-related (diet and activity level) condition. Understanding its implications on chronic disease such as osteoarthritis may further the efforts for obesity prevention. In recent projects, our group focused on the effects of adipose tissue-derived factors such as adipokines and free fatty acids in synovial tissues in the context of rheumatic diseases [20–23].

The destruction of the bone, however, is a central cause of permanent and irreversible damage to the affected joints and ultimately leads to complaints and disabilities of the patient. Therefore, in recent years the analysis of adipokines in arthritically-altered bone and cartilage has increasingly come to focus [24, 25]. Overall, it was found that elevated levels of adipokines such as adiponectin and visfatin were present in the area of joint destruction (compared to healthy controls) in both RA and OA [26]. Adipokines were additionally induced by the presence of pro-inflammatory stimuli, as found in chronic inflammatory autoimmune disease such as RA.

4 Osteoarthritis

OA is the most common form of arthritis, inflicting pain, locomotor disability and impairment of life quality on patients, as well as posing a huge challenge for health-care providers and health systems [1]. OA affects approximately 10% of male and 18% of female individuals worldwide and a total of 60% of the elderly population, with the incidence increasing significantly with age. The condition has long been seen as a degenerative, *wear-and-tear*-related condition resulting from aging and the accumulation of trauma to the joint. However it is now recognized as a systemic, metabolic disease with an imbalance between joint degeneration and insufficient repair processes [4].

Age is the most important risk factor for the development of OA. Other factors are high mechanical stress (e.g. due to obesity or malpositioning), former injury to the joint and genetic predisposition (e.g. collagen mutations producing a weaker joint cartilage). Metabolic risk factors include female sex (especially the altered hormone secretion in post-climacteric women), obesity and obesity-related hormone-production.

Risk factors for developing OA also differ for the site of the clinical manifestation. Obesity for example is an important risk factor for knee OA, but less significant in hip and hand OA, whereas genetic factors affect hand, knee and hip OA at similar levels [27].

4.1 Clinical presentation

OA may potentially affect any joint, yet it is most commonly seen in those of the knee, hip, hand, wrist and spine. The most prominent symptom of OA is joint pain - which is also the most common reason for patients to seek a physicians' advice. The pain related to OA is described by patients to change during the day and vary largely from week to week, often described to change in relation to weather conditions and barometric pressure [28]. Patients often report a poorly localized pain, that may be referred distally from the joint actually affected. The pain experienced by OA patients is also associated with poor sleep, fatigue, changes in mood and physical activity, all of which lead to significant impairment of quality of life.

The quality of the pain varies depending on its point of origin and may indicate the

underlying pathology. Pain after physical exercise, for example, is often caused by so-called bone angina due to subchondral ischemia. Other symptoms of osteoarthritis include joint stiffness, instability and reduced function of a joint or a crunching or clicking noise (crepitation) during movement. Clinical signs include tenderness, swelling with or without effusion, hard tissue enlargement and deformation.

Tissue damage in joints affected by OA includes damage to joint cartilage, menisci, capsule and surrounding tissues. Articular cartilage damage is the hallmark of OA, leading to abnormal, damaged and fissured cartilage, exposing the subchondral bone to the joint space. Cartilage debris and subchondral materials such as collagen, proteoglycans, enzymes and cytokines trigger a local inflammatory response in the synovium.

Fig. 3: Clinical presentation of OA. Top left: Photograph of the hands of an OA patient with common features of OA: affection of the distal interphalangeal joints with the formation of hard knobs ("Heberden's nodes") and the first carpometacarpal joint (base of the thumb, "Rhizarthrosis"). Another feature of OA is the formation of knobs at the proximal interphalangeal joints (Bouchard's nodes). Top right: Surgical resectate of knee joint cartilage with severe abrasions. Bottom left: X-ray of an OA-affected knee with asymmetrical joint space narrowing. Bottom right: Magnetic resonance imaging (MRI) of an OA-affected knee. High intensity (light color) indicates inflammation of the synovium as well as the bone lining.
Pictures used with the kind permission of Prof. Dr. Uwe Lange, Dept. of Rheumatology and Clinical Immunology, Campus Kerckhoff, Justus-Liebig University Giessen.

Because neither the bone covering cartilage, nor the menisci contain nerve endings themselves, they are merely an indirect source of the clinical pain. Subchondral bone however is highly innervated and causes pain when exposed to the joint space or in an ischemic state after physical activity. Corresponding diagnostic findings are subchondral bone lesions and cysts. Another source of pain and discomfort is the periosteum, which is usually stretched and injured due to the formation of osteophytes, intra-articular exostoses along joint margins.

Debris and subchondral material accumulates in the synovial fluid of OA-affected joints. Cytokines released from subchondral compartments cause inflammation. Nerve ends in the synovium may release substance P and calcitonin gene–related peptide (CGRP) which further pain and inflammation. Mechanical stress to the capsule by an excess of synovial fluid (swelling and effusions) as well as loose bodies in the joint ("joint mice") are further sources of pain [29].

4.2 Diagnosis

The diagnosis of OA is made by reviewing clinical history and by examination. Only in cases of atypical presentation specialized imaging be used [30]. Further imaging techniques usually include X-Ray imaging of the affected joints to evaluate subchondral abnormalities (cysts, dt: "Geröllzysten"), cartilage loss and (asymetrical) joint-space narrowing, osteophyte formation, malpositioning, bone sclerosis and ossification. More specialized diagnostics may include magnetic resonance imaging (MRI), bone scintigraphy and ultrasound. Biochemical markers in blood, urine or synovial fluid may be used to further verify and quantify the progression of the disease [29][31].

4.3 Management

The EULAR ('European League Against Rheumatism') Guidelines for management of OA patients recommend an individualized strategy depending on site and severity of the symptoms, prevalent co-morbidities, other medications being used and the compliance and therapy acceptance of the patient. Non-pharmacological treatments should build the

basis, complimented by drug treatment where necessary. All therapy regimes should include education and an exercise program. Paracetamol is recommended as a first-line medication with a variety of other treatment options to select from, depending on the patient's needs and acceptance.

Exercise should focus on the strengthening of the musculoskeletal system to reduce pain, increase joint stability and to help prevent further injury (tendency to fall). This should include a strategy to enhance the overall level of physical activity [32]. Patients also benefit from secondary outcomes of physical activity like improved well-being and sleep quality, as well as having a preventive effect on common co-morbidities (e.g. obesity). A patient-centred pain management with a focus on increasing the general activity level, lifestyle, controlling body weight and providing education have proven safe and effective [33].

Symptoms of OA are often episodic, with pain being the preliminary reason for patients seeking the advice of a physician. Pharmaceutical pain therapy is a good option to quickly reduce pain during exacerbation. Paracetamol and topical non-steroidal anti-inflammatory drugs (NSAIDs) should be the first option for treatment [34]. Pharmacological treatment should take into account other medications being taken by the patient.

Surgical treatment options like osteotomy, arthrodesis, arthroscopic debridement and lavage as well as prosthetic joint replacement should be considered for the individual patient, depending on the stage of the disease and the individual burden of disease.

4.4 Pathophysiology

The pathophysiology of OA is multifactorial. It primarily affects the joint cartilage, but extends to the entire functional unit of the joint. This includes subchondral bone, capsule and synovial membrane and the surrounding muscles and ligaments. Over the course of OA, characteristic changes in cartilage tissue are observed up to the final loss of cartilage and exposition of subchondral bone. Pritzker et al. proposed a grading system for OA providing a diagnostic overview of the histological alterations to the joint cartilage and bone structures [35][4][31].

In early OA, the cartilage structure is impaired when physical or proteolytic processes damage its collagen network (Grade 1). Matrix edema with increased water content and swelling of proteoglycans is observed in conjunction with chondrocyte proliferation, hypertrophy and apoptosis. The softened cartilage is further damaged by physical wear, causing surface matrix fibrillations and surface discontinuity. Cracks start to build in parallel to the cartilage surface (Grade 2). Proteoglycan contents decrease and cells lose their proper chondrom column orientation. As the damage continues, vertical fissures (clefts) extend into the mid and deeper cartilage zones (Grade 3). Histologic findings of cell death, edema and proteoglycan loss progress deeper into the cartilage. Over time, more and more cartilage substance is lost due to repeated trauma and proteolytic activity. In turn, calcified cartilage zones increase in thickness and micro-cracks form in the calcified cartilage which initiate subchondral bone remodeling. As a result subchondral cysts and sclerosis begin to build up and can be observed in x-ray imaging (Grade 4). As matrix is lost completely, the underlying bone surface is exposed (Grade 5). Microfractures initiate bone remodeling, leading to severe deformation (Grade 6).

4.5 Obesity and adipokines in OA pathology

Obesity is as major risk factor for patients developing OA. By understanding OA as a result of mechanical wear and tear of the joint, it is obvious that obese individuals would suffer a higher risk of developing OA in weight-bearing joints. The increased mechanical stress not only directly damages the cartilage matrix structure but also stresses chondrocytes. While this is a necessary stimulus to keep up cartilage homeostasis in healthy individuals, excessive stimulation activates pro-inflammatory and catabolic pathways.

There is also an association between obesity and OA in non-weight-bearing joints such as in the hand and wrist. This indicates a non-stress-related connection between obesity and OA. Obesity is associated with both an altered gait profile and a diabetic metabolic state, both affecting the joint integrity. Excessive proliferation of adipose tissue also increases the amount of adipokines and metabolic factors secreted by adipose tissues. Some of these adipokines like leptin and visfatin have been shown to act as pro-inflammatory cytokines and catabolic factors, disrupting cartilage metabolism [36]. Others, like adiponectin, were shown to ameliorate inflammatory processes.

5 Cells involved in osteoarthritis

OA is a systemic metabolic process with an imbalance between joint degeneration and insufficient repair processes [4]. OA affects the whole functional compartment of the affected joint, which itself is comprised of a number of specialized tissues and cell types. This chapter will give an overview of the anatomical structures of the joint, with a focus on cells involved in OA development.

Joints or articulations are the dynamic connection of bones enabling functional movement. Different types of articulations exist with different degrees of freedom, ranging from the extremely mobile shoulder to joints with very limited movement like intervertebral amphiarthrosis or skull sutures.

Synovial joints (diarthrosis, freely movable articulations) consist of the proximal and distal epiphyseal bones that are covered by articular cartilage. The space between the cartilage surfaces, the synovial space or cavity, is surrounded by a capsule with synovial lining tissue and filled with synovial fluid serving as a lubricant. The shapes of the cartilage surfaces, menisci, intra and extra articular ligaments and muscles, stabilize the joint and guide movement and degrees of freedom.

Bone is a specialized, rigid organ composing part of the endoskeleton of vertebrates. The skeletal system is important both as a supporting structure and for maintenance of mineral (calcium, magnesium, phosphate) and acid-base status of the whole organism. Bones protect the inner organs and serve as insertion points for muscles and tendons hereby enabling movement. The soft tissue inside trabecular bones, the bone marrow (myeloid tissue), is the site of hematopoesis, required for the formation of red and white blood cells.

Bone tissue (osseous tissue) is a highly specialized type of connective tissue. Bone cells produce and maintain the bone matrix that needs to be stabile but still flexible to some extent. This is reflected in its composition of elastic organic components and rigid, mineralized, an-organic salts. The organic matrix consists mainly of collagen type I (up

to 95%), with other components including proteoglycans, osteopontin and osteocalcin. Hydroxyapatite and other salts of calcium and phosphate make up the majority of the bone mineral accounting for its stability and 70% of its mass.

Bone cells Bone is a dynamic tissue that is continuously remodelled and adapted. This process is balanced by two groups of bone cells. Osteoblasts are bone-forming cells producing and mineralizing the base substance to generate new bone tissue. Osteoblasts eventually immure themselves in bone matter, where they settle and differentiate into osteocytes. These cells make up the vast majority of bone cells and can be found all across the bone tissue.

Osteoclasts are the functional counterpart to osteoblasts. These multi-nucleated cells secrete hydrogen ions (acid) and hydrolytic enzymes to dissolve and resorb the bone matrix.

5.1 Osteoblasts

Osteoblasts are specialized mesenchymal cells that produce and maintain the bone matrix and regulate bone homeostasis. Similar to fibroblasts they originate from mesenchymal stem cells (MSCs).

Active osteoblasts organize in groups on the bone surface and are interconnected with gap junctions, allowing them to act as a functional unit. For bone production and mineralization, a layer of osteoblasts seals the site of ossification. Osteoblasts secrete matrix components leading to the osteoid formation, the base substance of bone tissue. The vast majority of all osteoid proteins is collagen type I. This type of collagen is densely cross-linked and is secreted by osteoblasts in an oriented, alternating pattern. Other organic components in the osteoid are proteoglycans (such as hyaluronic acid), osteocalcin and osteopontin. For mineralization, osteoblasts secrete Ca^{2+} which allows for precipitation of hydroxyapatite crystals from calcium and phosphate. The hydrogen ions released during this reaction is removed from the apical compartment and transported to the basal side of the osteoblasts. In the process of bone formation, osteoblasts surround themselves with

solid matrix and settle in bone niches (lacunae), where they differentiate into osteocytes. Osteocytes keep their previously formed gap junctions and hereby remain interconnected. Embedded in the bone matrix, osteocytes play a role in regulating bone remodeling and repair processes mainly by producing the Receptor Activator of NF-$\varkappa$B (RANK)-Ligand (RANKL), sclerostin (SOST) and Dickkopf-related protein 1 (DKK1) in response to mechanical and hormonal stimuli. Sclerostin and DDK1 inhibit the WNT signaling pathway, a promotor of osteogenic differentiation in osteoblast precursor cells. RANKL directly regulates osteoclast formation and activation. Hereby osteocytes regulate bone formation by activating osteoclasts and down-regulating osteogenic differentiation [37].

Osteoblasts express a number of extracellular receptors on their cell surface that linking their function to systemic metabolic processes. They are able to receive activating stimuli from the parathyroid hormone (PTH), which is secreted by the parathyroid gland, and from calcitriol (Vitamin D3) released from the kidneys. These signaling cascades lead to the activation of osteoblast function, which in turn activates the osteoblasts via RANKL. By increasing bone turnover, the organism can quickly increase the calcium level in the serum.

Osteoblasts that do not remain in the bone matrix in the form of osteocytes either undergo apoptosis or become bone lining cells covering the bone surface.

5.2 Osteoclasts

Osteoclasts are large, multi-nucleate cells formed by the fusion of up to ten monocytes. As siblings of macrophages, osteoclasts originate from the hematopoietic lineage. Osteoclasts dissolve and resorb the bone matrix during bone homeostasis or e.g. at the site of microfractures. The process of resorption takes place within the resorption pit (Howship's lacune). This localized area is sealed off from the environment by strong attachment of the plasma membrane to the underlying bone ("sealing zone"). Through the bone facing apical side of the osteoclasts, the ruffled border, osteoclasts release hydrogen ions which dissolve the mineralized bone matrix within the resorption pit. To digest the organic matrix components, hydrolytic enzymes like matrix metalloproteinases (MMPs))

are released.

Osteoclast formation and activation is regulated by osteoblasts and their precursors via the release of RANKL and macrophage colony-stimulation factor (M-CSF). Both factors activate osteoblasts and their precursors by binding to osteoclast surface receptors (c-Fms, RANK). M-CSF stimulates hematopoetic stem cell proliferation and osteoclastogenesis. RANKL triggers a signaling pathway to further differentiate and activate osteoclasts.

The functional counterpart of RANKL is osteoprotegerin (OPG) expressed by various osteoblast lineage cells, B-cells, dendritic cells and others. OPG is a decoy receptor for RANKL which binds secreted RANKL, hereby down-regulating osteoclastogenesis and bone resorption. OPG expression is up-regulated by estrogens. Estrogen deficiency in postmenopausal women and other conditions such as ovariectomy, ovarian failure, anorexia and hyperprolactinaemia therefore results in lower OPG levels and subsequently higher osteoclast activation and the development of osteoporosis [38].

5.3 Mesenchymal stem cells (MSC)

Mesenchymal stem cells (MSCs) are an integral part of bone homeostasis, growth and regeneration e.g. after bone fractures. MSCs are a heterogeneous population of cells with the potential to differentiate into a specific set of somatic cell lineages including osteoblasts and adipocytes. They react to chemo-attractants released from injured tissues, infiltrate the area and locally differentiate according to the local micro-milieu to promote tissue recovery [39].

After their initial discovery, MCSs where described as multi-potent progenitors of mesodermal cells [40]. They have been shown to be capable of differentiating in vitro into mature-like cells from all three germ layers [41, 42]. MSCs can be found in almost all types of tissues, with the highest concentrations in the bone-marrow and in adipose tissues [43]. Depending on their site of origin, there are considerable differences in differentiation potential and growth characteristics [44]. Isolation of MCSs is possible from almost any tissue, yet the highest numbers can be retrieved from bone marrow (bone-marrow derived MCSs, BM-MCSs), adipose tissue (AD-MCSs) and umbilical cord blood (CB-MSCs).

Isolating MSCs from other donor tissues in the laboratory is a major challenge. Since a complete purification is difficult to achieve, mixed populations rich in MSCs are usually used in experiments. The term mesenchymal stromal cells is therefore often used to highlight the fact that a studied population of MSCs is to some extent contaminated with cells of other types.

In vitro, MSCs can be described as plastic adherent cells with a fibroblast-like appearance. They can easily be distinguished from non-plastic-adherent hematopoetic stem cells. Since MSCs originate from the hypoxic conditions of the bone-marrow, they need to be cultured in-vitro at low-oxygen levels. Mesenchymal stem cells were shown to have high variability between samples even from the same donor in terms of colony growth and expansion activity [45], making comparisons between populations difficult. The variability within the group also increases with the number of passages in culture [46]. Therefore, only populations in low passages (<3 passages) have been used in experiments conducted for this study.

Besides their multipotency, MCSs are a valuable subject of research for their immunologic characteristics. They are accessible for autologous or heterologous transplantation, easy to isolate and to expand ex-vivo and can be genetically modified making them a viable target for therapeutic use. They are described as being MHC II, CD40, CD80 and CD86-negative, which makes them nearly invisible for the immune system and allows for allogenic transplantation without immunosuppression [43].

5.4 MSC differentiation

Mesenchymal stem cells are the precursor of all connective tissue cell lineages. They rest in a hibernation state in the bone marrow, circulate within the blood stream and reside in all types of tissues. On specific stimuli (e.g. tissue injury) MSCs migrate to the required sites of action and differentiate into the adequate mesenchymal cell phenotype.

Adding a proper stimulus, MSCs can successfully be differentiated in vitro. Differentiation of osteoblasts can be divided in three stages: proliferation, matrix maturation and matrix mineralization. To analyse osteogenic differentiation in vitro, bone specific

markers AP, OC and collagen type I (produced by mature osteoblasts) can be measured. Staining methods can be used to visualize calcium deposits and hereby matrix mineralization as a marker for successful differentiation and for *in vitro* bone formation [47].

Osteogenic differentiation is regulated by specific transcription factors. Whereas SOX9 is a marker for all osteoblast progenitor cells, Runt-related transcription factor 2 (Runx2) is essential to osteogenic differentiation [37]. Runx2 shifts the differentiation of MSCs away from chondrogenic and adipogenic towards osteogenic differentiation. Subsequently, Runx2 sets the stimulus for the cells to express osteocalcin (OCN) and osterix (OSX), essential proteins to mineralize the surrounding matrix. In mature cells, activating transcription factor 4 (ATF4) regulates the expression of OCN and metabolic functions of osteoblasts [37].

6 Adipokines

Adipokines or adipocytokines [48] are proteins that are produced and secreted by the adipose tissue. In this publication the term *adiopkines* will be used according to the recommendation of Trayhun et al. because many adipose tissue secreted factors are cytokines or cytokine-like (see table 1 on the following page). This does, however, not comprehensively summarize all adipose-tissue-secreted hormones [49]. Other known products of adipose tissues are free fatty acids, tumor necrosis factor (TNF) alpha, the interleukines IL-6 and IL-1, monocyte chemoattractant protein 1 (MCP1), platelet-activator inhibitor (PAI)-1, and complement components.

Since the discovery of leptin as the first adipokine in 1994 [50], a wide variety of other adipose tissue derived proteins has been shown to have effects on metabolic functions such as lipid and energy metabolism, appetite, blood pressure, angiogenesis and haemostasis in an endocrine, paracrine and autocrine manner [49]. Adipose tissue therefore has been recognized not only as an energy depot but as a bioactive organ that is involved in inflammatory reactions and autoimmune disorders such as RA and OA [51–54]. Adipose-tissue-derived proteins include cytokines, acute-phase and inflammation-related proteins. Pro-inflammatory cytokines secreted by adipose tissues include tumor necrosis

factor alpha (TNFα) [55] and interleukin 6 (IL-6) [56]. Both cytokines have been found to be increased in obese individuals and were linked to insulin resistance. Table 1 gives an oversight on different adipokines.

cytokines	acute-phase proteins	inflammation related	adipokines
TNFα	PAI-1	NGF	Adiponectin
TGF-b	Haptoglobin	MCP-1	Chemerin
IL-1b	Serum amyloid A		Leptin
IL-6	(α1-Acid glycoprotein)		LCN2
IL-8	(24p3)		Omentin
IL-10	CRP		Resistin
(IL-17D)			Visfatin
(IL-18)			Apelin
			Oncostatin M
			Osteopontin

Tab. 1: Overview on proteins secreted by adipose tissue, mainly but not exclusively, by adipocytes. CRP: C-reactive Protein; IL: Interleukin; NGF: Nerve Growth Factor, ILN2: Lipocalin 2; PAI-1: Plasminogen Activator Inhibitor-1; TGFβ: Transforming Growth Factor β; TNFα: Tumor Necrosis Factor α; MCP-1: Monocyte Chemoattractant Protein 1. Based on [19, 49].

Adipokines, obesity and inflammation Pro-inflammatory adipokines may be a causing factor of low-grade inflammation in obesity, a condition that is regularly associated with increased risk of cancer, type 2 diabetes, cardiovascular, autoimmune, and inflammatory diseases [17, 19]. Obesity and chronic low-grade inflammation is linked by various signaling pathways [57]. These pathways include pro-inflammatory mediators like IL-6 [58] and TNFα [55], linking inflammation and glucose metabolism.

Adipokine serum levels have also been shown to be increased in obesity, to correlate with body-weight and to be modulated by weight loss [59, 60]. In particular the effects of the adipokine leptin on inflammation and immunity are well recognized [36].

6.1 Leptin

Leptin is a primarily adipose tissue derived hormone that was discovered in studies with mice bearing a spontaneous mutation in the leptin-coding gene [61]. Other tissues expressing leptin are the placenta, ovaries, skeletal muscle, stomach, pituitary gland and liver [62]. Leptin-deficiency was observed to lead to obesity and diabetes development [61] and total leptin levels correlate with the amount of body fat and BMI. By central effects on the hypothalamus, leptin regulates appetite and suppresses food intake [63]. Energy consumption, on the other hand, is stimulated by leptin [63]. In the periphery, leptin modulates insulin sensitivity [64] and the innate and adaptive immune response [65]. Like other adipokines, leptin has pro-inflammatory properties [65] up-regulating inflammatory cytokines including TNFα and IL-6.

The role of leptin in bone metabolism is not fully understood and is currently controversially discussed. Both anabolic and catabolic effects have been observed in different studies. The involvement of leptin in the pathophysiology of diseases such as OP, OA and RA is also subject of various investigations. Higher systemic (serum) and local (synovial fluid) levels of leptin were shown in OA and RA patients [66, 67] - yet the effects of leptin and its potential diagnostic or therapeutic value needs to be further investigated.

6.2 Resistin

Upon its discovery in 2001, the adipokine resistin was first linked to insulin resistance [68]. Further studies revealed its involvement in other processes like inflammation and bone remodeling. Resistin is secreted by adipose tissues in adult mice, in human adults, however, the main sources of resistin are monocytes and macrophages. Studies have shown promoting effects on osteoblast proliferation as well as osteoclastogenesis [69]. Pro-inflammatory effects include the activation of the NFkB promotor leading to an increased expression of IL-1, IL-6, IL-12 and TNFα [70]. Elevated serum levels of resistin have been found in patients who were over-weight or suffering from diabetes. In synovial fluid, higher levels of resistin were found in RA as compared to OA samples [71], suggesting the involvement of resistin in pro-inflammatory processes [72, 73].

6.3 Visfatin

Visfatin was first discovered as a cytokine involved in pre-B cell colony formation and therefore named pre-B-cell colony-enhancing factor 1 (PBEF1) [74]. Because it is a co-enzyme in the nicotinamide recovery pathway, visfatin is also known as nicotinamide phosphoribosyltransferase (Nampt).

The gene coding for PBEF1/Visfatin was isolated by Samal et al. in 1994 from a human peripheral blood lymphocyte cDNA library. Visfatin mRNA is encoded in the *NAMPT* gene on 7q22.3 [74, 75]. Visfatin forms a homo-dimer of two proteins consisting of 491 amino acids. Each monomer contains two structural domains with a total of 19 β-strands and 13 α-helices [76].

Like other adipokines, systemic visfatin activity is linked with various metabolic states such as obesity, visceral fat mass and diabetes [77–79].

Visfatin as a cytokine Samal et al. first described visfatin under the name pre-B-cell colony-enhancing factor (PBEF1) as a secreted cytokine. They demonstrated the effect of stem cell factor (SCF) and IL-7 on murine pre-B-cell colony formation to be significantly enhanced in the presence of PBEF1. PBEF1 was found to be expressed in bone marrow stromal cells as well as in activated human lymphocytes, acting on lymphocyte maturation and inflammation regulation. High tissue concentrations of visfatin were found in liver and kidney tissue, muscle and bone marrow [80–84].

Visfatin as an enzyme Rongvaux et al. described visfatin as a rate limiting component in the nicotinamide salvage pathway, an alternative pathway for nicotinamide adenine dinucleotide (NAD) biosynthesis from niacin and nicotinamide [85]. Visfatin as a co-enzyme in the nicotinamide salvaging pathway is therefore also referred to as nicotinamide phosphoribosyltransferase (Nampt or NAmPRTase).

NAD is an important co-factor in the metabolism of every living cell, serving as an electron carrier in redox reactions. It is a co-enzyme to many oxidoreductases in beta oxidation, glycolysis and the citric acid cycle. It provides electrons (as NADH) for ATP production in the mitochondrial electron transport chain. Many other enzymes depend on

NAD, such as ADP-ribosyltransferases, sirtuins (NAD-dependent deacetylase) and DNA ligases.

NAD can be synthesized de-novo from the essential amino acid tryptophan (or aspartic acid in plants and some bacteria) or salvaged from the food nutrient vitamin B_3 (nicotinic acid, nicotinamide and nicotinamide riboside, also referred to as vitamin B_3 complex). Vitamin B_3 or tryptophan deficiency can cause pellagra in humans - Nampt inhibition was shown to reduce intracellular NAD+ levels and induce cell-senescence in vitro [86].

Visfatin as a fat-derived hormone Nampt/PBEF1 was re-identified as a "new visceral fat-derived hormone" in an intensively discussed SCIENCE publication by Fukuhara et al. from 2005 [1], suggesting an insulin-mimetic effect of visfatin on glucose control. The proposed ability of visfatin to bind and activate the insulin-receptor has been questioned, generating a retraction by the author in 2007 [88].

The adipokine was found to be enriched in visceral fat of both humans and mice in contrast to subcutaneous fat, thus it was named visfatin ("*vis*ceral *fat* cytok*in*e"). Visfatin was reported to exert insulin-mimetic effects in cultured cells by binding and activating the insulin receptor at a site different from the binding site of insulin. In mice, lower plasma glucose levels after visfatin application and higher levels in heterozygous mutated individuals were observed, suggesting a possible role for visfatin production as a compensatory response to insulin resistance [89].

After the retraction, other studies confirmed a visfatin effect on osteoblast glucose uptake, proliferation, matrix mineralization and collagen I and osteocalcin production [90]. Of these osteoblast functions, glucose uptake, proliferation, and type I collagen production were described to be mediated by the insulin receptor (IR) transduction pathway, that was activated by both insulin and visfatin, confirming the initial hypothesis.

Visfatin was shown to be expressed by cells found in adipose tissue, adipocytes and macrophages, with no production by osteoblasts and osteoblast precursors [90, 91]. Osteoblasts are, however, a functional target of visfatin [90].

[1] The retracted paper is purposely not formally cited as recommended by Teixeirada et. al [87].

6.3.1 Visfatin and inflammation

In 2007, Moschen et al. started looking at the immunological and inflammatory functions of the - at that time – recently identified adipokine visfatin [91]. Upon stimulation of human monocytes with recombinant visfatin, they found the production of the pro- and anti-inflammatory cytokines IL-1β, IL-1R, IL-6, IL-10, and TNF-α to be up-regulated in in a dose dependent manner. In parallel, the cluster of differentiation (CD) surface markers CD80 and CD40, both involved in the communication of antigen-presenting cells (APCs) and T-lymphocytes were found to be up-regulated. ICAM-1 (CD54), another T-cell promotor, was induced by visfatin stimulation. In addition, cellular functions such as an increased phagocytosis were reported in human monocytes. In addition, the authors hypothesized APCs to be a source of visfatin themselves [91].

The most predominantly up-regulated cytokine in macrophages stimulated *in vitro* with visfatin was IL-6. This finding was confirmed in the serum of visfatin injected mice with highest levels of visfatin expression in gut tissue [91]. The adipose tissue was not explicitly sampled. However, the high expression of IL-6 mRNA in gut tissue compared to lung, liver and spleen described by Moschen et al. likely pointed to the visceral adipose tissue as the main site of increased IL-6 production.

The multifunctional interleukin IL-6 plays a critical role in a variety of immunological processes. It belongs to the IL-6-family of cytokines that share the common glycoprotein gp130 as a critical component for signal transduction. Only hepatocytes and leucocytes express the membrane-bound IL-6 receptor (IL-6R) that binds and transduces the IL-6 signal via gp130. All other cell types do express gp130 on their membrane but require the soluble receptor IL-6R (sIL-6R) for activation. IL-6 is involved in activating the acute phase response (and as an endogenous pyrogen inducing fever), B cell maturation, T cell activation and proliferation, inflammatory chemokine induction and leukocyte recruitment, as well as haemopoesis and tissue regeneration [92]. Several studies have shown a correlation between visfatin and IL-6 levels [93]. Visfatin seems also to be a stimulus for TNFα expression [94].

Interleukin 6 is involved in many autoimmune disorders and inflammatory conditions

such as diabetes [95], atherosclerosis [96], systemic lupus erythematosus [97], Behçet's disease [98], rheumatoid arthritis [99], major depression [100], Alzheimer's disease [101], as well as malagnancies [102, 103]. Monoclonal antibodies against the IL-6R have successfully been developed and are frequently used for the treatment of rheumatoid arthritis.

The role of visfatin in OA was described by Chen et al. in 2010 [104]. Elevated visfatin levels where observed in serum and synovial fluid of OA patients compared to controls. As a local source of visfatin in the joint, the infra-patellar fat pad, the synovium and osteophytes could be identified [5, 104, 105]. In addition to adipocytes, immunohistochemical staining for visfatin was positive in OA osteoblasts, osteoclasts and chondrocytes [5]. Visfatin was found to positively correlate with cartilage degradation markers [106] and was inversely correlated with the clinical severity of OA [107], further suggesting an involvement of visfatin in the pathophysiology of OA. Likewise, clinical studies have shown a response of visfatin in serum to mud bath therapy in OA patients [108].

Preliminary projects of our group showed that the shift of stem cell differentiation in patients with osteoporosis towards adipogenesis leading to reduced osteogenic potential is not altered by visfatin. However, visfatin affects the release of MMPs, inflammation mediators and matrix mineralization during osteogenesis [109].

McNulty et al. (2011) demonstrated how visfatin but not other adipokines acted synergistically with IL-1β to activate nitric oxide, proteoglycan production and MMP activity and to degrade cartilage and meniscus in an experimental porcine tissue model [110].

6.3.2 Visfatin in osteogenic differentiation

Visfatin is an adipose tissue derived hormone, also expressed in and released by connective tissue mesenchymal cells. Altered visfatin levels have been reported in various autoimmune and inflammatory conditions including obesity. MSCs as multi-potent connective tissue stem cells are essential for tissue maintenance and regeneration. MSCs migrate to the site of tissue injury and differentiate to the appropriate somatic cell type. In conditions like OA and other rheumatic diseases this interplay of systemically and locally altered adipokine level and osteogenic differentiation of MSCs may be a leading cause in

pathophysiology and disease progression.

Visfatin has shown pro-osteogenic effects on human osteoblasts, proliferation, type I collagen production through insulin receptor (IR) phosphorylation in osteoblasts [90]. Inhibition of visfatin during osteogenic differentiation resulted in a reduction of the activity of alkaline phosphatase (ALP), Runx2, OCN and OPN, as well as bone mineralization [111], visfatin deficiency promoted adipogenesis and reduced osteogenesis in mice [112].

Tsiklauri et al. focused on the impact of adipokines on adipogenic and osteogenic MSC differentiation. Visfatin was shown to shift the differentiation potential of MSCs towards osteogenic differentiation. Differentiation markers were altered and matrix mineralization in vitro was enhanced. MMP production was increased, as well as IL-6, IL-8 and MCP-1 production [109].

This study therefore took a closer look on the link between visfatin, its pro-inflammatory effects and the impaired bone tissue structure and composition in OA and other inflammation and age-related conditions.

7 Regulatory RNA

Less than 2% of the human genome is protein-coding information. Only this small fraction of information is transcribed and translated to proteins. The rest was considered evolutionary remnants involved in DNA stability or merely junk. The identification of functional, non-protein-coding genes in this 'genomic dark matter' [113] is a challenge to science, sparking endeavors like the HUMAN GENOME PROJECT and 1000 GENES PROJECT to further understanding of 'our' genetic code.

The total amount of RNA produced by a cell is known as their transcriptome. Information is transcribed to pro-messenger RNA (mRNA) that get processed by the spliceosome and other small nuclear ribonucleoproteins (snRNP) containing snRNA. The resulting mature mRNA is translated into a protein sequence by the ribosome. This molecular protein production facility itself is a complex of ribosomal RNA (rRNA) and proteins. Further RNA molecules like signal recognition particles (SRP RNA) and transfer RNA (tRNA) are directly involved in this process. These types of RNA are examples of non-protein

coding RNA molecules (ncRNA). Information about their structure is stored in genomic DNA and they are (to current knowledge) transcribed into RNA via similar processes as protein coding DNA sequences.

The first ncRNA to be discovered was the product of the H19 gene. The resulting mRNA is transcribed by the RNA polymerase II and poly-adenylated like any other. Upon their discovery Brannan et al. noted in their 1990 publication: "[...] we suggest that the H19 RNA is not a classical mRNA. Instead, the product of this unusual gene may be an RNA molecule." [114]

Due to their nucleic acid structure, many ncRNAs are found at the interface of the nucleic acid and the protein world, facilitating and regulating the flow of information between them [115]. The 'world' of non-coding RNA molecules ranges from RNAs involved in the translation machinery and its regulation (rRNAs, tRNAs, small interfering RNAs and micro RNAs), RNA processing (splicing) [116, 117], to the large and heterogeneous class of long non-coding RNAs (lncRNAs). These RNA molecules with lengths of more than 200 bases have been shown to be involved in the formation of the dense chromosome structure [117]. ncRNAs are often incorporated in ribonucleoproteins (RNPs) which then act as an adapter molecule between proteins and nucleic acids. Other mechanisms of functional/regulatory RNA molecules are described below and an overview of the different types of coding and non-coding RNAs is shown in figure 4 on the following page.

One way to categorize ncRNAs is by their length. This distinguishes lncRNAs with more than 200 nucleotides from micro RNAs (miRNAs) that often consist of only 20 nucleotides. Other classes of small ncRNAs include small interfering RNAs (siRNAs), Piwi-interacting RNAs (piRNAs), small transfer RNAs (tRFs), small nucleolar RNAs (snoRNAs), small nuclear RNAs (snRNAs), and small cytoplasmic RNAs (scRNAs). All of these types of RNA are not strict categories as there are examples of lncRNAs consisting of parts or fragments of protein coding RNA or lncRNAs being later spliced into smaller regulatory units. Therefore lncRNAs can be further categorized based on their association with annotated protein-coding genes or other DNA elements [118–120].

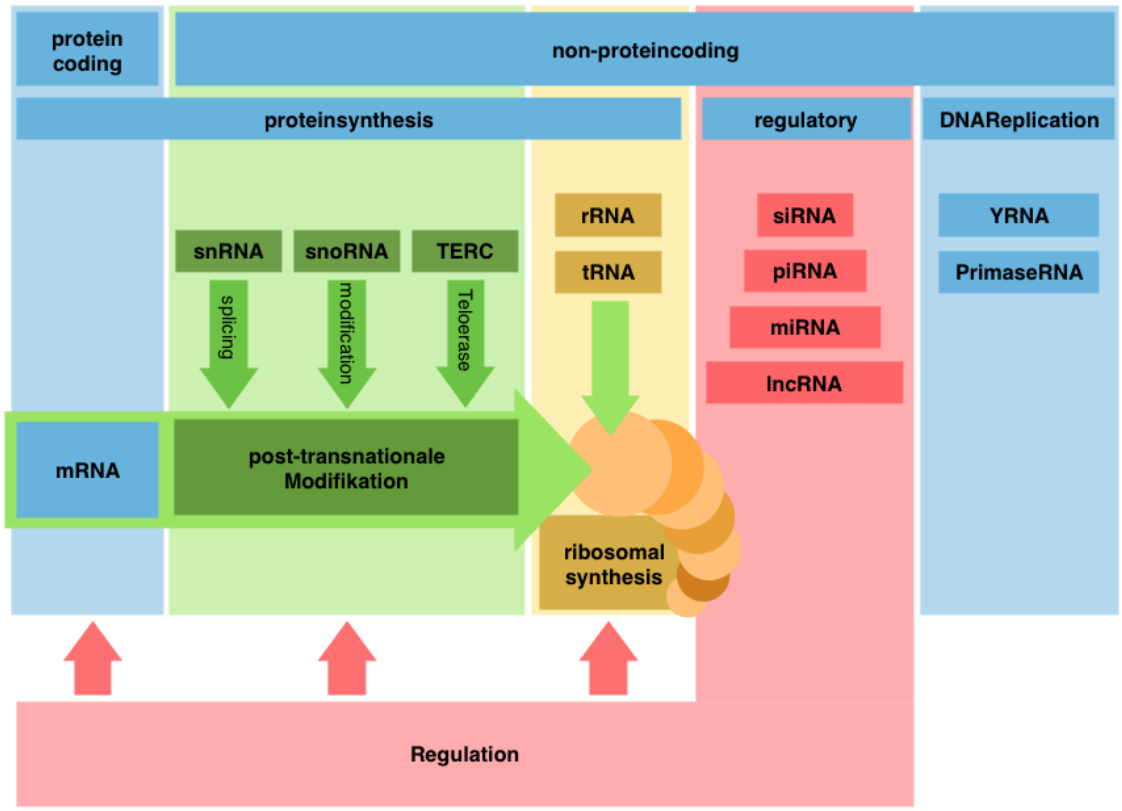

Fig. 4: Overview on different types of RNAs. Protein coding mRNA (blue) is modified by different molecules including RNA molecules (green) and finally transcribed into proteins (yellow). These (and other) processes are regulated by non-conding RNAs (red). Other non-protein-coding RNAs play a role e.g. in DNA maintenance and replication (blue, rightmost column).

7.1 Micro RNA

Micro RNAs (miRNAs) are small 20- to 25-nucleotide-long ncRNAs that play a role in the regulation of translation and processing of mRNA - hereby "fine-tuning" gene expression of a particular cell. Imbalances in the network of miRNAs have been observed in many medical conditions including cancers and rheumatic diseases.

After the discovery of the let-7 family of miRNAs and their role as down-regulated tumor suppressors in many cancers, the topic of miRNAs in oncogenesis quickly emerged. The search for *oncomiRs*, cancer-associated miRNAs, has since led to the identification of new prognostic biomarkers and drug targets. Interestingly some miRNA have been identified as regulators of osteogenic differentiation such as miRNA29b [121], miRNA 34a [122], miRNA 138 [123], miRNA 140 [124] and miRNA 542 [125].

Like mRNA, miRNA is transcribed into a primary miRNA (pri-miRNA) by RNA

polymerase II and like mRNA, they are processed with a 5' cap and 3' polyadenylated. Most pri-miRNA carry one miRNA, yet some have been found to be *polycistronic,* coding for more than one miRNA. miRNAs are then processed into shorter (~65-nucleotide-long) precursor RNAs (pre-miRNAs) which form a secondary hairpin structure and gets transported from the nucleus to the cytoplasm. Here, the pre-miRNA is further processed and a double-stranded miRNA duplex is released. One strand of miRNA is then incorporated with other proteins into the RNA induced silencing complex (RISC). As part of this complex, the miRNA serves as a template to recognize and cleave the target mRNA, a process called RNA interference.

miRNAs may also be encoded within the sequence of lncRNAs, for example two miRNAs (miRNA 675-3p and -5p) are encoded inside lncRNA H19 [126].

7.2 Long non-coding RNA

Long non-coding RNAs (lncRNAs) are defined as non-protein coding RNA molecules longer than 200 nucleotides. This rather arbitrary limit distinguishes lncRNAs from other regulatory RNAs such as micro RNAs or small-interfering RNA. The current version of the GENCODE library lists a total of 17.957 human and 13.197 murine lncRNA genes[127] and the LNCBOOK accounts for 3.772 lncRNA associated with 462 diseases and 28 MeSH disease terms [128].

The majority of lncRNAs are transcribed by RNA polymerase II, and they are often spliced (and even alternatively spliced) during RNA processing. Many lncRNAs are similar to mRNAs polyadenylated and receive a 5' cap [129]. Some, however, are processed differently such as cancer-associated MALAT1, which is processed by RNase P at the 3' end (that is otherwise known to process the 5' ends of tRNAs) [130].

Over 20% of the genome is comprised of intronic material which is spliced off upon RNA processing. This may be a large source of 'intronic' lncRNA. There are, however, lncRNAs encoded in between protein coding genes or on opposite strands as well. These associations with known genes may be responsible for many of their functions, for example enabling positive and negative feedback loops. On the other hand, these associations

have become a basis for classification and organization of the plentiful lncRNAs that are emerging in recent years.

7.2.1 Classification of lncRNA

A widely used classification system of lncRNAs is based on their association with known protein-coding genes and was established by Rinn et al. in 2012 [115]. Relative to the encoding genes, they can be classified as either sense or anti-sense, and can thus be located on the same (sense) or on the opposite strand (anti-sense) of DNA. On the same strand, an lncRNA can be either close to (intergenic, divergent) or within the transcribed DNA fragment. As part of the protein-coding fragment, lncRNAs can be restricted to intronic sequences or even overlap potentially protein-coding exons [118].

Anti-sense ncRNAs are encoded on the opposite strand of a protein-coding gene, either initiated inside of [115] or overlapping its exonic sequence [131].

Sense ncRNAs are located on the same strand as a protein coding gene.

Intergenic ncRNAs (lincRNAs) reside in between coding gene sequences. Hence their transcription is not triggered by a coding genes initiation complex, they have separate transcriptional units from protein coding genes [115].

Bidirectional (divergent) ncRNAs initiate within the same complex as a protein coding sequence, but are transcribed in the opposite direction [115].

intronic ncRNA reside within intronic sequences of protein-coding genes. Characteristically the initiate inside an intron of a protein-coding gene without overlapping its exons. In a strict definition they sometimes are referred to as totally intronic ncRNAs (TINs) [118]. When transcribed with a coding gene, these ncRNA-coding introns may escape de-branching and accumulate in the cell as intronic circular RNA (icRNA) further regulating the expression of their parent gene [132].

sense-overlapping ncRNA overlap with or share the same DNA-sequence as protein coding genes. They are further characterized as unspliced sense partially intronic RNAs (PINs) and spliced transcripts, that may combine exons from coding and non-coding genes.

7.2.2 lncRNA modes of action

Wang et al. (2011) defined archetypes of lncRNA function based on their structural ability to bind specific DNA/RNA sequences as well as form complexes with proteins [133]. In this publication, the authors also pointed out that transcribed lncRNAs can also act as *signal* for other cellular processes as well as a specific sign for the particular transcriptional state a cell is in. Many of the first lncRNAs described exhibit enhancer-like functionality, promoting gene-expression. Signal lncRNAs herein may stay attached to their site of transcription, regulating further expression in cis, or may form DNA loops affection expression of other sequences in trans.

Decoy The most simple mode of action for a lncRNA is to serve as decoy, carrying the same nucleic acid sequence targeted by for example a transcription factor. In titrating other molecules away from their target gene, lncRNAs can specifically alter gene expression.

Similarly to the decoy mechanism, lncRNAs may bind one or more miRNAs, titrating them away from their sites of action. This behavior is often referred to as sponge.

Scaffold Given their ability to bind proteins, lncRNAs can act as adaptors for the formation of protein complexes, hereby bringing active sites of different proteins together in a structured manner.

Guide Taking together both, the ability to specifically target a nucleotide sequence and build specific, localized protein complexes, lncRNAs can serve as a guide, leading a protein complex to a targeted location of the genome for specific action. Notably, lncRNAs can bind DNA in both, cis- and trans-configuration.

8 lncRNA H19

lncRNA H19 was discovered as the first functional RNA in 1990 by Brannan et al. An RNA molecule was identified in mice and found to be transcribed by RNA polymerase II, spliced and polyadenylated like typically seen in mRNAs; however, it lacked an open reading frame and could be found outside of the nucleus in the cytosol. It therefore was believed to function as an untranslated RNA molecule [114].

As H19 was confirmed to be a functional RNA molecule [134], the lncRNA became a subject of further research. It was found highly expressed in embryonal tissues of endo- and mesodermal origin and to play a role in foetal growth and tissue differentiation and its expression declined after birth [135, 136]. A lack of H19 expression resulted in an over-growth phenotype, while postnatal growth was reduced in mice with H19 over-expression [137]. Embryological disorders Beckwidth-Wiedemann-Syndrome and Silver-Russell-Syndrome, pre-eclampsia and a variety of neoplasms such as Wilms tumor, osteosarcoma or colon and gastric cancer showed a differential regulation of H19 [138–141]. These results indicate a role of H19 in the regulation of growth and tissue differentiation. H19 expression is decreased in all tissues except heart and skeletal muscle after birth. Yet it has been shown to be involved in the regulation and differentiation of mesenchymal stem cells and to mediate their faith towards osteogenic, adipogenic, tenogenic and chondrogenic lineage. Stuhlmuller et al. introduced H19 to the field of rheumatology, finding H19 expressed in chronically inflamed synovial tissue of RA and OA patients [142].

These findings are the basis for the research discussed in this thesis: lncRNA H19 in the context of both osteogenic differentiation and under the influence of the pro-inflammatory adipokine visfatin.

8.1 Structure of lncRNA H19 and endogenous micro RNAs

LncRNA H19 is a monoallelically expressed and highly conserved [134] ncRNA encoded on chromosome 11p15 in humans and on chromosome 7 in mice [114, 143].

The allele-specific expression of H19 is based on epigenetic imprinting. H19 itself has been suggested to control the expression of other imprinted genes via an *imprinted gene network* during embryonic development [137]. The lncRNA consists of 5 exons as shown in figure 5. Exon 1 contains two miRNAs miRNA- 675-5p and miRNA-675-3p, that in turn themselves were shown to play a role in cell proliferation and cancer development [126, 144–146] (shown in figure 6). These micro RNAs can be released from the lncRNA molecule by alternative splicing [126]. The two mature micro RNAs act as co-operators of H19 in the regulation of cellular differentiation [147].

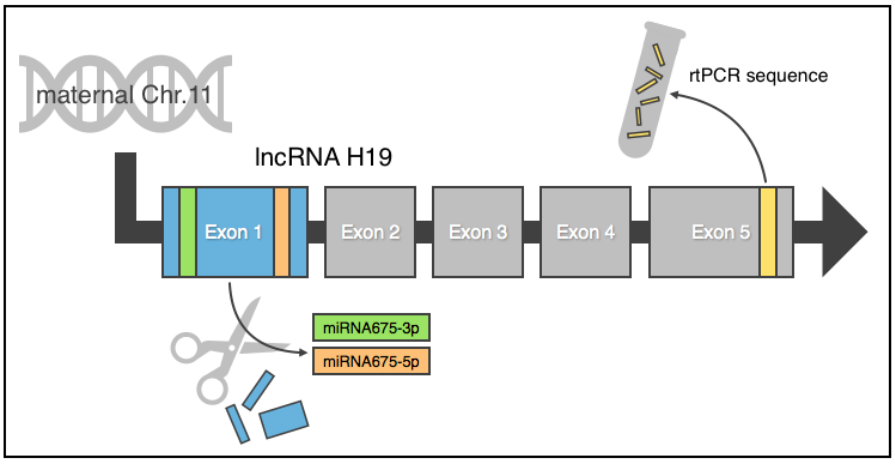

Fig. 5: Structure of lncRNA H19. The coding gene for H19 is located on 11p15, and is only expressed from the maternal chromosome. H19 consists of 5 exons, shown as exon 1-5. The two intrinsic micro RNAs miRNA675-3p and miRNA675-5p are located in exon 1 and may be released by alternative splicing. To detect the total amount of lncRNA H19, we used a sequence in exon 5 for real-time PCR quantification. This method is therefore naive to the amount of alternative splicing and results always reflect the total amount of H19 produced.

lncRNA H19 and IGF2

Insulin-like growth factors (IGFs) are polypeptides with a highly homologous structure to insulin. Like their better-known sibling, they stimulate growth and differentiation in various foetal and adult tissues. The IGF-pathway consists of the two substrates IGF1 and 2, membrane receptors IGF1R and IGF2R and IGF binding proteins IGFBP-1-to-6. IGFs

Fig. 6: Sequence of lncRNA H19. Shown in bold are the included microRNAs 675-5p (in the line starting at 4621) and 675-3p (4681) and the forward and reverse primer target sequences used for rtPCR analysis.

have been shown to promote cell proliferation and inhibit apoptosis.

As they play a role in physiological growth, they are also associated with pathological processes and cancer development. It was suggested that IGF2 is more active in the early stages of development, whereas IGF1 is an important regulator of later stages of growth and development.

IGFs have the ability to bind to the IGF1-receptor, the IGF2-receptor (IGF1R & -2R), as well as to the insulin receptor (IR). IGF1 has the highest affinity to IGF1R, a receptor tyrosin kinase, similar to the IR. The IGF2R has no known downstream signaling mechanisms and is proposed to attenuate IGF2 and its effects.

The H19 gene shares a common imprinting control region (ICR) and a common set of enhancers with the IGF2 gene. Whereas H19 is only expressed from the maternally-inherited chromosome, IGF2 is only expressed paternally. Methylation of the ICR either prevents or allows gene expression. CTCF (CCTC-binding factor) and c-myc proteins bind the un-methylated ICR, preventing the binding of enhancing factors. Hereby, only one of both regions is transcribed physiologically. Recent studies have suggested a role of the H19 antisense gene, 91H.

lncRNA H19 and 91H

On the opposite strand of the gene coding for lncRNA H19, an antisense RNA named 91H was proposed [148]. Research conducted by Vennin et. al. indicated that 91H may be involved in maintaining the differential methylation of the H19/IGF2 locus and may

induce expression of these genes by masking the common ICR, hereby promoting H19 and IGF2 expression.

8.2 lncRNA H19 in osteogenic differentiation

lncRNA H19 was shown to be up-regulated in osteogenic differentiation of MSCs [147, 149]. Osteogenesis inducers such as TGF-β 1, BMP2 and BMP4 likewise increased the expression of H19. H19 over-expressing MSCs showed significantly up-regulated matrix mineralization and osteogenesis marker expression (ALP, OCN, Runx2) [147]. Recent studies found an increased level of serum H19 in osteoporosis patients, in keloid tissues or at sites of increased calcification [150–152]. Yet the regulatory mechanisms and the role of H19 in osteoblast differentiation remains a current subject of research. Wang et. al performed a lncRNA microarray on mesenchymal stromal cells after induction of osteogenic differentiation. The up-regulation of H19 was verified using rtPCR in this study. A detailed analysis of the H19 expression trend during differentiation showed a significant rise between day 0 and 7 and a steady, yet insignificant trend until day 21. These results are coherent with other group's findings [147]. An inverse regulation for H19 was shown in the osteogenic differentiation of adipose-derived stem cells (ASCs) [153]. Knock-down of H19 was shown to induce adipogenic differentiation in ASCs [154].

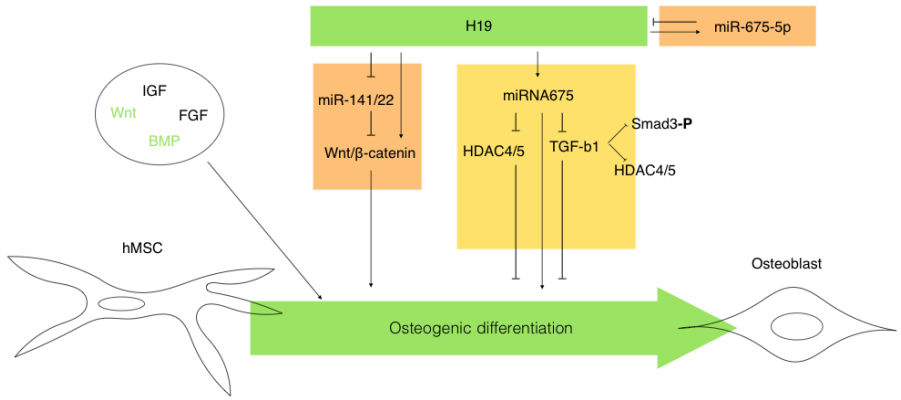

Fig. 7: Overview on H19 downstream mechanisms. Green arrow: osteogenic differentiation (OD) of human mesenchymal stem cells (hMSCs) towards osteoblasts. Established regulators of OD are IGF, FGF, Wnt and BMP. Two proposed downstream mechanisms are the H19/miR-675/TGF-β1/Smad3/HDAC-pathway (yellow, [155]) and the H19/miR-141/-22/Wnt/β-catenin-pathway (orange, [147]) as well as the feedback loop with ectopically expressed miRNA 675-5p (orange).

8.2.1 H19-dependent TGF-β1 signaling pathway

Huang et al. in 2015 reported a lncRNA-miRNA-mRNA network of H19 during osteogenic differentiation. This pathway was suggested to promote osteogenic differentiation by suppressing the H19/miR-675/TGF-β1/Smad3/HDAC signaling pathway. Their findings and the key elements of this pathway are discussed below.

miRNA 675 is a micro RNA located within the RNA sequence of H19, where it is encoded on the exon 1 of H19. It therefore can be expressed by alternate splicing of H19 and may mediate some of the regulatory functions of lncRNA H19.

Huang et al. demonstrated that miRNA 675 was up-regulated in parallel to H19 during OD [155]. Ectopic miRNA 675 expression showed similar effects on osteogenic markers as the over-expression of the complete H19 lncRNA. This could be demonstrated in standard growth medium and the effect was even stronger after OD induction. Over-expression led to increased levels of ALP, OCN and Runx2 as well as increased mineralization. Inverse effects where shown in miRNA deficient MSCs. The osteogenic effect of H19 could be partially restored in miRNA 675 transfected H19 deficient MSCs and were lost after miRNA 675 mutation, indicating that the osteogenesis promoting effects of H19 are partially mediated by its contained miRNA 675.

TGFβ1 Transforming growth factor beta 1 (TGFβ1) is a cytokine from the *TGF*β *superfamily*. With other growth regulating ligands such as bone morphogenetic proteins (BMPs), growth and differentiation factors (GDFs), anti-Müllerian hormone (AMH) and activin, TGFβ1 is mainly involved in control of cell growth, proliferation, differentiation, and apoptosis. It is produced by a wide range of cell types and its effects have been shown to vary, depending on the differentiation stage of the target cell. Mainly acting as an auto- and allocrine negative growth factor, TGFβ1 released by T cells down-regulates T, T helper and cytotoxic T and B cells and inhibits the expression of various cytokines and interleukins. In suppressing myeloic cells, it may also function as a chemoattractant hereby up-regulating the monocytic immune response.

All TGFβ superfamily members bind to a membrane bound TGFβ1 type 2 recep-

tor which recruits and phosphorylates a type 1 receptor. This hetero-tetrameric complex phosphorylates and activates an R-SMAD (a group of signal transducers of TGF-beta-receptors) which in turn phosphorylates a coSMAD (e.g. SMAD4). This complex can alter gene expression by binding transcription promotors or cofactors after entering the nucleolus.

H19 was found up-regulated after treatment with TGFβ1 for seven days and over-expression of H19 led to increased tendon growth [156]. H19 and its splice product miRNA-675 were demonstrated to negatively correlate with TGFβ1 in prostate epithelial cells, which led to higher motility and less apoptosis in tumor cells [157]. Target prediction analysis revealed binding sites for miRNA675-3p and -5p in the TGFβ1 transcript. miRNA675-3p and -5p transfected MSCs showed a reduction of TGFβ1 both on mRNA and protein level [155].

TGFβ1 deficient mice were found to exhibit reduced bone growth and impaired mineralization capacity [147] and down regulated osteogenic differentiation of MSCs. TGFβ1 induces a phosphorylation of SMAD 3 via the TGFβ1-receptor type 1 and 2 pathway which interacts directly with class IIa histone deacetylase (HDACs) 4 and 5 down-regulating Runx2 expression at the osteocalcin promotor [158, 159].

H19 and its endogenous miRNA 675 bind to TGFβ1, hereby inhibiting the TGFβ1 pathway, leading to an overall increased osteogenic differentiation potential [155].

8.2.2 H19 - miR-675-5p feedback loop

The contained miRNAs of H19 exhibit functional/regulatory roles by themselves. They show no coordination with H19 expression during osteogenesis. Ectopic expression of miRNA- 675-5p, however, shows an inhibitory effect on H19 via targeting a specific binding site in its host gene, hence forming a negative feedback loop [147].

8.2.3 H19-dependent Wnt/β-Catenin signaling pathway

A possible effector mechanism of lncRNAs is the inherent ability to bind to other nucleic acids such as messenger or micro RNAs. This may be another pathway for H19's osteogenesis promoting capacity. By acting as a miRNA sponge for miRNA-141 and miRNA-22, it may hinder their inhibitory effects and hereby activate the pro-osteogenic Wnt/β-Catenin pathway [147].

Micro RNA 141/22 The two micro RNAs 141 and 22 were identified as negative regulators of osteogenesis markers BMP2, ALP, MSX2, OCN, collagen A1 and Runx2, as well as matrix mineralization as shown by Alizarin Red staining.

β-Catenin was determined to be a potential target for miRNA-141 and 22. Both micro RNAs where shown to be negative regulators of β-Catenin expression [147].

miRNA 141 is part of the miRNA200-family that is involved in the formation and progression of numerous malignancies, including nasopharyngeal, esophageal, breast and colon carcinoma.

miRNA-22 also was found to be differentially regulated in tumor cells, with its targets being myc binding protein (MYCBP) and histone deacetylase 4 (HDAC4).

Wnt/β-Catenin-pathway The canonical Wnt/β-Catenin-pathway was shown to play a fundamental role in osteogenesis and embryonic bone formation and bone remodeling [37, 160]. β-Catenin is an essential element for bone development. its presence was demonstrated in the cytoplasm and nuclei of metabollicaly active osteoblasts [161] and in cell-cell contacts, where it directly links cadherins and the actin cytoskeleton [162].

In the absence of Wnt, plasmatic β-Catenin is bound in the β-Catenin-destruction-complex, where it is phosphorylated, priming it for ubiquitination and consecutively proteasomal degradation. The β-Catenin concentration is held at a constant, low level when Wnt signaling is inactive. Upon extracellular binding of Wnt, the destruction complex is deactivated, allowing β-Catenin to accumulate in the cytoplasm and to relocate to the nucleus, creating transcription activating complexes. High levels of β-Catenin can preserve pluripotency in stem cell lines as well as promote differentiation and retard apoptosis.

A loss-of-function APC, an element of the β-Catenin-destruction-complex, leads to constitutive high β-Catenin levels and plays a role in the development of colorectal cancer [163, 164].

H19 over-expression was shown to up-regulate the Wnt/β-Catenin pathway. This effect was silenced after H19 miRNA binding site mutation and complete down-regulation of H19 via siRNA. These results suggest that H19 may act as a sponge for miRNA 141 and 22, hereby neutralizing its β-Catenin inhibitory effects [147].

H19 also associates with the enhancer of zeste homolog 2 (EZH2), also leading to Wnt-pathway activation, a decreased expression of the tumor suppressor E-cadherin and ultimately increased bladder cancer cell metastasis [165].

Other H19 sponge activity Studies have shown a number of other ribonucleoproteins that may form complexes with H19. H19 was shown to act as a molecular sponge for let-7 family members, de-repressing several protein-coding genes targeted by let-7. H19 over-expression was also found to down-regulate the let-7 targets DICER and HMGA2 [166]. Similarly, H19 could also act as a decoy for miRNA-138 and miRNA-200a [167].

Part II. Aims and research questions

Destructive bone diseases like osteoarthritis concern a large group of patients and lead to chronic pain, disability and reduced quality of life. Injury of the joint as well as local and systemic chronic inflammation contribute to cartilage damage and bone erosion. As a part of this process, the physiological bone remodeling machinery, the continuous resorption and production of bone matrix, is severely dysregulated. An important component of this system are the mesenchymal stem cells, which migrate to sites of tissue destruction and differentiate into osteoblasts to support bone repair. Pro-inflammatory adipokines like visfatin that are secreted primarily from adipose tissues throughout the body as well as locally within the joints have been shown to alter the activation of the differentiating osteoblasts [109]. Visfatin stimulation of MSCs during osteogenic differentiation led to an increase in matrix mineralization with higher MMP and MCP-1 production as well as an increase in interleukins (IL-6 and -8), and create ultimately an inflammatory milieu with production of a less elastic, brittle bone structure [109]. Because of these findings, the experimental approach of this thesis focussed on the role of visfatin in osteoarthritis, although having the potential to be relevant also in other bone diseases such as osteoporosis.

Since their initial discovery, regulatory RNAs like long non-coding RNA molecules, with their ability to facilitate crosstalk between the protein and RNA worlds and regulating transcription processes, have emerged as a relevant new field of research.

Based on these findings, the aim of this thesis was to evaluate lncRNAs with respect to their role in the response of osteoblasts to inflammatory conditions and their effects on MSCs during osteogenic differentiation. To identify potential candidates for lncRNAs, the results of a micro-array analysis covering a large number of lncRNAs with osteoblasts from different patient collectives (osteoarthritis, rheumatoid arthritis) was evaluated with respect to their response to inflammatory conditions. One candidate was then investigated, specifically its regulation during OD including potential mechanisms of action.

The lncRNA array analysis was performed based on the following questions:

- Are the lncRNAs, which are included in the array, differentially regulated?
- Can this differential regulation be confirmed in individual cell populations?
- Which of these lncRNAs included are potential targets for further research?

lncRNA H19 was chosen as the most promising candidate. To investigate the role of H19 in MSCs during OD, the following questions where addressed by the experiments presented in this thesis:

Do adipokines affect the regulation of lncRNA H19 during OD?

In MSCs stimulated with visfatin, H19 was differentially regulated when compared to other adipokines (leptin, resistin) or unstimulated controls. Based on these findings, the following experiments focused on visfatin and its effect on H19 regulation.

Is lncRNA H19 differentially regulated in adipogenic differentiation of MSCs?

MSCs can also be differentiated towards adipocytes. To evaluate, whether the regulation of H19 was specific to osteogenic differentiation, H19 regulation in adipogenic differentiation was evaluated and compared to OD.

Is the differential regulation of lncRNA H19 a visfatin-specific effect?

Given the pro-inflammatory effects of visfatin, the H19-regulatory effects of TNFα as another pro-inflammatory stimulus were investigated and compared.

What is the mechanism of lncRNA H19 affecting osteogenic differentiation?

Three potential downstream mechanisms of lncRNA H19 were evaluated: WNT/β-Catenin and TGFβ1 pathways, as well as differential regulation of the two micro-RNAs known to be encoded within the sequence of H19.

Part III. Materials

8.3 Tissue specimen

phMSCs primary human MSCs

were available from the research groups biobank. Human tissue samples were collected following joint replacement surgery in the department of Orthopedics and Trauma Surgery, Agaplesion Markus Hospital in Frankfurt, Germany. Informed consent was given by all patients prior to the intervention. Isolation and scientific use of human tissue samples was approved by the ethics commission of the Medical Faculty of Justus-Liebig-University, Giessen, Germany (Aktenzeichen 66/08, 74/05).

hMSC Human MSCs from healthy donors were bought from Lonza, Allendale, USA.

8.4 Materials and chemicals

Description	Source
Visfatin *recombinant, human*	Biovendor, Heidelberg, Germany
Resistin *recombinant, human*	PeproTech, Rocky Hill, USA
Leptin *recombinant, human*	Biovendor, Heidelberg, Germany
TNFα	Sigma Aldrich, Taufkirchen, Germany
Porcupine (PORCN), WNT-C59	R&D Systems, Wiesbaden, Germany
LY2109761	Selleckchem, Munich, Germany
Trypsin EDTA	GE Healthcare, Chicago, USA
RNasin	Promega, Mannheim, Germany
AMV Reverse Transcriptase	Promega, Fitchburg, WI, USA

Tab. 2: Enzymes and proteins

Description	Source
ABSOLUTE QPCR SYBR GREEN CAPILLARY MIX	Thermo Scientific, Roche
QUANTIKINE® ELISA HUMAN IL-6 IMMUNOASSAY	R&D Systems, Wiesbaden, Germany
QUANTIKINE® ELISA HUMAN TNF-α IMMUNOASSAY	R&D Systems, Wiesbaden, Germany
QUANTIKINE® ELISA HUMAN TGF-β1 IMMUNOASSAY	R&D Systems, Wiesbaden, Germany
RNEASY^{TM} MINI KIT	Qiagen, Hilden, Germany
MIRNEASY^{TM} MINI KIT	Qiagen, Hilden, Germany
RNASE-FREE DNASE SET	Qiagen, Hilden, Germany

Tab. 3: Kits for molecular biology and immunological assays

Description	Source
FCS *foetal calf serum*	Sigma Aldrich, Taufkirchen, Germany
Pipet Tips	Corning, Wiesbaden, Germany
Falcon Tubes	Greiner, Frickenhausen, Germany
Cell Scraper	Greiner, Frickenhausen, Germany
Cell culture flasks	Greiner, Frickenhausen, Germany
Stripettes	Corning, Wiesbaden, Germany
Pasteur pipettes	Carl Roth, Karlsruhe, Germany
Light Cycler Capillaries	Roche, Mannheim, Germany
PCR reaction tubes	Carl Roth, Karlsruhe, Germany
MgCl	Sigma Aldrich, Taufkirchen, Germany
rt-PCR grade water	Roche, Mannheim, Germany
HCl	Carl Roth, Karlsruhe, Germany
NaOH	Carl Roth, Karlsruhe, Germany
β-Mercaptoethanol	Carl Roth, Karlsruhe, Germany
PBS buffer	Biochrom Gmbh, Berlin, Germany
Ethanol	Carl Roth, Karlsruhe, Germany
Random Primer-Hexamer	Sigma Aldrich, Taufkirchen, Germany
PCR dNTP-Mix	Roche, Mannheim, Germany
AMV-RT-Puffer 5x	Promega, Mannheim, Germany
RNase away	Carl Roth, Karlsruhe, Germany
Dexamethasone	Sigma Aldrich, Taufkirchen, Germany
β-Glycerophosphate	Sigma Aldrich, Taufkirchen, Germany
Ascorbic acid	Sigma Aldrich, Taufkirchen, Germany
Alizarin Red	Sigma Aldrich, Taufkirchen, Germany
Ammonia solution	Carl Roth, Karlsruhe, Germany
Penicillin	PAA, Coelbe, Germany
Streptomycin	PAA, Coelbe, Germany
MEM + GlutaMAX-I including HEPES buffer	Gibco, Carlsbad, CA, USA
MSC Growth Medium Bullet Kit	Lonza, Cologne, Germany

Tab. 4: Applied chemicals and other materials

8.5 Oligonucleotides (primers)

Custom primer design

For a variety of genes, no commercial primers were available. Therefore, custom primer sequences had to be designed and were ordered from Sigma Aldrich, Taufkirchen, Germany. Gene sequences for the corresponding genes were obtained from online databases e.g. NCBI (National Center for Biotechnology Information, U.S. National Library of Medicine). Primer sequences were designed using web tools like Primer3 and selected for best matching the primer sequence criteria. Sequences matching these criteria where

BLAST-checked (e.g. with NCBI) to ensure primer specificity.

Selected primers at an ideal product length of 100 bp where then ordered from Sigma Aldrich and optimized for realtime PCR (rtPCR).

Primers where then optimized (see 13.5 on page 56) and the product analyzed using agarose gel-electrophoresis (see (13.4)) for sufficient amount and specificity.

lncRNA H19 primer was designed with its target in exon 5 (of 5) of lncRNA H19. This was especially important to distinguish the lncRNA from its containing miRNAs 675-3p and 675-5p on exon 1.

18s housekeeping gene was used as a reference to normalize rtPCR results.

Random hexamer primer mix was used for reverse transcription (Roche, Rotkreuz, Switzerland).

Oligo Name		Sequence	Mg_2Cl [mM]	Ta [°C]	Gelelectrophoresis
XLOC_001719	for	TGAGACCAACAGACAGCCAAG			
	rev	TGAGCTATATCTGCACTGCC			
XLOC_009281	for	TTGGCTGCTGACACCTATGA			
	rev	GCAGTCAGGCAGGAGGGAG			
XLOC_010981_1	for	GCAAGTCCAAGTCCCACAG	3	58	
	rev	GGCACATTCCAAGGTTTCCA			
XLOC_010981_2	for	CCCCATCTTGTACCGTTCCT	3	54	
	rev	CCTCCCTCCTCATTTCCCCTC			
U52111.14	for	CAGACAAACCAACCCAGAGC			+
	rev	TGCCATATCCAAGGTCGTGA			
RP11-79H23.3	for	GGGACACAGGAGCCAAACAAT			+
	rev	GAGGGAGGGAAGGAAGGAAG			
NR_023924	for	AGGTCGCTCACTGGATTGTT			+
	rev	CCCACCTCTCTCCCTTTCAC			
RP11-298D21.1	for	TCCTGAATGAACTCCCGACC			
	rev	GGGATGGTTTTGTCACTGGG			
RP11-761I4.1	for	GGCTGATAGTCTCCACCGAA	3	57	+
	rev	TGATAAGAGGGCACACACTGT			
Xloc_012442	for	GAAGGGAAGTGACTTGGCAA	3.5	59	+
	rev	AGGCTCCTCTGCTTGGCAA			
Xloc_007047	for	TCAAAAGCGTGAAAGAGATCCT			+
	rev	TCAGAGGGACATAGCAAGTCT			
LINC00277	for	GAAGTGTCTGGCAAGGAACA			
	rev	AGGTGGAGAAGAGGGACAAT			
AC010136.2	for	GGGCGAGACACAGAAAGAAA			
	rev	AGGAGAATTGCTGAACCTGG			
AK310441	for	CAGACACTGTGGAGCAACAT	3.5	60	+
	rev	AGCAGACTGGACAGGAAGAT			
AK056982	for	GACTGAAATACACCCTGGTCTC	3	57	+
	rev	AGAGAGTTTGAGAGCAGACAAC			
H19	for	AAGCCTCCACGACTCTGTTT	3	57	+
	rev	CTCACACTCACGCACACTC			
18s	for	CGGCTACCACATCCAAGGAA			
	rev	GCTGGAATTACCGCGGCTGC			
β-Catenin	for	GAAAATCCAGCGTGGACAAT			
	rev	TGGTAAAGGCAATCCTGAGG			

Tab. 5: Oligonucleotide primers used for reverse transcription and real time PCR. All oligonucleotides were purchased from Sigma Aldrich, Taufkirchen, Germany and diluted with ddH_20 to a working concentration of 100pmol/µl. The table shows the oligo namea and the sequences of the forward (for) and reverse (rev) primers.

8.6 Equipment

Description	Source
LightCycler 1.5	RocheDiagnostics, Mannheim, Germany
GeneAmp PCR System 9700	PE Applied Biosystems
HERASafe KS	Thermo Scientific, Langenselbold, Germany
Toplightmicroscope Axiovert 25	Carl Zeiss, Germany
SunriseBasic	Tecan, Crailsheim, Germany
Binder Incubator *at 37°C with 5% CO2*	Binder, Tuttlingen, Germany
NanoDrop ND-1000	Peqlab Biotechnologie, Erlangen, Germany
LC Carousel Centrifuge 2.0	Roche Diagnostics, Mannheim, Germany
Vortex Genie 2	Bender & Hobein, Ulm, Germany
inoLab pH Level 1	Wissenschaftlich Technische Werkstätten, Weilheim, Germany
Water-bath *at 37°C*	GFL, Burgwedel, Germany
Multifuge 3 S-R	Kendro, Osterode, Germany
UVC 500 UV Crosslinker	Hoefer

Tab. 6: Equipment

8.7 Software

Description	Source
LightCycler Software Version 3.5	Roche Molecular Biochemicals, Mannheim, Germany
Magellan 5.0	Tecan, Crailsheim, Germany
NanoDrop 1000 V 3.8.1	Thermo Fisher SCIENTIFIC
RStudio 1.0.143	RStudio: Integrated Development for R, RStudio Team, RStudio, Inc., Boston, MA, USA
R: A Language and Environment for Statistical Computing 3.4.0 (2017-04-21) - "You Stupid Darkness"	R Foundation for Statistical Computing, R Core Team, Vienna, Austria
R-package: ggplot2	Original author: Hadley Wickham, Winston Chang, License GPLv2
R-package: gridExtra	Author: baptiste Auguie, License GPLv2
R-package: plyr	Author: Hadley Wickham, License MIT
R-package: tidyr	Author: Hadley Wickham, License MIT
LyX - The Document Processor 2.3.3 & 2.2.2	The LyX Team, http://www.lyx.org/

Tab. 7: Software

Part IV. Methods

9 Tissue sampling

All cells used for subsequent experiments were available from our research groups biobank and had been isolated according to the local protocol:

Primary human (ph) MSCs were isolated from spongiosa following joint replacement surgery. The tissue was collected and cut in approximately 2 cm^2 fragments and incubated in culture flasks with MEM + GLUTAMAX^{TM}-I, 20 % FCS, 100 U/ml penicillin, 10 µg/ml streptomycin and cultured at 37 °C, relative humidity of 95 % and with 5 % CO_2. Culture medium was changed every three days, non-adherent cells where removed by washing with PBS buffer. After reaching approximately 80 % confluence, cells were passaged or cryo-conserved for later use.

10 Cell culture

All tasks including living cells were performed in a class II safety cabinet. Cells were incubated at 37°C with 5 % CO_2 in a Binder incubator.

Primary human cells (RAOB, OAOB, phMSC) Primary human cells were cultured in standard cell culture medium (CCM) consisting of MEM + GLUTAMAX^{TM}-I with 10 % FCS, 10 U/ml penicillin and 10 µg/ml streptomycin.

Commercially obtained hMSCs Commercially obtained hMSCs where cultured in MSC GROWTH MEDIUM BULLET KIT which was recommended and provided by the manufacturer. The MSC GROWTH MEDIUM BULLET KIT contains MSC BASAL GROWTH MEDIUM, MSC GROWTH SUPPLEMENT, L-glutamine and GA-10000.

10.1 Unfreezing and seeding

Vials of cryo-conserved cells were briefly left to partly thaw in 37 °C water bath and immediately added to twice the volume of warm culture medium. The solution was cen-

trifuged for 10 minutes at 300 xg and the supernatant discarded. The pellet was subsequently dissolved in 2 ml culture medium and seeded into expansion format.

10.2 Expansion

Cells were expanded in an incubator at 37 °C with 5 % CO_2. Medium was exchanged twice a week. Depending on the expansion format, a residual amount of medium was left over to conserve growth factors. Cells were grown to 90 % confluence, then passaged or frozen according to the respective protocols.

10.3 Cell transfer and harvest

Medium was discarded and incubated for 10 minutes with an appropriate amount of 10% trypsin solution. Adequate detachment of the cells was verified under a top light microscope and an equal amount of culture medium was added (containing FCS to inactivate the trypsin). After a thorough rinse, the solution was pelleted by centrifuging for 10 minutes at 300 xg, then the supernatant was discarded by careful aspiration.

For cell transfer, the pellet was dissolved in 2 ml culture medium and seeded in the respective new format. After 24 hours, the medium was discarded and the culture washed with PBS buffer solution and fresh warm medium was added.

Cells were then used for cryo-conservation or preparation of cell lysates as described below.

10.4 Cell lysis

Cell lysis and subsequent RNA purification was conducted according to the RNEASY MINI KIT (Quiagen) instruction manual. The harvested medium free cell pellet (refer to 10.3) was dissolved in RLT buffer by carefully pipetting the solution for a few times. Dissolved cell lysates were immediately purified (see 13.1) or stored at -80 °C for later use.

Cryo-conservation For cryo conservation, cells were harvested as stated above. The pellet was dissolved in FCS + 10 % DMSO solution and immediately transferred to a cryo tube and slow-frozen in a freezing container in -80 °C freezer.

Contamination test Before cryo-conservation, every cell population was tested for mycoplasma infection via DAPI staining. Cells were cultured to 50 % confluence in 4-/8-well slides, washed with PBS, fixated with 100 % ethanol and air dried. DAPI (4',6-Diamindino-2-phenylindol) was diluted 1 µl with 5 ml MeOH. The slides were stained with the solution and stopped with excess PBS. After 1 day drying in the refrigerator, contamination microscopy test was conducted under the fluorescence microscope.

Cell count and density

Cell count was conducted in a Neubauer counting chamber. After detachment with trypsine, 10 µl of cell suspension was pipetted into the chamber, all four quadrants were counted individually and the average was used for calculation:

$$cells/ml = average\,cell\,count \times 10^4$$

Cell density was evaluated visually under a top light microscope.

11 Cell differentiation and stimulation

11.1 Osteogenic differentiation (OD)

For osteogenic differentiation, cells were expanded to 90 % confluence in CCM. To induce osteogenic differentiation, cells were transferred to a 6-well plate format and differentiation medium (DM) containing CCM, 0.1 µM dexamethasone, 10 mM β-glycerophosphate and 0.06 mM ascorbic acid was added for a total of 21 days. DM was changed every two days. At all sampling time points (2, 7, 14 and 21 days), supernatants were collected and cells harvested for RNA isolation according to the respective protocols. An additional

well per population was prepared for the mineralization array on day 21.

Adipokine stimulation during OD During the 21d osteogenic differentiation, cells were constantly stimulated with 0.1 µg/ml visfatin, 0.02 µg/ml resistin or 0.01 µg/ml leptin, respectively. Medium exchange, RNA and supernatant sample collection and mineralization assays were conducted according to the osteogenic differentiation protocol stated above.

TNFα stimulation during OD During osteogenic differentiation, cells were pulse-stimulated with 1 ng/ml TNFα, over the course of 21 day differentiation. The medium exchange to TNFα containing medium for an inflammatory pulse was performed 48 hours prior to sample collection. Sample collection and storage followed the established protocol as outlined above.

11.2 TNFα stimulation

For TNFα stimulation, cultures were expanded and transferred to 6-well plates. 24 hours after transfer, the cells were washed with PBS buffer solution and again cultured for 24h in growth medium. TNFα was added to medium at 5 ng/ml (or 10 ng/ml when specifically indicated) and incubated for 24h. The supernatant was immediately frozen for ELISA analysis, cells were lysed and the RNA extracted according to the respective protocol. Extracted RNA samples were used for lncRNA microarray analysis and for individual and pooled rtPCR as indicated in the respective experiments.

12 Pathway inhibitions

For pathway analysis, commercially obtained hMSCs were differentiated according to our established protocol. On day 7, specific pathway inhibitors were added and supernatant and RNA samples collected after 48 hours (day 9 of differentiation) and after 7 days of inhibition (day 14 of differentiation).

Inhibitors were dissolved in DMSO, a negative control containing DMSO was run alongside.

The inhibitors used are indicated below.

Wnt/β-Catenin pathway For Wnt/β-Catenin pathway analysis, the commercially available inhibitor of Porcupine (PORCN), WNT-C59 was used. WNT-C59 was dissolved in DMSO and added on day 7 of osteogenic differentiation at a concentration of 100 nM.

TGFβ1/Smad2 pathway To investigate TGFβ1/Smad2 signaling, we used LY2109761, a selective TGFβ receptor type I/II inhibitor. LY2109761 was dissolved in DMSO and added at a concentration of 5 µM on day 7 of osteogenic differentiation.

13 Expression analysis

RNA was extracted from cell lysates and reverse transcribed to cDNA for stabile storage. For semi-quantitative expression analysis, real-time PCR was conducted using the ABSOLUTE QPCR SYBR GREEN CAPILLARY MIX (= SYBR Green) system and a Roche LightCycler 1.5. All pipet work including RNA samples was performed using sterile pipet tips and a reserved set of pipets.

13.1 RNA purification

RNA was extracted from cell lysates (see 10.4) using the RNEASY^{TM} MINI KIT (Quiagen) according to the manufacturers instructions. TaqMan analysis were conducted by Prof. Dr. Dr. Ospelt at the collaborating Center for Experimental Rheumatology at the University of Zurich, Switzerland (13.8). The MIRNEASY^{TM} MINI KIT (Quiagen) was used according to the manufacturers protocol for compliance with the TaqMan protocol used and to preserve micro RNAs extracted from lysates.

With the RNEASY^{TM} MINI KIT, some optional steps contained in the protocol were performed and the full procedure used for RNA purifications is described here.

Cell lysates were thawed or used directly after harvest from the culture flasks. 70% ethanol was added in an equal amount as the buffer RLT. The homogenized solution was transferred to RNeasy spin columns, binding RNA to the column membrane. The membrane was washed with the RW1 buffer and DNase I in buffer RDD and incubated for 15 minutes for DNase digestion to remove DNA contamination of the specimen using the RNASE-FREE DNASE SET (Quiagen).

DNase was washed off with the RW1 buffer and twice with the RPE buffer. Leftover buffer was eliminated by an extra centrifuging step. Purified RNA was then eluted off the membrane with RNase free H_2O.

Successful extraction was verified by the NanoDrop ND-1000 OD260/280 ratio. Purified RNA samples were immediately transcribed to cDNA or stored at -80 °C.

13.2 Reverse transcription

For reverse transcription of isolated RNA to cDNA for later rtPCR analysis, RNA with RNAsin and ddH_2O was mixed, denatured and chilled on ice. The remaining reagents were added (see 8), centrifuged and placed in a GENEAMP PCR SYSTEM 9700. The reaction was incubated for the intervals and temperature settings given in 9.

	[µl] / 50 µl
RNA	*100-1000 ng*
ddH_2O	ad 50 µl
RNAsin	1
add after chilling:	
AMV-RT-Puffer 5x	10
PCR dNTP-mix	5
Random hexamer primer	1
AMV-Rev transkriptase	2

Tab. 8: Reverse transcription reaction: RNA solution and RT master mix for reverse transcription. The RNA sample was filled ad 31 µl with ddH_2O and 1 µl of RNase was added. The reaction was then denatured at 70 °C for two minutes and immediately placed on ice to chill for 5 minutes. The remaining reagents were mixed and 18 µl added to each reaction.

Transcribed cDNA was stored at -20 °C until further use.

70°C	2 min
ice water	5 min
25°C	10 min
37°C	30 min
42°C	30 min
70°C	10 min

Tab. 9: Reverse transcription temperature profile.

13.3 Real-time PCR

Real-time PCR (reverse transcription-polymerase chain reaction, rtPCR) is the most sensitive method for quantifying different types of nucleic acids. We used a Roche LightCycler capillary system with THERMOFISHER SYBR GREEN as a detection system. SYBR Green reagent binds to double-stranded DNA, which accumulates over the course of repeated PCR. The SYBR Green-DNA-complex absorbs yellow light at 494 nm and emits green light at 521 nm. An increase in PCR product can be detected by the increasing fluorescence of the reaction.

A standardized program for rtPCR was used, consisting of a denaturation stage where double-stranded cDNA is split into single strands, a cycle of repeated polymerization steps and a final melting curve step. In the last stage, the temperature is continuously increased up to 100°C. This slowly decreases the fluorescence level detected as the double-stranded PCR products denatured. At the point of the products specific melting point, the detected fluorescence drops as the one desired product melts and breaks the SYBR Green-DNA-complex.

	Temperature	Duration	Repetition
Initial denaturation	94°C	10 min	1x
Denaturation	95°C	10s	35-55x
Annealing	Ta	25s	
Elongation	72°C	30s	
Melting curve analysis	50°C → 99°C	0.1°C/s	1x

Tab. 10: rtPCR standard amplification program used for all rtPCR analysis. Ta: individual annealing temperature, retrieved by primer optimization 13.5 on the next page.

The SYBR Green system is based on the binding of the detection reagent to any sort of double-stranded DNA but is not specific to the desired product. It therefore also binds

to primer-primer-dimers or side products of the reaction. Therefore, the efficiency of the PCR reaction had to be optimizeed to only create very distinctive peaks in the melting curve analysis (see 13.5).

rtPCR Reaction A primer mix was diluted from stock solutions of forward and reverse primers with a final concentration of 10 µM. For each reaction, a master mix of SYBR Green, primer mix, MgCl-solution and PCR-grade RNase free ddH2O was prepared. To each reaction capillary the cDNA template was added , sealed and centrifuged. For rtPCR a Roche LightCycler 1.5 was used.

SYBR Green Mix	(contains 25 mM MgCl)	10 µl
Primer Mix	10 µM	1 µl
MgCl	25 mM	*add to adjust c[MgCl]*
cDNA template		*standard: 2µl*
ddH_2O (RNase free)		ad 20 µl

Tab. 11: rtPCR reaction mix

13.4 Agarose gel electrophoresis

Gel electrophoresis was used to verify rtPCR product lengths and amounts. Samples were extracted from Light Cycler capillaries either directly after rtPCR or stored at -20 °C before analysis.

A 1.5 % agarose gel in in TAE buffer (1x) was prepared. Samples were diluted with bromphenolblue loading buffer, TAE (1x) served as running buffer and the chamber was set to 70-100 V. DNA marker ladder with a range from 1000 bp to 100 bp served as standard. After a sufficient runtime, the gel was stained in ethidium bromide solution for a minimum of 15 minutes.

Results were detected in a UV trans-luminator and photographed for documentation.

13.5 Primer optimization

For rtPCR, the optimal annealing temperature (T_2) and $MgCl_2$-concentration for each primer had to be determined. Therefore, different master mixes (containing different

concentrations of $MgCl_2$) against serial dilutions of cDNA templates were evaluated. The amount of ddH_2O was adjusted to make a total volume of 20 µl per reaction capillary. For optimization, pooled RA and OA osteoblast cDNA samples were used.

		$MgCl_2$			
serial dilution	template dilution	3mM	3.5mM	4mM	mock-concentration
1:2	1:2				9000
1:3	1:6				3000
1:3	1:18				1000
1:3	1:54				333

Tab. 12: Example of rtPCR primer optimization protocol. 'Serial dilution' shows the relative dilution of each template sample, 'template dilution' is the absolute dilution. To generate a standard curve in the LightCycler Software, an arbitrary concentration value is given according to the serial dilution.

To find the most efficient annealing temperature (Ta), the first optimization was run at a temperature ~ 5° below the lowest of the two primers (forward and reverse) melting temperature as stated by the manufacturer.

Each step of the optimization was evaluated by examining the 'efficiency' of the current setting and the resulting melting curves.

Efficiency was calculated from the slope of the linear regression of the Log(concentration) (x-Axis) the cycle number (y-Axis). The slope is calculated within the LightCycler Software, the efficiency is $efficiency = 10^{-(1/slope)}$ with an optimum of $2 \pm 0,1$.

The melting curves were examined for having a unique, specific peak.

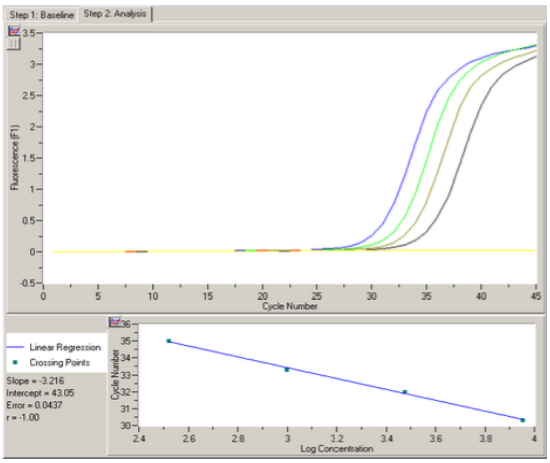

(a) Top: Fluorescence values over the course of 45 rtPCR cycles. Bottom: Efficiency curve showing the cycle number at which the cycle threshold (ct, 13.6) is reached over the log transformed 'mock' concentrations given. Slope, intercept, error and r are calculated by the software.

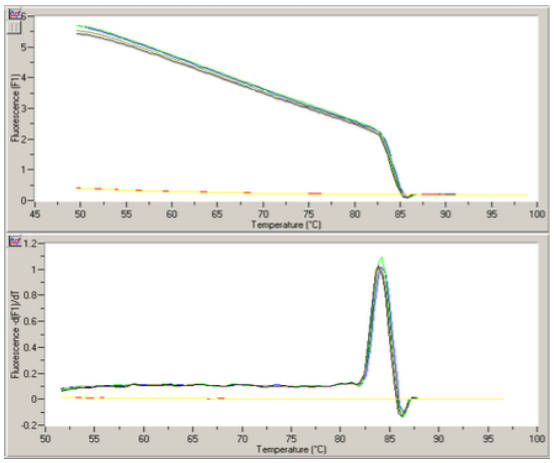

(b) Melting curve shown as absolute fluorescence (top) and as slope/derivative (bottom) over the temperature profile (50 to 100°C).

Fig. 8: Output of the LightCycler Software showing an example of the successful optimization of oleonucleotide primer XLOC_10981-2. This optimization was run at 54 °C with 3mM $MgCl_2$. The given slope was -3.216, the efficiency 2.046. The melting curve shows a specific peak around 84 °C. The yellow line ist the negative control, containing only Master mix and no cDNA template.

13.6 Real-time PCR data analysis

For semi-quantitiative RNA measurements via rtPCR, the comparative threshold method was used. It compares the ct (cycle threshold)-values of the sample of interest to a non-regulated housekeeping gene. The ct value is defined as the cycle number at chich the detected fluorescence crosses a defined threshold which is significantly above the background fluorescence. It therefore provides a relative measure of the concentration of the PCR product of interest. The ct value of 18s RNA of the small homo sapiens sub-unit of the eukaryotic ribosome was used as a non-regulated housekeeping gene to normalize ct values.

$$dct = ct(product\,of\,interest) - ct(18s) \tag{1}$$

This dct (delta-ct) value was then adjusted to the amount of RNA initially used for the PCR and can be compared amongst different populations of origin. To express differential expression of a gene for example over the course of a differentiation or compared to a

negative control and a stimulated sample, the dct values of the product of interest can be compared to a control dct value.

$$ddct = dct(product) - dct(control) \tag{2}$$

This gives a ddct (delta-delta-ct) value which is a measure for the regulation of a product, adjusted to the amount of RNA used and in relation to a chosen control.

For $ddct \leq 0$:

$$RF = 2^{-ddct} \tag{3}$$

For $ddct > 0$:

$$RF = -(2^{ddct}) \tag{4}$$

The regulatory factor (RF) was then calculated based on the ddct value (formula 3 and 4) . Base 2 results from the intended efficiency reached in the primer optimization 13.5 on page 56.

For down-regulated products (where ddct is higher than 0 hence the product crossed the cycle threshold *after* the control) the negative reciprocal value is used (4) . The reference product will result in an RF of 1, as ddct is 0 (equal subtrahend and minuend in (2)).

13.7 lncRNA Microarray

For a lncRNA micro array analysis, RNA from two RA and three OA osteoblast populations, stimulated with 5 ng/ml TNFα and unstimulated controls was isolated according to the above mentioned protocol. Samples were pooled (OA+TNF; OA control; RA+TNF; RA control) and sent to a commercial laboratory for analysis.

The initial attempt to ship the samples at ambient temperature using the RNAstable kit led to degraded samples when reaching the company's laboratory. Therefore, samples were once more sent on dry ice after isolation resulting in a sufficient amount of sample in a appropriate quality (measured by NanoDrop OD260/280 ratio and agarose gel electrophoresis) for analysis.

The array ("Arraystar Human LcnRNA Microarray V3.0") and data analysis were performed by Arraystar Inc., testing for differential expression of 30.586 human lncRNAs and 26.109 coding transcripts:

cDNA was synthesised using SUPERSCRIPT II RT kit to transcribe 1 µg of RNA per sample to cDNA.

Sample labelling and array hybridization were performed according to the companies modification of the AGILENT ONE-COLOR MICROARRAY-BASED GENE EXPRESSION ANALYSIS protocol (Agilent Technology). mRNA was purified (MRNA-ONLY™ EUKARYOTIC MRNA ISOLATION KIT, Epicentre), amplified and transcribed into fluorescent cRNA (ARRAYSTAR FLASH RNA LABELING KIT, Arraystar). The labeled cRNA was then fragmented and dispensed into microarray slides. After 17 hours at 65°C in an Agilent Hybridization Oven, the slides were washed, fixed and scanned using the Agilent DNA Microarray Scanner (part number G2505C).

The raw array data was analyzed with the Agilent Feature Extraction software (version 11.0.1.1). Quantile normalization and subsequent data processing were performed with using the GeneSpring GX v12.0 software package (Agilent Technologies). Resulting data sets were then provided for analysis in an Excel spreadsheet format.

Primer selection Based on the array results we selected a total of 16 sequences to further analyze. Primers were ordered from SIGMA-ALDRICH. See list of primers on page 47.

13.8 micro-RNA analysis

Measurements of micro-RNA expression were performed by Prof. Dr. Dr. med. Caroline Ospelt at the Center of Experimental Rheumatology, Department of Rheumatology, University Hospital of Zurich, according to local protocol:

150 ng of RNA was reversed transcribed using the High-Capacity cDNA Reverse Transcription Kit with specific primers for miR-675-5p, miR-675-3p, RNU44 and snU6. Quantitative real-time PCR was performed using TaqMan™ Universal Master Mix II

without uracil-N-glycoslyase and TaqMan™ primers for miR-675-5p, miR-675-3p, RNU44 and snU6 (all Thermo Fisher). Data were analysed with the semi-quantitative ddCT method using RNU44 or snU6, respectively as housekeeping genes.

14 Matrix mineralization assay

To quantify osteogenic differentiation and increased matrix mineralization by osteoblasts, the matrix mineralization was evaluated at day 21 of osteogenic differentiation. Alizarin Red S staining to specifically stain calcium deposits as a marker for successful in-vitro bone formation was used. The matrix mineralization assessment was performed according to the PROMOCELL *Detection of Calcium Deposits (Mineralization)* protocol.

During osteogenic differentiation, a well was used for matrix mineralization assessment. After 21 days of differentiation, cells were washed with PBS and fixed twice with 10 % formalin for 10 minutes at room temperature. A 2 % Alizarin Red S (Sigma) solution in ddH_2O was adjusted to a pH of $4,2 \pm 0,1$ with HCl and filtered. The cells were then stained with the staining solution for 45 minutes. Wells where then washed with PBS to remove excess dye and immediately photographed for documentation.

For quantitative analysis, Alizarin Red stained wells were incubated with 10% ascorbic acid (Sigma) for 30 minutes and scraped off. The material was then incubated for 10 minutes at 85 °C, cooled for 5 minutes on ice and centrifuged. 20 µl of 10 % ammonia solution was added to 80 µl of supernatant. We then determined the optical density with the NanoDrop at 492 and 515 nm wave length.

15 Enzyme-linked immunosorbent assay (ELISA)

ELISAs were performed using the corresponding QUANTIKINE® ELISA IMMUNOASSAY (R&D Systems) according to the respective protocol. Samples where then evaluated in the supplied 96 well plates with a SUNRISEBASIC ELISA Reader (Tecan, Austria) using the Magellan 5 Software.

IL-6 Supernatants from TNFα-stimulated cell cultures at different time points of osteogenic differentiation were analyzed with the Human IL-6 QUANTIKINE ELISA KIT according to the manufacturers protocol.

TGFβ1 Supernatants sampled from hMSCs at different time points over the course of osteogenic differentiation were analyzed with the Human TGFβ1 QUANTIKINE ELISA KIT according to the manufacturers protocol.

16 Statistical analysis

The statistical analysis of the data was created with Microsoft Excel and R-Studio. The programming language R and the packages listed in table 7 are open source software. For analysis of rtPCR data, a set of R-scripts was used according to 13.6 on page 58. The graphical representations were created using the packages 'gglot2' and 'gridExtra'. For statistical hypothesis testing, Student's T-test was performed. To represent the values, arithmetic averages were calculated from the biological replicates. Statistical significance was defined as a p-value < 0.05.

Part V. Results

17 IL-6 response of osteoblasts to TNFα stimulation

IL-6 secretion of osteoblasts was evaluated by ELISA assay of culture supernatants. RA and OA osteoblasts were stimulated with 0 ng/ml, 5 ng/ml or 10 ng/ml of TNFα over 24 hours (concentrations chosen within its biological activity range of 0.05–20ng/ml). The results are shown in detail in figure 9. This confirmed a stable IL-6 response to pro-inflammatory stimuli, that was significant in both lower (5 ng/ml) and higher (10 ng/ml) TNFα concentrations in all RA and OA groups. Notably, in all settings, the OA response was lower than that of RA osteoblasts and significantly lower in the 5 ng/ml stimulation.

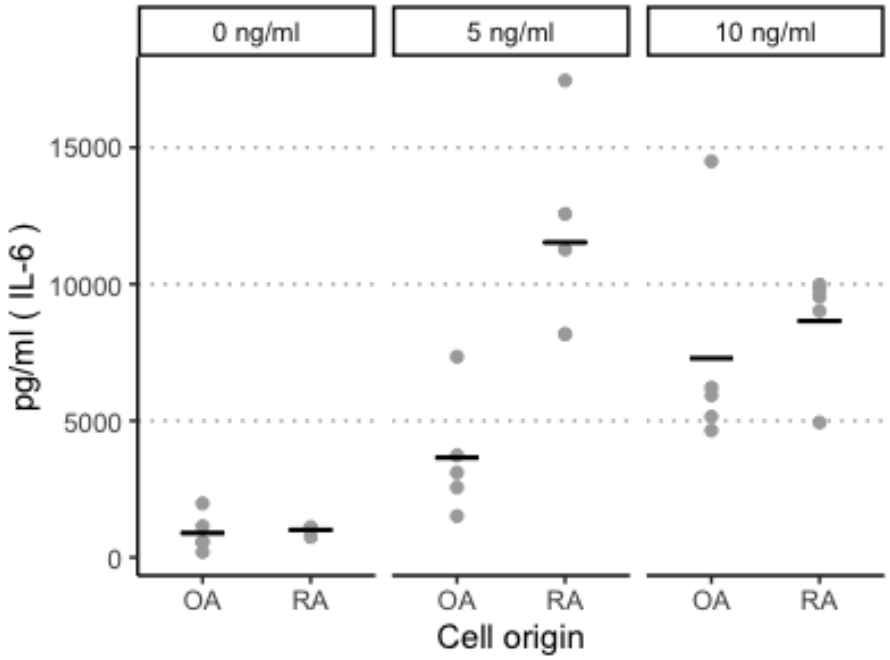

Fig. 9: IL-6 concentrations as measured with ELISA assay in supernatants form osteoarthritis (OA, n = 5) and rheumatoid arthritis (RA, n = 5) osteoblasts after 24 hour stimulation with 0 ng/ml, 5 ng/ml or 10 ng/ml of TNFα. Black lines indicate group means. 0 ng/ml: OA (mean = 891.3 pg/ml), RA (mean = 1004.42 pg/ml). 5 ng/ml: significant up-regulation of IL-6 compared to 0 ng/ml in OA (mean = 3650 pg/ml, p = 0.047) and RA (mean = 11.536.52 pg/ml, p = 0.0035). At 5 ng/ml, the IL-6 response was significantly higher (p = 0.006) in RA than in OA groups. 10 ng/ml: significant increase in IL-6 concentration compared to 0 ng/ml in both OA (mean = 7286.2 pg/ml, p = 0.02) and RA (mean = 8651.40 pg/ml, p = 0.0012).

18 osteoblast lncRNA-response to TNFα microarray

A microarray (ARRAYSTAR HUMAN LCNRNA MICROARRAY V3.0) capable of detecting 30.586 human lncRNAs and 26.109 coding transcripts was conducted by ARRAYSTAR INC. (Rockville, Maryland, USA).

Samples for the micro array were pooled OA and RA osteoblasts stimulated over 24 hours with/without 5 ng/ml TNFα. The microarray produced fluorescence data of labeled cRNA which was normalized to internal controls. The results are visualized in figure 10 and summarized in table 13. Table 14 lists the top 10 results of normalized results for each group evaluated.

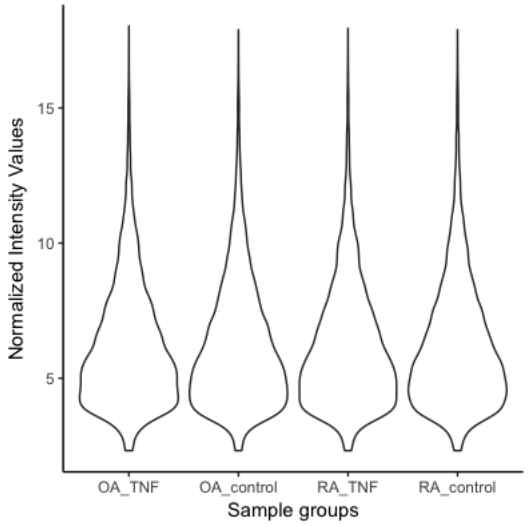

(a) Violin plot of normalized intensity values by cell population (OA or RA) and stimulation (+/- TNFα). The y-axis shows intensity values, width of the plot shows the distribution of values in each group. These data are summarized in table 13.

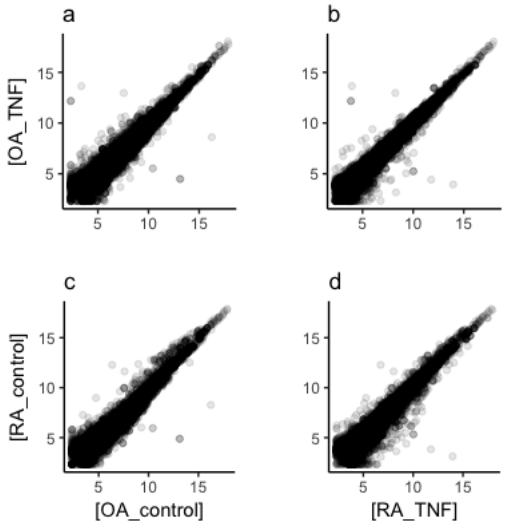

(b) Jitter plots comparing each setting to another. a) OA+TNFα vs. unstimulated controls b) OA+TNFα vs. RA+TNFα c) RA control vs. OA control d) RA control vs. RA+TNFα.

Fig. 10: Overview of the normalized microarray results.

Group		Minimum	Maximum	Mean	SD
OA	TNF	2.323644	18.03198	6.183497	2.278895
	control	2.323346	17.88997	6.205557	2.318289
RA	TNF	2.322518	17.94249	6.166033	2.282252
	control	2.322155	17.88997	6.196758	2.316753

Tab. 13: Descriptive data summary of normalized microarray results. The table shows minima, maxima, mean and standard deviation (SD) grouped by cell population (OA or RA) and stimulation (+/- TNFα). Each group contains 17.111 probes targeting 11.853 genes. The data is visualized in figure 10.

GeneSymbol	***OA control**	OA TNF	RA control	RA TNF
RP1-179N16.6	17.889969	17.731407	17.889969	17.850927
FTH1P10	17.850927	18.031982	17.753511	17.942493
XLOC_003181	17.608744	17.536535	17.669008	17.575808
cytochrome b	17.536535	17.422373	17.536535	17.608744
ACTG1	17.101553	17.00613	17.101553	16.992863
X07060	16.978752	17.608744	16.978752	17.459093
XLOC_011515	16.941153	16.917873	16.695526	16.775791
RP11-752G15.9	16.901634	16.679552	16.809017	16.746607
RPL6P27	16.672459	16.561302	16.657093	16.618486
RPL31P11	16.595253	16.56686	16.607937	16.633814

GeneSymbol	OA control	***OA TNF**	RA control	RA TNF
FTH1P10	17.850927	18.031982	17.753511	17.942493
RP1-179N16.6	17.889969	17.731407	17.889969	17.850927
X07060	16.978752	17.608744	16.978752	17.459093
XLOC_003181	17.608744	17.536535	17.669008	17.575808
cytochrome b	17.536535	17.422373	17.536535	17.608744
ACTG1	17.101553	17.00613	17.101553	16.992863
XLOC_011515	16.941153	16.917873	16.695526	16.775791
XLOC_002730	16.5798	16.765703	16.388454	16.457977
RP11-752G15.9	16.901634	16.679552	16.809017	16.746607
XLOC_003849	16.553726	16.618486	16.86767	16.595253

GeneSymbol	OA control	OA TNF	***RA control**	RA TNF
RP1-179N16.6	17.889969	17.731407	17.889969	17.850927
FTH1P10	17.850927	18.031982	17.753511	17.942493
XLOC_003181	17.608744	17.536535	17.669008	17.575808
cytochrome b	17.536535	17.422373	17.536535	17.608744
ACTG1	17.101553	17.00613	17.101553	16.992863
X07060	16.978752	17.608744	16.978752	17.459093
XLOC_003849	16.553726	16.618486	16.86767	16.595253
RP11-752G15.9	16.901634	16.679552	16.809017	16.746607
XLOC_011515	16.941153	16.917873	16.695526	16.775791
RPL6P27	16.672459	16.561302	16.657093	16.618486

GeneSymbol	OA control	OA TNF	RA control	***RA TNF**
FTH1P10	17.850927	18.031982	17.753511	17.942493
RP1-179N16.6	17.889969	17.731407	17.889969	17.850927
cytochrome b	17.536535	17.422373	17.536535	17.608744
XLOC_003181	17.608744	17.536535	17.669008	17.575808
X07060	16.978752	17.608744	16.978752	17.459093
ACTG1	17.101553	17.00613	17.101553	16.992863
XLOC_011515	16.941153	16.917873	16.695526	16.775791
RP11-752G15.9	16.901634	16.679552	16.809017	16.746607
RP11-159F24.2	16.515974	16.542208	16.5798	16.695526
RPL31P11	16.595253	16.56686	16.607937	16.633814

Tab. 14: Top 10 microarray results by sample groups (RA cpntrol, RA+TNFα, OA control and OA+TNFα). * indicates the group sorted by.

From the normalized intensity values, a regulation factor (Log(fold-change)) was calculated for 4 group comparisons: RA+TNFα vs. RActr, OA+TNFα vs. OActr, OActr vs. RActr and OA+TNFα vs. RA+TNFα. By our requirements, a threshold of 2-fold regulation (up or down) in 2 or more comparisons was set. After application of this threshold, 3.389 target sequences corresponding to 2.989 genes were chosen for further analysis. Box plots for all results are shown in figure 11 and the selected primers are highlighted in figure 12.

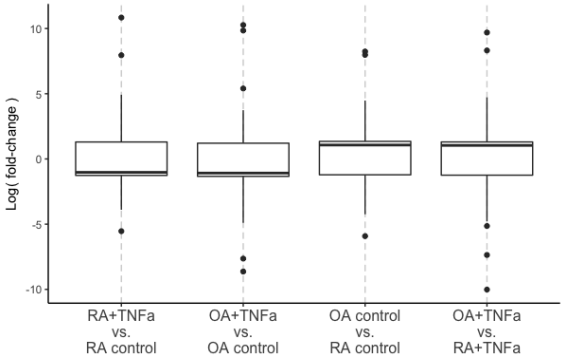

Fig. 11: Box plots with outliers of lncRNA microarray regulation results. Boxes extend from the lower to the upper quartile, the black band illustrates the 50% quartile (median). Whiskers (black vertical lines) extend to the lowest data point within 1.5 interquartile range (IQR). Outliers are shown as points and detailed in table 15.

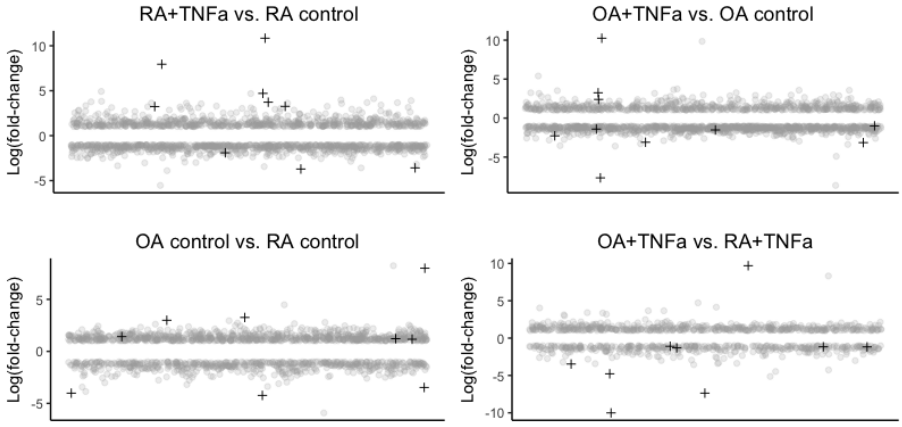

Fig. 12: Jitter plot showing the results of the lncRNA microarray comparing 2989 genes (3389 probes) in OA and RA stimulated with TNF and unstimulated controls. All results are shown in grey points. lncRNAs that were selected for further investigation are shown as black '+' in this plot and individually in figure 13 on page 69 and 14 on page 69. Top left: In the RA samples, 719 targets were found up-regulated, 833 were down-regulated upon stimulation. Top right: In OA, 623 were up-regulated, 948 down-regulated upon stimulation. Bottom left: In unstimulated OA samples, 826 targets were up-regulated and 587 down-regulated as compared to unstimulated RA samples. Bottom right: In the stimulated OA samples, 499 targets were up-regulated and 412 down-regulated, in comparison to stimulated RA samples.

GeneSymbol	RA+TNFa vs. RA ctr	OA+TNFa vs. OA ctr	OA ctr vs. RA ctr	OA+TNFa vs. RA+TNFa
AC002472.8		-4.896577	4.4783325	
AK054972		9.8489116		8.318675
AK056982			-4.2409265	
AK127889				-5.1421683
*AK310441		-7.639495	7.980515	
BC019880		5.4039482		4.720916
BX571672.3	4.9208023			
C17orf76-AS1	-5.5372286		-5.917614	
GBP1P1		3.7401085		
PCYT1B-AS1	-3.8949417			
RP11-467L20.10		-8.6315427	8.2373934	
*U52111.14				-4.7775211
*XLOC_001719	10.8417153			-10.0155742
*XLOC_009281	7.9535425			-7.36211
*XLOC_010981		10.2706965		9.6934193

Tab. 15: Outliers and last value within interquartile range in lncRNA microarray regulation data (corresponding to points and whisker ends in figure 11. '*' mark lncRNAs chosen for further investigation. Positive values indicate up-regulation, negative values indicate down-regulation in the respective comparison.

GeneSymbol	RA+TNFα vs. RA ctr	OA+TNFα	OA ctr vs. RA ctr	OA+TNFα vs. RA+TNFα
AC010136.2		-3.0721171	1.3996555	-1.1748206
AK056982	-3.7021563		-4.2409265	
AK310441		-7.639495	7.980515	
DHRS4-AS1		-3.1437764	3.270884	
H19		-1.415296	1.1667805	
LINC00277	-3.590718		-4.03057	-1.310842
RP11-298D21.1	-1.9072676		-3.4637649	-1.1627627
RP11-761I4.1		-2.2778133	2.974801	
RP11-79H23.3	3.716569	3.2525982		-1.097932
U52111.14	4.7022725	-1.0177326		-4.7775211
XLOC_001719	10.8417153		1.2300839	-10.0155742
XLOC_007047	3.2653085			-3.4681988
XLOC_009281	7.9535425			-7.36211
XLOC_010981		10.2706965		9.6934193
XLOC_012442	3.2366157	2.4126451		

Tab. 16: Microarray regulation data for the selected lncRNAs as log(fold-change) in the four comparison groups (RA+TNFα vs. RA ctr, OA+TNFα, OA ctr vs. RA ctr and OA+TNFα vs. RA+TNFα). For the microarray analysis, pooled samples were used and hence no statistical analysis could be calculated.

In the RA samples, 719 targets were found up-regulated, 833 were down-regulated upon stimulation. In OA, 623 were up-regulated, 948 down-regulated. In unstimulated OA samples, 826 targets were up-regulated and 587 down-regulated when compared to RA samples. In the stimulated OA samples, 499 targets were up-regulated and 412 down-regulated, in comparison to stimulated RA samples.

From literature research and the microarray results, 15 lncRNAs were selected for further examination (marked '+' in figure 12). Namely these were "XLOC_012442", "RP11-761I4.1", "U52111.14", "XLOC_007047", "RP11-79H23.3", "AC010136.2", "NR_023924", "AK056982", "AK310441", "XLOC_001719", "XLOC_009281", "H19", "LINC00277", "RP11-298D21.1", and "XLOC_010981" (microarray results are shown in detail in figure 13 and 14 on the following page). Corresponding primers were ordered from Sigma Aldrich. After PCR, successful cDNA replication was tested by agarose gel-electrophoresis. Nine of the selected primeres produced a specific product in gel-electrophoresis. Out of these, seven proved efficient and specific in rtPCR optimization. See corresponding table 5 on page 47.

Subsequently, the results of the microarray analysis were validated by real-time PCR analysis using samples from individual osteoblast populations.

As measured by rtPCR, lncRNA expression differed greatly between the individual osteoblast populations regardless of OA or RA patient background. The expression obtained by rtPCR on individual saples were also in-concordant with the microarray findings (shown in figure 15 on the following page).

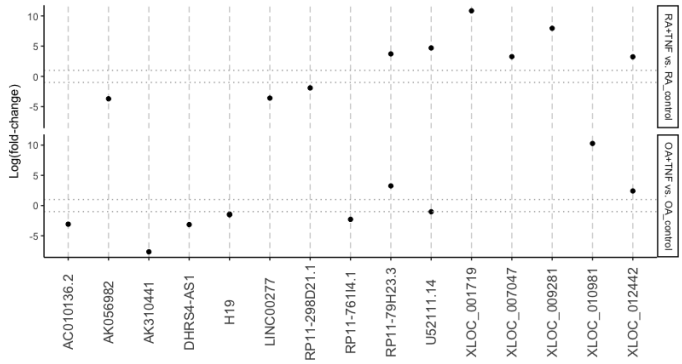

Fig. 13: Microarray regulation data for the 15 selected lncRNAs. Top row shows log-values of lncRNA fold-changes in RA samples with and without TNFα stimulation (RA+TNFα vs. RA control). Bottom row showes data from OA samples with and without TNFα stimulation (OA+TNFα vs. OA control).

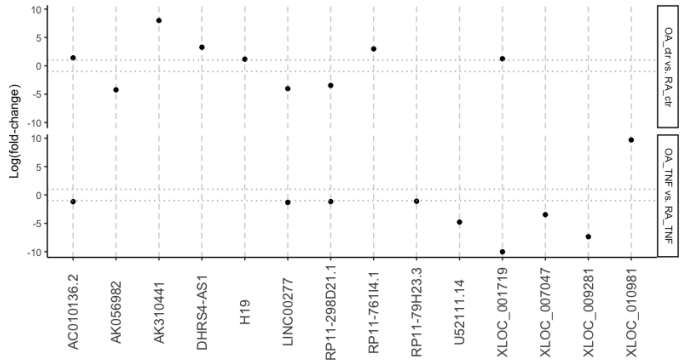

Fig. 14: Microarray regulation data for the selected lncRNAs ("XLOC_012443" not shown as it is not regulated in either of these categories). Top row shows log-values of lncRNA fold-changes of OA controls as compared to RA controls (OA control vs. RA control). Bottom row showes data from TNFα-stimulated OA samples compared to stimulated RA samples (OA+TNFα vs. RA+TNF).

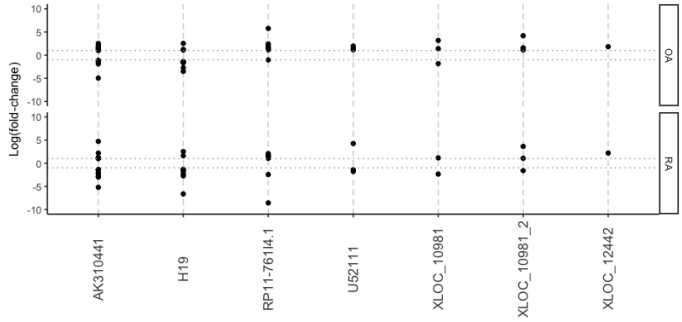

Fig. 15: rtPCR data validation of microarray results for 7 lncRNAs AK310441 (OA: n = 9, RA: n = 8), H19 (OA n = 9, RA n = 8), RP11-761I4.1 (n = 8), U52111 (n = 3), XLOC_010981 (n = 3), XLOC_10981_2 (n = 3), XLOC_12442 (OA n = 3, RA n = 4). The data shows the differential regulation of the respective lncRNA after TNFα stimulation compared to unstimulated controls in OA or RA osteoblasts.

19 Regulatory effects of visfatin on lncRNA H19

To evaluate the regulation of lncRNA H19 during osteogenesis over time, primary human hip MSCs were co-stimulated with either leptin, resistin, visfatin over the course of 21 days. OD with no stimulus served as control. As expected and previously reported by other groups, H19 was found up-regulated over the course of osteogenic differentiation in the control setting compared to day 2 of OD (value set to 1 for each setting). Samples stimulated with both resistin and leptin showed a similar up-regulation of the lncRNA.

Unexpectedly, H19 was down-regulated in the samples treated with visfatin. Results are shown in figure 16.

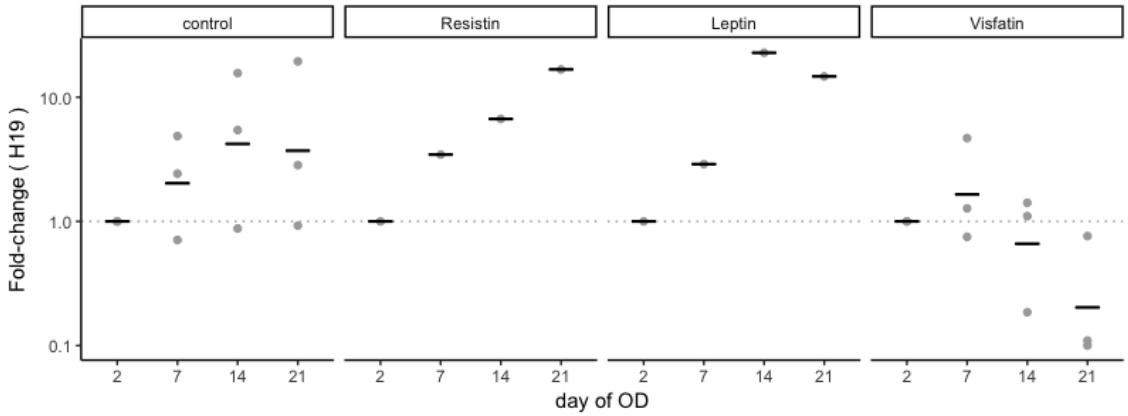

Fig. 16: lncRNA H19 regulation in hip-phMSCs over the course of OD. Values were calculated as fold changes compared to the values of day 2 (set to 1). Co-stimulation with resistin (n = 1), leptin (n = 1) or no stimulus (n = 3) showed a continuous up-regulation over the course of differentiation. Visfatin co-stimulated samples (n = 3) were differentially regulated and showed a steady decrease of H19 expression over the course of OD up to 10-fold down-regulation on day 21.

Experimental Condition	day 7		day 14		day 21	
	mean	mean(log)	mean	mean(log)	mean	mean(log)
Control (n = 3)	2.667	0.708*	7.326	1.438*	7.734	1.311*
Resistin (n = 1)	3.451	1.239	6.688	1.900	16.743	2.818
Leptin (n = 1)	2.892	1.062	22.801	3.127	14.703	2.688
Visfatin (n = 3)	2.237	0.500*	0.900	-0.414*	0.324	-1.594*
		*p = 0.8038		*p = 0.1599		*p = 0.0637

Tab. 17: Group means of lncRNA H19 regulation data in hip-phMSCs as mean and mean of the log transformed values per day of OD. p-values are shown comparing log transformed data of control and visfatin groups (*).

19.1 Visfatin mediated differential regulation of H19 over the course of OD

To confirm the effects of visfatin on H19 regulation during differentiation, the experiment was repeated using primary human MSCs of another origin (knee instead of hip) compared to commercially obtained hMSCs from healthy donors. In these experiments the observed H19-inducing effect of OD in knee phMSC was weaker and absent in hMSC from healthy donors (Figure 17). Yet, H19 expression was lower in the visfatin treated co-stimulated samples compared to the control setting in all sample groups confirming the H19-down-regulating effect of visfatin during OD.

Expression data for day 21 were not measured due to low RNA harvest from the highly mineralized matrix in the phMSC knee group.

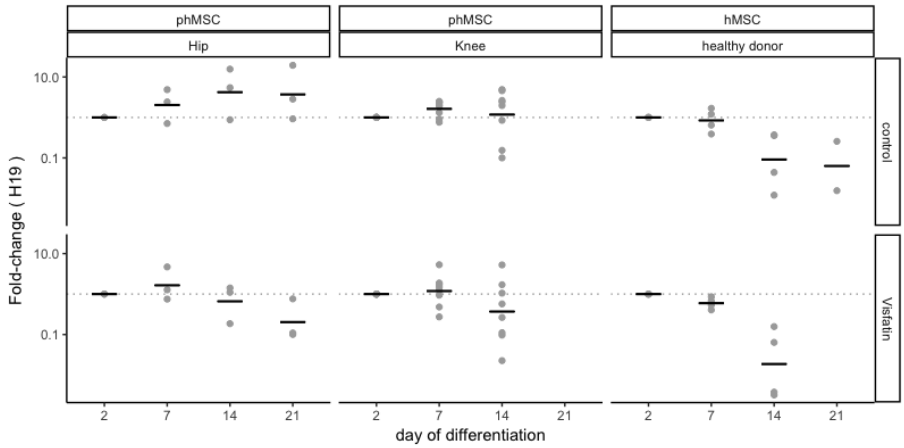

Fig. 17: lncRNA H19 regulation over the course of OD in different MSCs as compared to day 2 (set to 1, grey line). Hip-phMSCs (n = 3) showed a continuous up-regulation in the unstimulated control setting and a down-regulation when stimulated with visfatin. In knee-phMSCs (n = 8) and hMSCs (n = 4), lncRNA H19 was down-regulated in the visfatin stimulated samples and in the control setting for hMSC from healthy donors.

Cell origin :	Knee (n = 8)				healthy donor (n = 4)			
Experimental condition	day 7		day 14		day 7		day 14	
	mean	mean(log)	mean	mean(log)	mean	mean(log)	mean	mean(log)
control	1.77	0.488	2.2	0.163	0.981	-0.168	0.196	-2.393
Visfatin	1.669	0.172	1.135	-0.996	0.619	-0.518	0.057	-3.98
		p = 0.3965		p = 0.1789		p = 0.1789		p = 0.2678

Tab. 18: Group means of lncRNA H19 regulation data in knee-phMSCs and hMSC as mean and mean of the log transformed values per day of OD. p-values are given for log transformed values comparing controls and visfatin stimulated groups.

19.2 Comparison H19 in adipogenic vs osteogenic differentiation

H19 levels were also evaluated in hip phMSC samples during adipogenic differentiation as shown in figure 18. Like in OD, H19 was up-regulated over the course of 'control' adipogenic differentiation. In contrast, the down-regulation of H19 observed in the OD samples was not visible in AD samples.

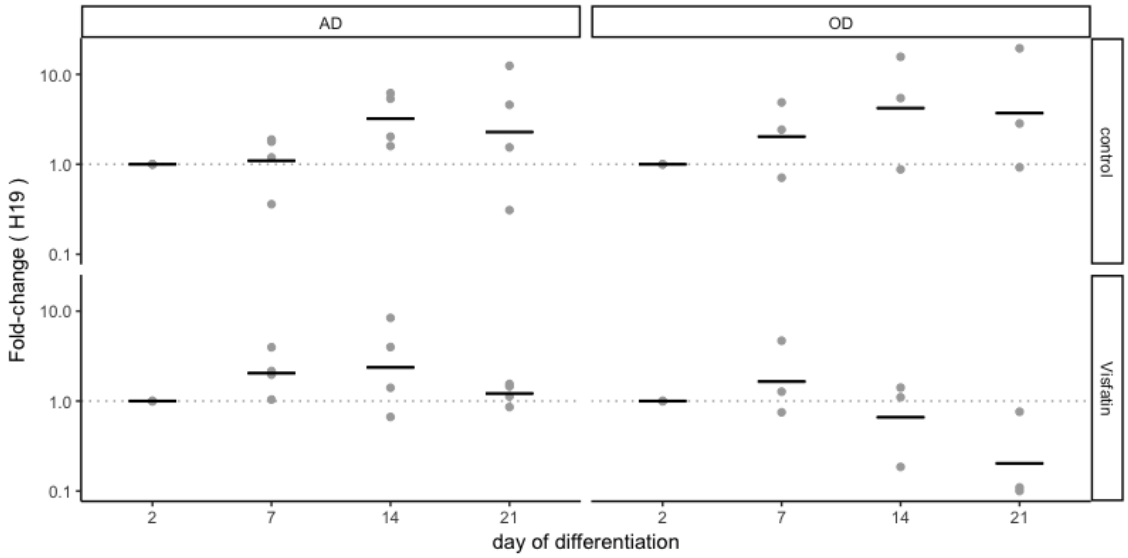

Fig. 18: LncRNA H19 levels over the course of adipogenic differentiation in hip phMSCs (n=4). Left: H19 regulation as compared to day 2 (value set to 1) of adipogenic differentiation. In the unstimulated control and in the visfatin stimulated group, H19 was continuously up-regulated at days 7 and 14 and showed a decline on day 21. Right: individual regulation of each sample compared to the corresponding control during OD at the same time points. Reference was set to 1 (gray dotted line). Visfatin stimulation led to a down-regulation of H19 compared to unstimulated controls at all time points evaluated.

Experimental Condition	day 7		day 14		day 21	
	mean	mean(log)	mean	mean(log)	mean	mean(log)
Control (n = 4)	1.304	0.091	3.790	1.168	4.714	0.825
Visfatin (n = 4)	2.282	0.715	3.617	0.862	1.247	0.195
		p = 0.2392		p = 0.6599		p = 0.4863

Tab. 19: lncRNA H19 fold-change during AD in unstimulated controls and visfatin stimulated MSCs. p-values are calculated between the means of the log transformed values of both groups per day of AD.

19.3 Visfatin down-regulates lncRNA H19 in OD

Even though lncRNA was down-regulated in the unstimulated control and visfatin setting in hMSCs and knee phMSCs as shown in figure 17, the group means were lower in the visfatin stimulated samples when compared to the controls. To evaluate the kinetics of each individual sample, each visfatin stimulated sample was compared to the corresponding unstimulated control. As shown in figure 19 visfatin down-regulated the H19 expression over the course of OD in each individual OD differentiation culture.

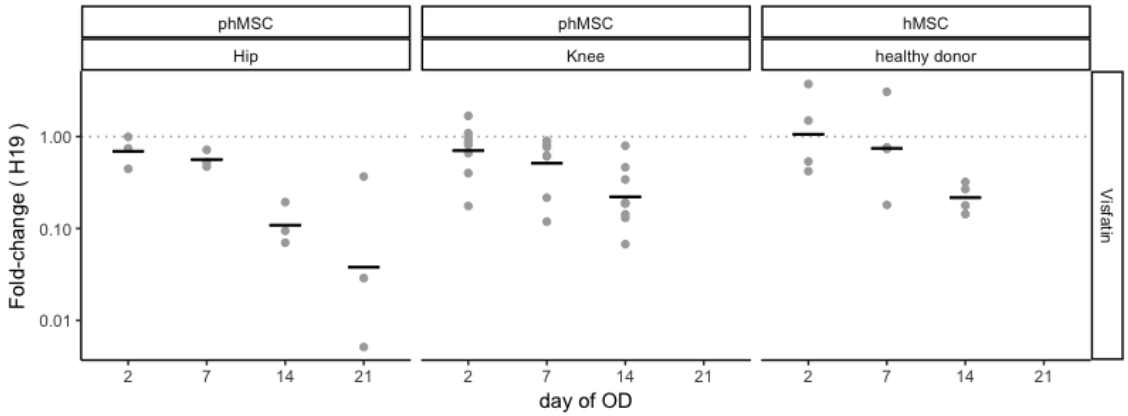

Fig. 19: lncRNA H19 expressions compared individually to the corresponding control of the same cell origin and day of OD. Controls were set to 1 (grey dotted line). A continuous down-regulation of lncRNA H19 over the course of OD could be observed in all groups. hMSC (n = 4), phMSC knee (n = 8), hip (n = 3).

Cell Origin	day 2		day 7		day 14		day 21	
	mean	mean(log)	mean	mean(log)	mean	mean(log)	mean	mean(log)
Hip (n = 3)	0.729	-0.369*	0.571	-0.577	0.119	-2.22	0.134	-3.274
				p = 0.4915		p = 0.009694		p = 0.1396
Knee (n = 8)	0.836	-0.352*	0.615	-0.668	0.29	-1.511		
				p = 0.3961		p = 0.007532		
healthy donor (n = 4)	1.546	0.057*	1.187	-0.293	0.228	-1.53		
				p = 0.6641		p = 0.04402		

Tab. 20: lncRNA H19 expression compared individually to the corresponding control of the same cell origin and day of OD. p-values are calculated for log transformed values at day 2 (*) and the following days of OD (day 7, 14, 21).

19.4 H19 response types upon visfatin stimulation

While the relative down-regulation by co-stimulation with visfatin was observed in the individual comparisons shown in figure 19, the down-regulation was not seen in all samlpes. To identify potential sub-groups in our samples with different response types to visfatin stimulation, we further analyzed the expression data of H19. In figure 20, the individual fold-change of H19 compared to the corresponding negative control (as depicted in figure 19) was depicted vertically and all day 2 values were set to 1. Figure 20 shows a constant down-regulation in all hip-phMSC samples, in 5 out of 8 knee-phMSC samples and in 3 out of 4 hMSC samples. In one knee-phMSC sample, a down-regulation was observed until day 7, reaching a plateau at day 14. In two knee-phMSC samples no down-regulation was observed.

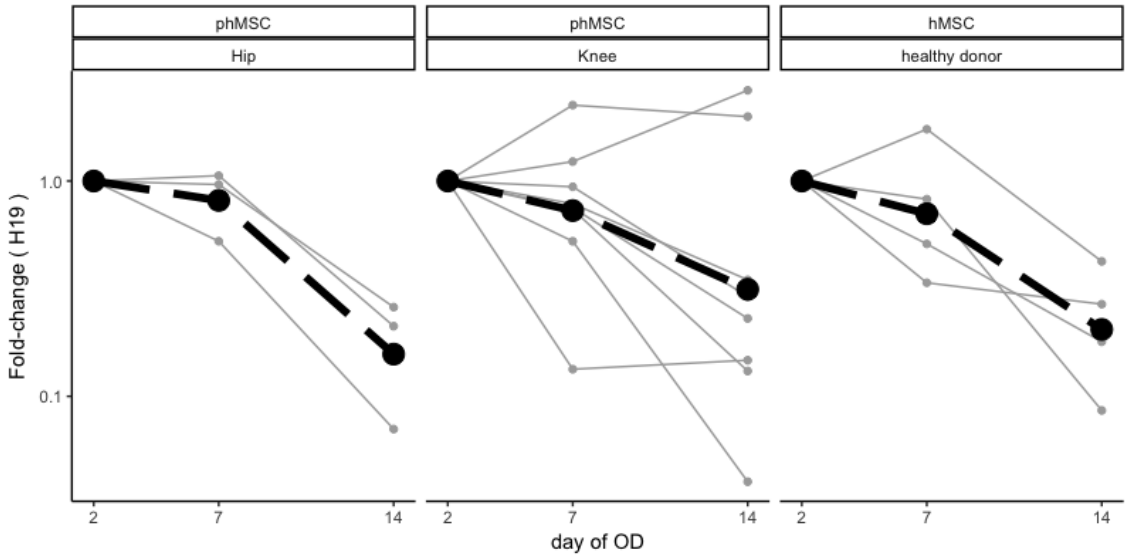

Fig. 20: H19 regulation compared to unstimulated control (analogous to figure 19). The individual values for each donor or patient sample of day 2 were set to 1 and fold changes calculated for each differentiation time point. Individual population data points (grey) are connected with grey lines. Group means per day are shown in black and connected with dashed lines.

20 Visfatin enhances matrix mineralization in OD

Successful osteogenic differentiation was validated using a mineralization assay after 21 days of differentiation. Calcium precipitates are stained in red using this method. Positive calcium staining in the unstimulated setting indicates a successful in-vitro osteogenesis and serves as control (figure 21 below). In the visfatin treated wells, a much stronger reaction indicates that visfatin enhances matrix production in osteogenic differentiation as previously observed and quantified [109].

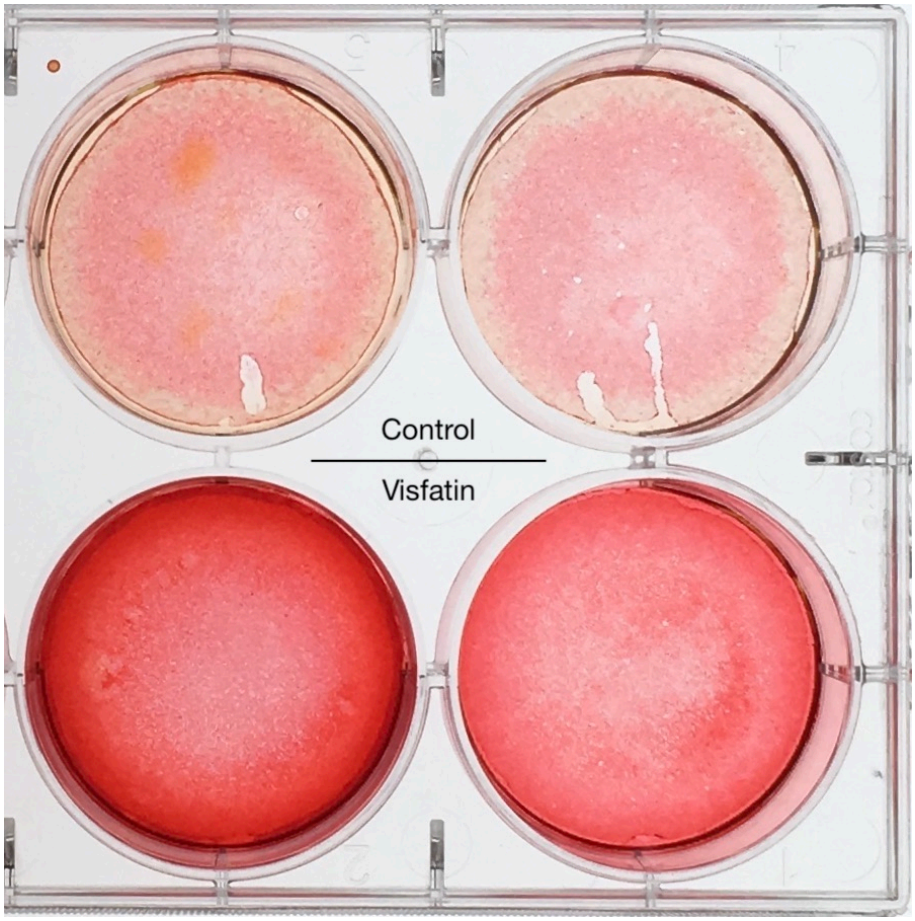

Fig. 21: Representative example of matrix mineralization assay with Alizarin Red staining. Calcium precipitates were stained red, indicating a stronger matrix mineralization and hence osteoblast activity in the visfatin-stimulated setting. Samples were stained at day 21 of osteogenic differentiation. The visfatin treated samples (bottom row) show a stronger staining than the controls (top row). Each column represents cells of one individual donor.

21 Visfatin and inflammatory effects on H19 expression

21.1 Pro-inflammatory effects of visfatin

Over the course of the 21 day osteogenic differentiation, IL-6 secretion was measured by ELISA in the culture supernatants. As shown in figure 22, IL-6 was highly induced in the visfatin-stimulated group as compared to unstimulated controls. The increase in IL-6 was time dependent, with a small difference at day 2 and a continuous increase over the rest of OD.

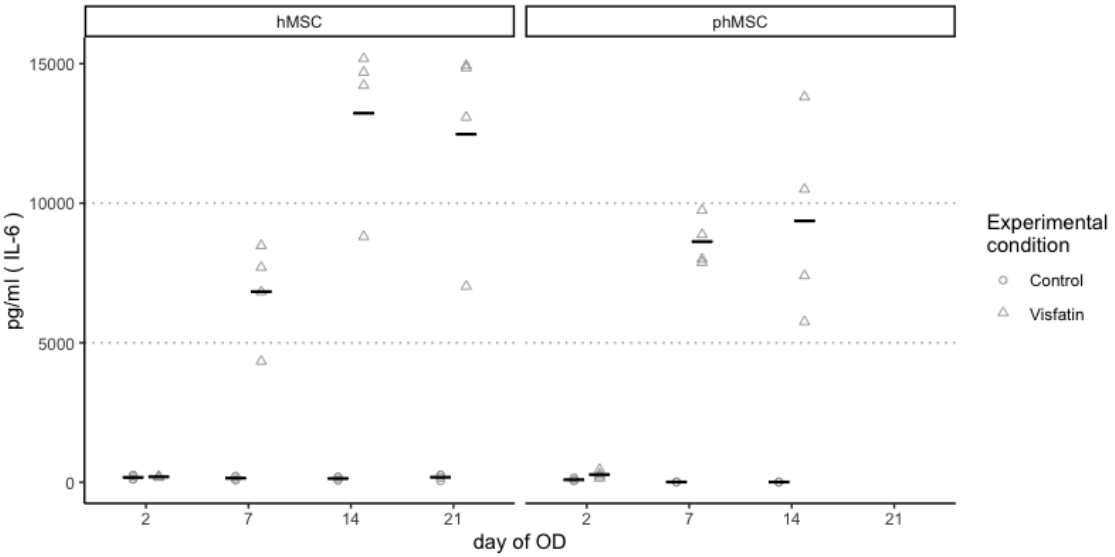

Fig. 22: IL-6 concentration was measured by ELISA in culture supernatants at different time points over the course of OD in both hMSC (n = 4) and phMSC (n = 4) populations. Black lines indicate group means. In visfatin-stimulated populations, IL-6 levels increased significantly (see table 21) but remained near base level in unstimulated controls .

Cell type	Experimental condition	mean(day 2)	mean(day 7)	mean(day 14)	mean(day 21)
hMSC (n = 4)	NK	175.38	148.21	134.92	181.71
	Visfatin	194.55	6832.9	13224.52	12471.05
		p = 0.6549	p = 0.004997	p = 0.003076	p = 0.007095
phMSC (n = 4)	NK	90.34	9.64	7.24	
	Visfatin	276.57	8624.4	9365.33	
		p = 0.06063	p = 0.0002807	p = 0.01337	

Tab. 21: Mean IL-6 concentrations in culture supernatants of hMSCs and phMSCs over the course of OD. In the visfatin stimulated groups, IL-6 was significantly up-regulated on the later time points of OD (day 7, 14 (and 21, only in hMSC cultures)).

21.2 IL-6 response to TNFα stimulation during OD

Visfatin differentially regulated lncRNA H19 expression and enhanced matrix mineralization over the course of osteogenic differentiation of MSCs. Visfatin acts as a pro-inflammatory stimulus during OD. It could therefore be hypothesized that the differential regulation of H19 is merely a response to the visfatin-induced inflammatory milieu. To follow up on this hypothesis, the effects of TNFα, a pro-inflammatory cytokine, as a stimulus during osteogenic differentiation was examined.

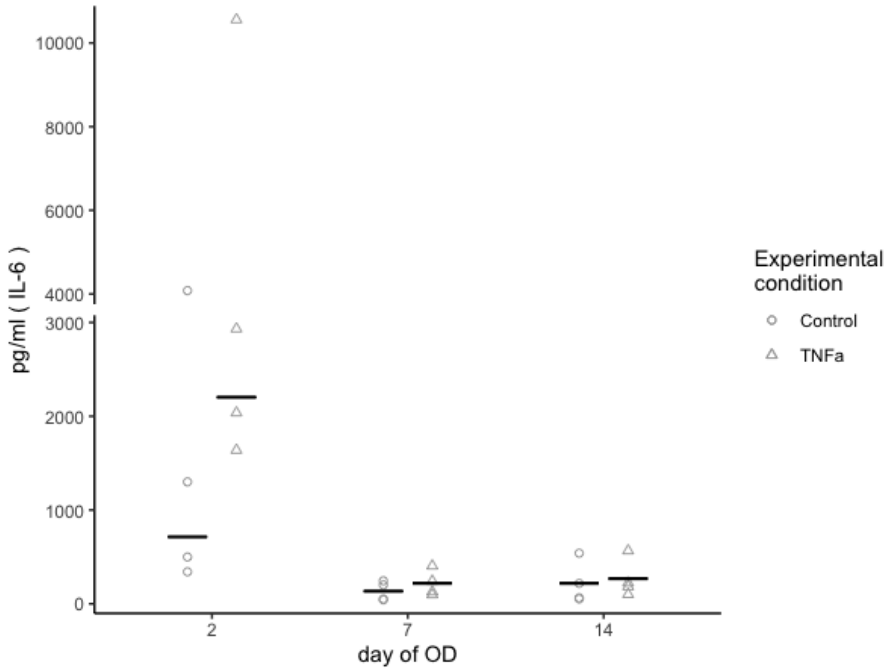

Fig. 23: IL-6 expression from phMSCs upon stimulation with (n = 4, triangle) or without (n = 4, circle) TNFα during OD. Black lines indicate mean values. At day 2, one population showed much higher values than other groups. These were excluded from group mean calculation.

Experimental condition	day 2 (n = 3)	day 7 (n = 4)	day 14 (n = 4)
Control	713.97	135.3	218.75
TNFα	2203.23	218.85	268.93
	p = 0.040	p = 0.374	p = 0.754

Tab. 22: Mean IL-6 concentrations in supernatants of phMSC cultures at three time points of OD, with and without TNFα stimulation. At day 2, one population showed much higher IL-6 levels in both the control and the stimulated group (see figure 23) and was therefore ommited from this analysis (day 2 control: 4080 pg/dl, TNFα: 10559 pg/dl).

21.3 TNFα does not down-regulate H19

During osteogenic differentiation with either TNFα or visfatin as stimulus, cell lysates were collected. TNFα-stimulated controls did not show the same regulation, leading to the suggestion that the regulation of lncRNA H19 is due to visfatin rather than to the pro-inflammatory effects on MSCs.

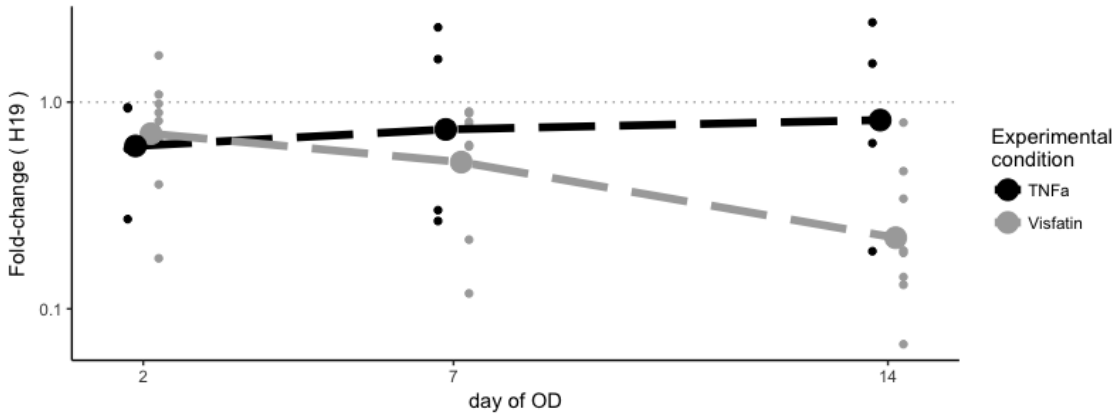

Fig. 24: Differential regulation of H19 by TNFα compared to visfatin stimulation of knee-phMSCs. Visfatin co-stimulation (grey, n = 8) during OD showed the previously observed down-regulation over the course of OD whereas this effect was not visible in TNFα treated samples (black, n = 4).

Experimental condition	day 2		day 7		day 14	
	mean	mean (log)	mean	mean (log)	mean	mean (log)
TNFα (n = 4)	0.685	-0.488	1.12	-0.304	1.197	-0.2
Visfatin (n = 8)	0.836	-0.352	0.615	-0.668	0.29	-1.511
		p = 0.7313		p = 0.5851		p = 0.09634

Tab. 23: Differential regulation of H19 by TNFα compared to visfatin stimulation of knee-phMSCs. p-values are calculated for log(mean) values comparing TNFα and visfatin stimulated groups at day 2, 7 and 14 of OD

21.4 TNFα does not stimulate matrix mineralization

Visfatin and TNFα-stimulated populations were stained with Alizarin Red after 21 days of osteogenic differentiation. As established above, visfatin enhanced matrix stimulation as compared to the negative controls. This effect was not observed in the TNFα co-stimulated populations. Figure 25 shows exemplary populations stained after 21 days of differentiation.

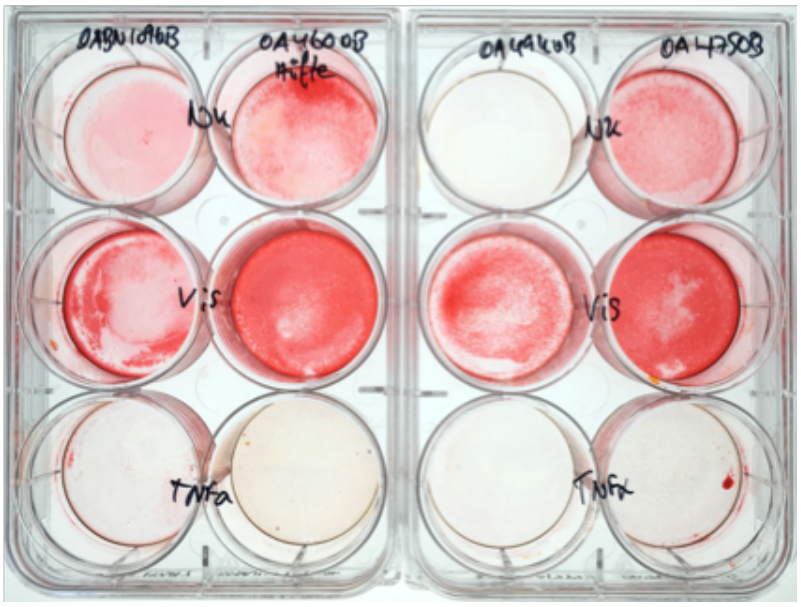

Fig. 25: Visfatin stimulated matrix mineralization is shown by Alizarin Red staining of 4 representative populations of knee-phMSCs after 21 days of OD. Alizarin Red stains calcium precipitates as a measure of in-vitro bone formation. Visfatin-stimulated cultures (middle row, “Vis”) showed a stronger mineralization compared to unstimulated controls (top row, “NK”) or TNFα-stimulated knee-phMSCs (bottom row, “TNFα”).

22 Effects of visfatin on TGFβ1 release during OD

Involvement of the TGFβ1 pathway was one of the potential mechanisms for lncRNA H19 to affect osteogenic differentiation. To evaluate the relevance of the TGFβ1 pathway in the visfatin-mediated effect during OD, TGFβ1 concentrations in the culture supernatants were measured over the course of OD. As illustrated in figure 26, a decrease of TGFβ1 at the early stage of OD (up to day 7) was observed in phMSCs. In addition, TGFβ1 concentrations were reduced in visfatin-stimulated phMSCs. These effects were not observed in hMSCs.

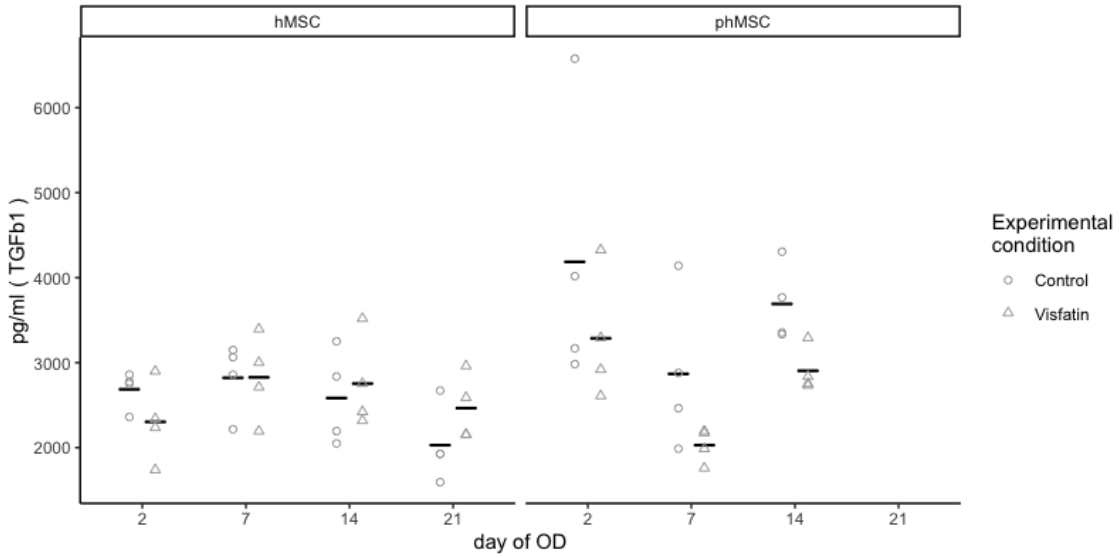

Fig. 26: TGFβ1 concentrations in culture supernatants of hMSCs (n = 4) and knee-phMSCs (n = 4) over the course of OD with visfatin stimulation (triangles) and in unstimulated controls (circles). Black bars indicate group means.

Cell type	Experimental condition	mean(day 2)	mean(day 7)	mean(day 14)	mean(day 21)
hMSC (n = 4)	control	2686.88	2821.45	2583.14	2028.78
	Visfatin	2303.42	2826.57	2754.08	2464.11
		p = 0.2141	p = 0.9881	p = 0.6771	p = 0.1981
phMSC (n = 4)	control	4186.21	2867.73	3690.68	
	Visfatin	3287.06	2028.88	2904.34	
		p = 0.3763	p = 0.166	p = 0.03225	

Tab. 24: Mean TGFβ1 concentrations in culture supernatants of hMSCs (n=4) and knee-phMSCs (n=4) on day 2, 8, 14 and 21 of OD [pg/ml]. p-values are given for individual observations comparing visfatin-stimulated to control samples.

23 H19 downstream pathway analysis

To evaluate different pathways for the potential H19 downstream effects on OD, two pathway inhibitors, Porcupine (PORCN, Wnt-C59) for the WNT/β-Catenin pathway and LY2109761 for the TGFβ1 pathway, were added to hMSC cultures. hMSCs were treated according to the established protocol over the course of early OD. On day 7, the pathway inhibitors were added and RNA and supernatant samples were collected on day 9 of OD (after 2 days of inhibition) and on the regular time point day 14 (day 7 of inhibition). For both inhibitors, dimethyl sulfoxide (DMSO) was used as an organic solvent. In the inhibition experiments, DMSO-controls were introduced next to unstimulated negative controls to identify potential DMSO-effects.

23.1 Pathway inhibition and visfatin induced IL-6 production

Visfatin stimulated samples were treated with TGFβ1- and WNT- pathway specific inhibitors LY2109761 and Porcupine as well as DMSO as control. Culture supernatants were collected on day 9 and 14 of OD and IL-6 concentrations were evaluated in ELISA assays. Figure 27 on the next page shows the expected increase in the visfatin-stimulated samples in the control group. IL-6 secretion was lower in the DMSO- and inhibitor-treated samples. The DMSO-values at day 9 were comparable to the control setting at day 7 and lower at day 14. In comparison to the pathway inhibitors no effect on the cytokine production or the ability to react to the visfatin stimulus of the hMSCs in-vitro compared to the DMSO solvent control was observed.

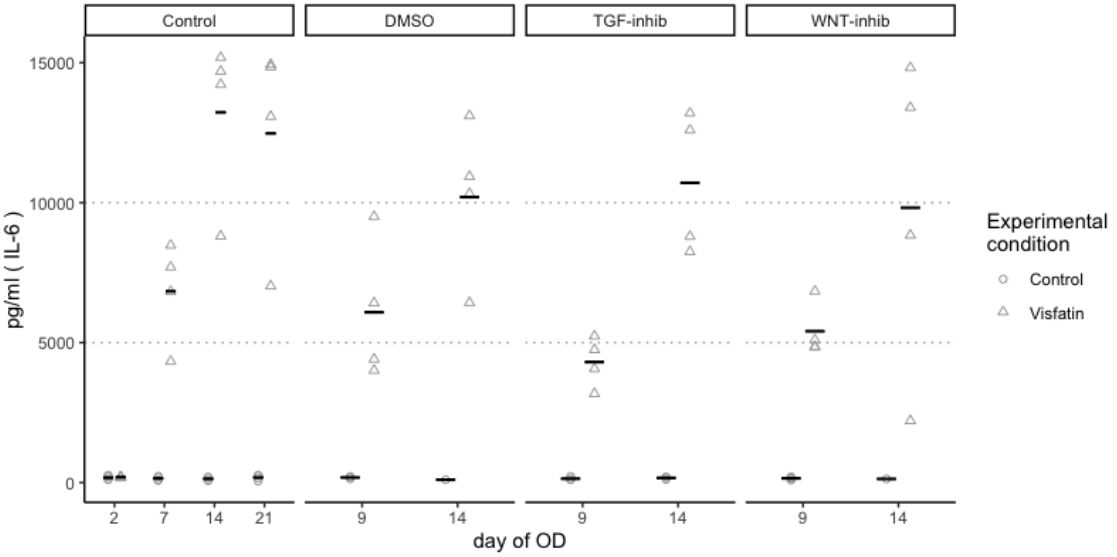

Fig. 27: IL-6 concentrations with pathway inhibition over the course of OD. The specific pathway inhibitors Porcupine (PORCN, Wnt-C59,) for the WNT/β-Catenin pathway (WNT-inhib, n = 4) and LY2109761 for the TGFβ1 pathway (TGF-inhib, n = 4) were added on day 7 of differentiation. Culture supernatants were sampled on day 2 (day 9 of OD) and 7 (14 of OD) after inhibition. Controls were sampled on days 2, 7, 14 and 21. DMSO (n = 4) served as negative control for the inhibitor effect. On day 14, IL-6 concentrations were slightly lower than in the visfatin stimulated control setting compared to DMSO. No difference between DMSO solvent control and inhibitors was observed.

Experimental condition		mean(day 9)	mean(day 14)
DMSO (n = 4)	NK	181.45 (n = 3)	102.2 (n = 1)
	Visfatin	6083.38	10198.25
p = 0.01818			
TGF-inhib (n = 4)	NK	138.37	166.66 (n = 3)
	Visfatin	4306.32	10708.42
		p = 0.002537	p = 0.003686
WNT-inhib (n = 4)	NK	150.67	131.12 (n = 1)
	Visfatin	5407.85	9816.83
		p = 0.001599	

Tab. 25: IL-6 concentrations [pg/ml] with pathway inhibition over the course of OD. The specific pathway inhibitors Porcupine (PORCN, Wnt-C59) for the WNT/β-Catenin pathway (WNT-inhib) and LY2109761 for the TGFβ1 pathway (TGF-inhib) were added on day 7 of differentiation. Culture supernatants were sampled on day 2 (day 9 of OD) and 7 (14 of OD) after inhibition. DMSO served as negative control for the inhibitor effect. Added visfatin led to significantly higher IL-6 expression in all settings. Differences between DMSO negative control and inhibition experiments could not be observed.

23.2 Pathway inhibition and H19 regulation

The down-regulation of lncRNA H19 was observed in the setting without inhibitor. Inhibitor treated samples showed no down-regulation of lncRNA H19 over the course of OD compared to DMSO solvent control (figure 28). Whereas regulation on day 9 is rather comparable to the regulation in the base setting on day 7, the day the inhibitors were added, the mean of the day 14 values appear reduced in the DMSO solvent control. Unfortunately, some day 14 samples had low RNA yield and were not sufficient for rt-PCR analysis. Also in the day 14 samples, measurements are noticeably wide spread in contrast to prevous experiments indicating an solvent effect in culture.

To evaluate the effectiveness of inhibition, the fold-change in lncRNA H19 in the inhibitor settings were individually compared to the corresponding DMSO solvent control. The results showed little to no difference in H19 expression of the inhibited samples compared to the negative controls.

These results suggest merely a DMSO effect and no effect by pathway inhibition.

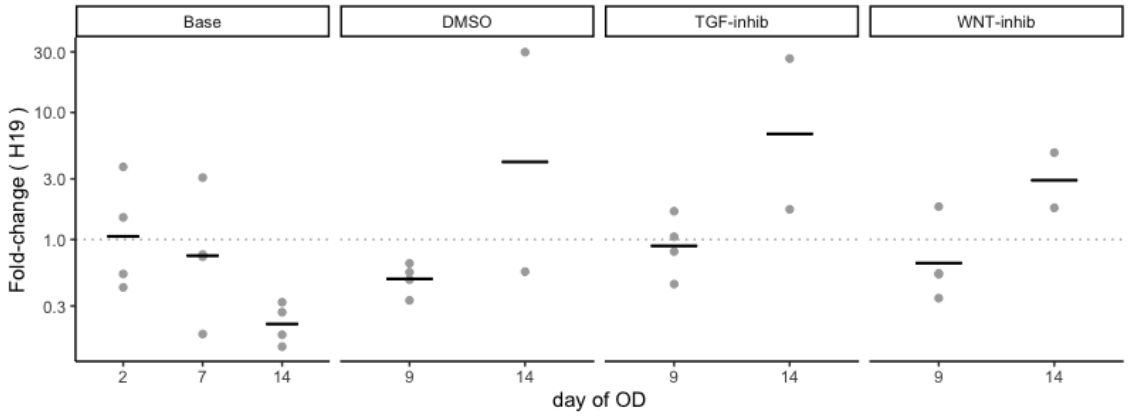

Fig. 28: lncRNA H19 regulation by visfatin in WNT/TGFβ1-inhibitor treated samples. The specific pathway inhibitors Porcupine (PORCN, Wnt-C59) for the WNT/β-Catenin pathway (WNT-inhib, day 9 n = 3, day 14 n = 2) and LY2109761 for the TGFβ1 pathway (TGF-inhib, day 9 n = 4, day 14 n = 2) were added on day 7 of differentiation. DMSO served as negative control (n = 4). 'Base' setting resembles visfatin effect during OD without inhibitors (n = 4). H19 regulation was evaluated in rtPCR on day 2 (day 9 of OD) and 7 (14 of OD) after inhibition.

24 Micro RNA expression profiles over the course of OD

TaqMan rtPCR of H19 endogenous micro RNAs miRNA 675-3p and 675-5p was conducted by Prof. Dr. Ospelt at the Center of Experimental Rheumatology, University of Zurich, Switzerland. A new set of 6 phMSC populations were differentiated according to the established protocol with and without visfatin co-stimulation. RNA from cell lysates was purified using the MIRNEASY MINI KIT (Qiagen, Hilden, Germany). H19 rtPCR was conducted to verify the established H19 kinetics over the course of OD. Samples were then sent to Zyrich and TaqMan analysis for the two endogenous micro RNAs of H19 was conducted there. Expression data were normalized to both of the two endogenous controls (RNU44, snU6).

24.1 Kinetics of miRNA 675-3p expression under visfatin stimulation

Figure 29 shows the regulation of miRNA 675-3p with and without visfatin over the course of OD. In the snU6 normalized data, 675-3p was continuously down-regulated over the course of OD in the unstimulated control group. Upon visfatin stimulation during OD, a weak down-regulation could be observed at day 7, but does not continue at day 14. On day 14, miRNA 675-3p levels return to the initial levels measured at day 2. This regulation is not observed in the RNU44 normalized data.

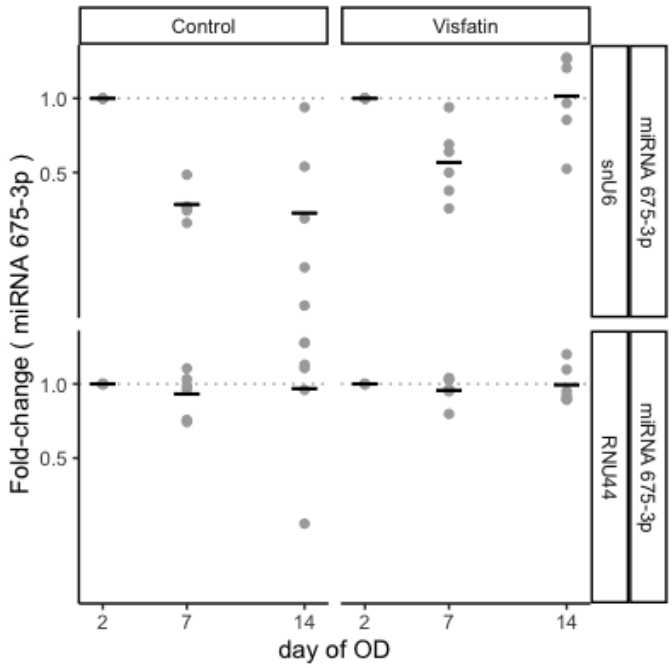

Fig. 29: Regulation of miRNA 675-3p over the course of OD in unstimulated controls and visfatin stimulated phMSCs. RNA samples of 3 different time points from 6 populations of phMSCs were analyzed by Taq-Man analysis. Two different endogenous controls (RNU44 and snU6) were used for normalization. In snU6 normalized data (upper panel), miRNA 675-3p was down-regulated over the course of OD in the control setting (left). In the visfatin stimulated group (right), miRNA 675-3p was first down-regulated from day 2 to day 7 (comparable to controls), from day 7 to 14, down-regulation is reversed and miRNA 675-3p returns to day 2 levels on day 14. This regulation is not observed in RNU44 normalized data (lower panel).

day of OD	Experimental condition	endogenous control			
		snU6		RNU44	
		mean	mean(log)	mean	mean(log)
7	Visfatin	0.576	-0.6	0.947	-0.06
	Control	0.375	-0.992	0.926	-0.094
			p = 0.038		p = 0.736
14	Visfatin	1.088	0.021	1.005	-0.009
	Control	0.425	-1.072	1.086	-0.044
			p = 0.025		p = 0.901

Tab. 26: Regulation of miRNA 675-3p over the course of OD in unstimulated controls and visfatin stimulated phMSCs, normalized to RNU44 and snU6 respectively. p-values were calculated for the log transformed values. Down-regulation of miRNA 675-3p was significant both at day 7 (p = 0.038) and day 14 (0.025) in the snU6 normalized data.

24.2 Kinetics of miRNA 675-5p expression under visfatin stimulation

Figure 30 shows the kinetics of miRNA 675-5p over the course of OD with and without visfatin stimulation. In both the RNU44 and snU6 normalized data, miRNA 675-5p was up-regulated over the course of OD in the control setting. In the visfatin stimulated group, however, an initial up-regulation until day 7 could be observed at day 14, miRNA 675-5p was down-regulated again to baseline (day 2) or even lower levels.

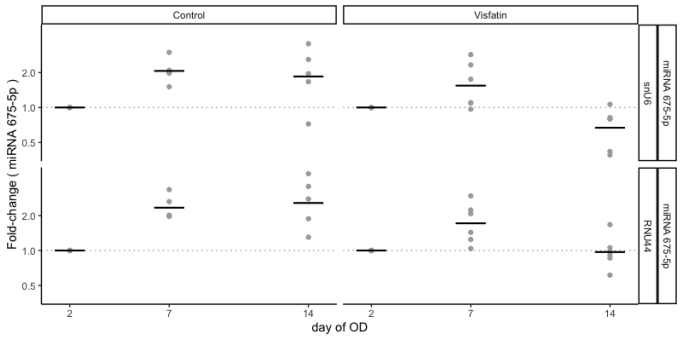

Fig. 30: Regulation of miRNA 675-5p over the course of OD in negative controls and visfatin stimulated phMSCs. RNA samples of 3 different time points from 6 populations of phMSCs were analyzed by Taq-Man analysis. Two different endogenous controls (RNU44 and snU6) were used for normalization. In the unstimulated controls (left), miRNA 675-5p was up-regulated over the course of OD. Visfatin stimulated populations (right) showed an up-regulation of miRNA 675-5p from day 2 to day 7 and a down-regulation in the later course of OD comparable to the level at day 2 (RNU44 normalized, bottom panel) or even below (snU6 normalized, top panel).

day of OD	Experimental condition	endogenous control			
		snU6		RNU44	
		mean	mean(log)	mean	mean(log)
2	Visfatin	1	0	1	0
	Control	1	0	1	0
7	Visfatin	1.683	0.434	1.831	0.540
	Control	2.117	0.726	2.394	0.850
			p = 0.211		p = 0.146
14	Visfatin	0.714	-0.402	1.0159	-0.03
	Control	2.098	0.616	2.825	0.943
			p = 0.015		p = 0.008

Tab. 27: Regulation of miRNA 675-5p over the course of OD in unstimulated controls and visfatin stimulated phMSCs, normalized to RNU44 or snU6 respectively. p-values were calculated for the log transformed values. On day 7, no significant difference between the visfatin stimulated and unstimulated groups could be detected. On day 14, miRNA 675-5p was significantly down-regulated in the visfatin stimulated groups (RNU44: p = 0.008; snU6: p = 0.015).

24.3 Visfatin mediated differential regulation of H19 endogenous miRNAs

To observe the regulatory effect of visfatin on H19's endogenous miRNAs, miRNA levels in the stimulated groups were compared to the corresponding controls of the same day of OD. The results are illustrated in figure 31. Figure 31a shows a continuous up-regulation of miRNA 675-3p upon visfatin stimulation over the course of OD. miRNA 675-5p, however, is down-regulated upon visfatin stimulation as depicted in figure 31b.

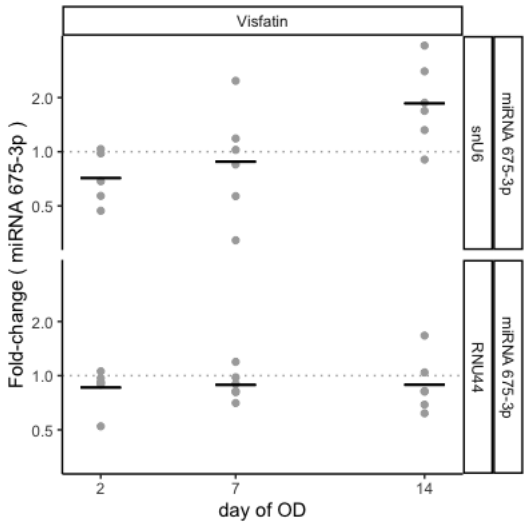

(a) miRNA 675-3p showed a continuous up-regulation over the course of OD in the visfatin stimulated group as compared to the respective control in the snU6 normalized groups (top panel). RNU44 normalized data showed a constant low expression of visfatin with no specific kinetics over the course of OD (lower panel).

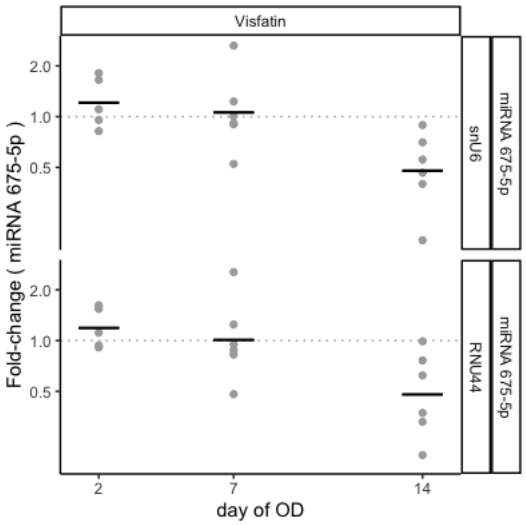

(b) miRNA675-5p was continuously down-regulated over the course of OD in both RNU44 and snU6 normalized results. On day 2 in visfatin stimulated samples, miRNA675-5p was 1.2 fold up-regulated as compared to the corresponding negative controls. By day 14, miRNA675-5p was significantly down-regulated 0.5 fold (RNU44: $p = 0.011$; snU6: $p = 0.008$).

Fig. 31: Visfatin mediated regulation of H19's endogenous micro RNAs 675-3p and -5p. miRNA 675-3p showed an up-regulation over the course of OD, whereas miRNA 675-5p was down-regulated by visfatin stimulation over the course of OD.

micro RNA	day of OD	RNU44			
		mean	log(mean)	vs. day 2	vs. miRNA 675-3p
miRNA 675-3p	2	0.879	-0.152		
	7	0.901	-0.118	p = 0.793	
	14	0.943	-0.117	p = 0.847	
miRNA 675-5p	2	1.224	0.173		p = 0.074
	7	1.156	0.009	p = 0.541	p = 0.61
	14	0.548	-0.736	p = 0.011	p = 0.056
		snU6			
miRNA 675-3p	2	0.748	-0.337		
	7	1.071	-0.127	p = 0.533	
	14	2.079	0.619	p = 0.006	
miRNA 675-5p	2	1.27	0.191		p = 0.041
	7	1.202	0.057	p = 0.626	p = 0.616
	14	0.534	-0.737	p = 0.008	p = 0.001

Tab. 28: Visfatin mediated regulation of miRNAs 675-3p and 5-p over the course of OD. Data shown was normalized to RNU44 and snU6 respectively. p-values were calculated for the log transformed values for both in-group comparison against day 2 and comparing miRNA 675-5p regulation to the regulation of miRNA 675-3p.
miRNA 675-3p was significantly up-regulated on day 14 compared to day 2 of OD (snU6: p = 0.006), whereas miRNA 675-5p showed a significant down-regulation against day 2 on day 14 of OD (RNU44: p=0.011; snU6: p = 0.008).
On day 2 of OD, miRNA 675-5p was significantly up-regulated as compared to miRNA 675-3p (SNU44: p = 0.074; snU6: p = 0.041). On day 14, miRNA 675-5p was significantly down-regulated as compared to miRNA 675-3p (SNU44: p = 0.056; snU6: p = 0.001).

The down-regulation of miRNA 675-3p was significantly reduced in the visfatin stimulated group on day 7 (p = 0.038) and day 14 (p = 0,025) compared to unstimulated controls as shown in figure 29. On day 14, visfatin stimulated miRNA 675-3p values returned to the initial values of day 2. miRNA 675-5p was up-regulated to a lesser extend upon visfatin stimulation, with its day 14 values staying below base levels at day 2. Visfatin mediated down-regulation was significant at day 14 (RNU44: p = 0.008, snU6: p = 0.015, see figure 30).

The kinetics of H19 and its endogenous miRNAs are compared in figure 32. Here we observed a parallel expression of H19 and miRNA 675-5p, whereas miRNA 675-3p follows an inverse expression pattern.

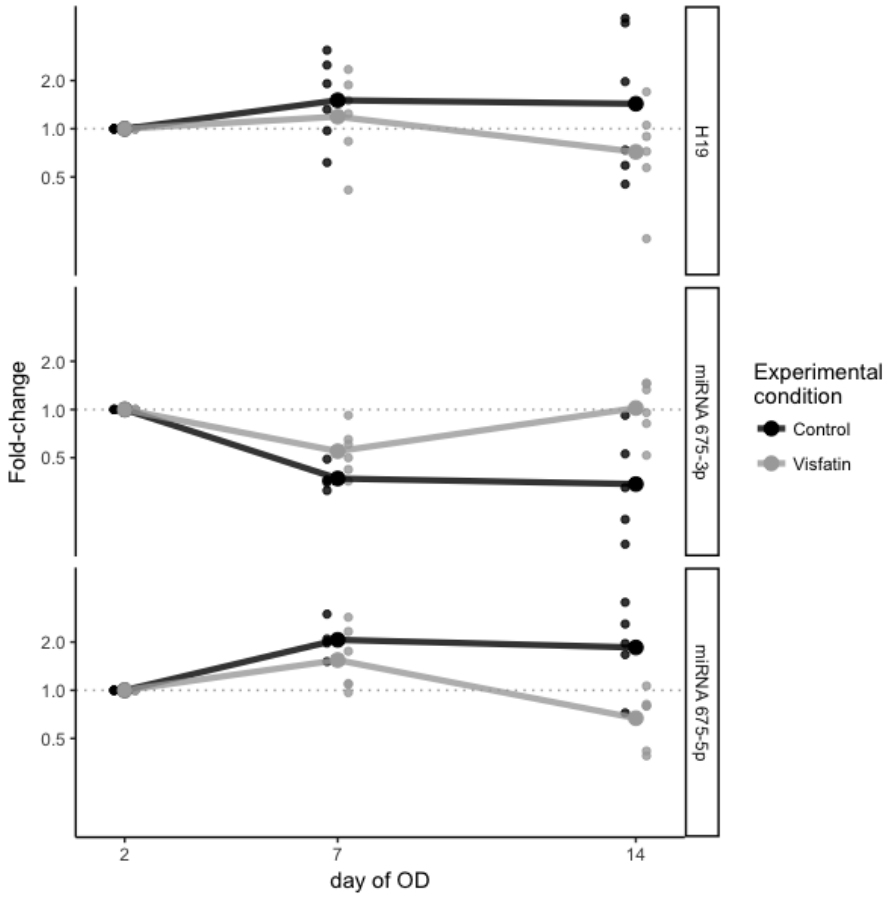

Fig. 32: Summary of the kinetics of H19 and its endogenous miRNAs 675-3p and 675-5p over the course of OD. Raw values were normalized to snU6 and day 2 values were set to 1. Six populations of phMSCs were analyzed using rtPCR (H19) and TaqMan (miRNAs) assay to evaluate fold-changes as compared to day 2 in early stage OD. As established in other cell populations, H19 levels increased continuously until day 14. In the visfatin stimulated group, H19 levels were supressed at day 7 and declined until day 14. miRNA 675-5p exhibits a parallel kinetic to H19, with rising levels in unstimulated controls and a supression between day 7 and 14. miRNA 675-3p shows an inverse kinetic to H19, with a continuous down-regulation in the unstimulated controls. Upon visfatin-stimulation, miRNA 675-3p levels decline to a lesser extent until day 7 and decline is reversed reaching day 2 levels on day 14 of OD.

Part VI. Discussion

Recent developments in sequencing techniques and computer-aided data analysis have opened the path to evaluating the vast majority of the human genome that does not hold protein-coding information. Amongst this “genomic dark matter”, a growing number of regulatory RNA molecules have been described over the last decades [113]. The goal of this thesis was to identify and evaluate long non-coding RNA molecules involved in the context of rheumatic diseases.

lncRNAs are defined as regulatory RNA molecules longer than 200 nucleotides and can be found in large numbers in mammals and humans. In recent years, there is increasing evidence that lncRNAs have a variety of functions in many cellular processes, especially in the regulation of gene transcription, post-transcriptional processing and epigenetic regulation [115–117]. Moreover, numerous studies have shown close associations of lncRNAs with various diseases and neoplasms [131, 168, 169].

A number of databases have been established to collect, validate and structure this body of data. For instance, the GENCODE library currently includes a total of 17.957 lncRNAs Frankish, Diekhans, Jungreis, et al. [127], and lncBook lists 3.772 lncRNA-disease associations with 462 diseases and 28 MeSH terms Ma, Cao, Liu, et al. [128].

25 lncRNAs in inflammatory conditions

In order to select promising lncRNAs from this large number of candidates, array analyses are an established method to identify differentially regulated lncRNAs under experimental conditions. We therefore analyzed a large data set containing 3.389 measurements of 2.989 genes of long non-coding RNAs in OA and RA patient samples for their regulation in response to TNFα, a pro-inflammatory stimulus.

Based on the array data and extensive literature research, 15 lncRNAs were selected for further evaluation. Expression and regulation of these lncRNAs proofed highly variable when evaluated individually using rtPCR. Regulation measured was differed largely depending on the type, quality and origin of cell populations. This was most likely due

to differences in baseline expression levels and individual donor patient background (e.g. prior medication and stage of disease) as well as the underlying disease itself. Hence, no definitive pattern for the (dys-)regulation of specific lncRNAs or lncRNA groups could be identified. For the purpose of this study we therefore selected lncRNA H19 for further evaluation, due to its particular interest based on literature research on the candidate lncRNAs.

26 lncRNA H19 in MSC differentiation

lncRNAs have been demonstrated in numerous studies to be involved in the regulation of the physiological and pathological differentiation of cell lines and development of tissues. In particular, lncRNA H19 has been described to be involved in osseous tissue formation, osteogenic differentiation and development of RA [142, 170–172].

H19 has also been shown to play a role in other physiological processes like embryogenesis, physiological growth and tissue repair, but also in a variety of pathogenic processes and neoplasms [135–138, 140, 141, 167, 173].

lncRNA H19 in osteogenic differentiation In the context of osteogenic differentiation of mesenchymal stromal cells (MSCs), other groups have published results showing H19 to be up-regulated *in vitro* and *in vivo* [147, 149]. In this study, we were able to confirm this up-regulation of lncRNA H19 over the course of OD in primary human MSCs from both hip and knee joints.

H19 was shown to be part of regulatory pathways of osteogenesis - it was shown to be up-regulated by osteogenesis inducing agents such as TGF-β1, BMP2 and BMP4, as well as being an inductor of osteogenesis, when over-expressed in MSCs [147]. In vivo studies found increased H19 levels at sites of increased osteogenesis [150–152].

These reports place lncRNA H19 in a central position for regulation of OD and potentially the development of pathologies such as RA. This study therefore aimes to further understand the regulatory mechanisms of H19 in the context of OD and H19s response to adipokine stimulation to explore potential involvement in the pathogenesis of osteoarthri-

tis and RA. An overview of proposed mechanisms for H19's regulatory effects on osteogenic differentiation has been given in figure 7 on page 37.

lncRNA H19 in adipogenic differentiation In addition, a similar but weaker up-regulation of H19 could be observed in primary human MSCs induced for adipogenic differentiation. These findings conflict with other groups reporting a down-regulation of H19 during adipogenic differentiation, as well as a shift towards adipogenic differentiation upon H19 knockdown in mice [174–176].

27 Visfatin effects on osteogenic differentiation of MSCs

Visfatin is a adipokine expressed predominantly in adipose tissue. It has been in the focus of research as a cytokine involved in pre-B-cell colony formation as well as a co-enzyme in the canonical nicotinamide salvage pathway [74, 85]. It acts as a pro-inflammatory stimulus and is associated with clinical risk factors of OA [91, 99, 104, 106]. The osteogenic differentiation of MSCs into osteoblasts is a crucial aspect of bone homeostasis and tissue regeneration after acute injuries as well as in chronic impairment of bone and joint tissue. Visfatin has been shown to alter osteogenic differentiation and the resulting osteoblast phenotypes [90, 109, 111, 112, 177, 178].

Our group previously established visfatins pro-osteogenic, proliferation-promoting effect on osteoblasts, resulting in increased matrix mineralization and reduced expression of type I collagen. This impairs bone remodeling and leads to a more fragile, brittle bone structure [109]. Dr. Tsiklauri's research focused on changes in osteogenic differentiation under the influence of adipokines such as visfatin. However, the details of the observed visfatin-mediated effects during OD remained to be clarified.

Given the regulatory capabilities of lncRNAs in general and H19s involvement in connective tissue regulations and dysfunctions, H19 was further evaluated as a potential link between adipokine stimulation and the resulting phenotypes described above.

28 Visfatin regulates lncRNA H19 during osteogenic differentiation

To assess whether adipokine stimulation would alter the H19 kinetics observed during OD, RNA samples from MSC cultures treated with the adipokines leptin, resist and visfatin were evaluated. The samples stimulated with leptin or resistin during OD showed an equivalent up-regulation to that observed in unstimulated controls as described above. The samples stimulated with visfatin, on the other hand, showed a continuous down-regulation, inverse to the unstimulated controls.

To be able to address this effect in more detail, additional specimens were evaluated. Among these were knee-MSCs collected from bone samples taken from OA and RA patients after knee-replacement surgery, as well as commercially obtained hMSCs from healthy donors. Like the initially used hip-phMSCs, these were verified to exhibit proper in-vitro bone formation and osteoblast function, comparable to the hip-phMSCs. Calcium precipitate staining confirmed the desired differentiation of MSCs as well as the enhanced matrix mineralization under the influence of visfatin during OD.

In evaluating these samples, H19 was confirmed to be up-regulated over the course of OD in unstimulated MSCs and down-regulated in the visfatin treated samples. We observed, however, that the previously described down-regulation was less prominent in non-hip-phMSCs. In hMSCs from healthy donors, the same visfatin-induced down-regulation of H19 was present. The up-regulation of H19 in the unstimulated controls, however, could not be observed (see figure 17).

MSCs are well recognized to be highly tissue-specific in many of their properties, including surface markers, proliferation and differentiation potential and metabolic activity [179–181]. To a lesser extent, this tissue-specificity also does apply to MSCs stemming from different joints. This tissue- and location-specificity may explain the observed differences in H19 regulation observed. As lncRNAs are involved in the regulation of gene expression and cell differentiation, tissue specific expression patterns have been observed by other groups [182, 183].

To correct for cell origin specific effects, populations stimulated with visfatin were

compared to their corresponding individual controls. Using this method, a relative down-regulation (or reduced up-regulation) of H19 could be observed in all of the samples evaluated. The visfatin induced down-regulation of H19 could be show to be a specific mechanism, that was independent of anatomic origin, baseline H19 expression, disease-affection or patient background.

lncRNA H19 may hereby proved a 'missing link' between visfatin stimulation and alteration of osteoblast phenotypes. Further studies are needed to establish this link and its physiologic relevance, in particular bringing together measurements of visfatin expression in vivo [104, 105], with corresponding H19 levels.

29 Visfatin specific effect versus inflammatory effect

The pro-inflammatory aspect of visfatin [91, 184] was replicated in terms of IL-6 induction in the context of OD. Over the course of OD, IL-6 was continuously up-regulated in visfatin treated samples, whereas IL-6 levels remained close to base line in unstimulated controls.

To distinguish between a visfatin-specific effect and an effect of the inflammatory milieu causing the differential expression of H19, TNFα served as a general inflammatory stimulus for further experiments. The pro-inflammatory effect of TNFα was likewise confirmed in terms of IL-6 induction.

H19's response to visfatin-stimulation was compared with TNFα-stimulation. In the TNFα treated samples, no down-regulation of lncRNA H19 could be observed compared to the unstimulated controls. A recent study in immortalized rheumatoid fibroblast-like synoviocytes (MH7A) showed even an up-regulation of H19 following TNFα stimulation [185].

Furthermore, induction of matrix mineralization at day 21 of OD in response to either visfatin or TNFα was evaluated. Matrix mineralization indicating in-vitro bone formation was seen in the unstimulated samples and was strongly enhanced in the visfatin stimulated group. TNFα stimulated samples, however, exhibited lower levels of mineralization even compared to controls, further indicating that the observed changes in osteoblast phenotype

are not inflammation-induced but a visfatin-specific effect.

TNFα stimulated samples had a significantly higher IL-6 concentration compared to unstimulated controls on day 2. As opposed to visfatin stimulation, however, IL-6 levels at later time points were lower than baseline in both stimulated and unstimulated groups. This may be due to in-stable TNFα stimulus used for the experiments. OD cultures were stimulated with either visfatin or TNFα 48 hours prior to sample collection. Instable TNFα molecules or an effect lasting for only a short period of time could have therefore remained undetected. TNFα stimulated samples measured after 24 hours of stimulation exhibited much higher IL-6 concentrations as shown in chapter 17 on page 63. Similarly, the IL-6 concentrations and the stimulatory effect of visfatin were markedly higher in day 2 samples than in the samples collected at day 7 and 14. This could be due to a loss of cell responsiveness to TNFα when the stimulus is applied over an extended period of time, or a loss of responsiveness of the cells as osteogenic differentiation proceeds.

To generate more reliable results in comparing the visfatin effect to a broad pro-inflammatory stimulus, this issue could be addressed by A) more frequent renewal of the TNFα-stimulus and shorter periods between medium exchange, B) over-expressing TNF in MSCs or C) by using other cytokines such as IL-1 as an alternative long-term pro-inflammatory stimulus.

30 Analysis of H19 downstream pathways

To further evaluate visfatin effects during OD, a number of potential downstream mechanismns of H19 were explored. Two proposed pathways found in the literature are the TGFβ1 and WNT/β-Catenin pathways [147, 155]. Other groups have described an osteogenesis-promoting effect of H19 in fibroblasts via the WNT/β-Catenin pathway [186].

TGFβ1 levels were measured over the course of OD. In hMCS but not in phMSC cultures, a trend to lower TGFβ1 levels could be observed over the 21 day period with significant reduction on the last day of differentiation.

Commercially obtained hMSCs are derived from deceased healthy donors. Unlike the used phMSCs, which were obtained from OA patients after joint replacement surgery.

Here, our laboratory could oversee the whole supply chain, including tissue origin and maintain low passage cycles until the experiments. phMSC cultures used are therefore assumed to closer represent the physiological composition of bone marrow cells as found in the osteoarthritic joint.

Furthermore, pathway inhibition experiments were conducted. Neither the TGFβ1 inhibitor (LY2109761) nor the WNT inhibitor (Porcupine) had any effect on the induction of IL-6 upon visfatin stimulation. On day 14 of OD after 7 days of inhibition, no down-regulation of H19 was observed in both inhibitor-treated groups as well as in controls containing DMSO, the solvent used for both inhibitors. All samples containing DMSO yielded a very low RNA harvest and only few were available for analysis. This was most likely an artifact produced by the long (seven day) exposure of the cells to the cytotoxic solvent DMSO, although it was used in low quantities.

In the RNA samples that were available for evaluation, the visfatin induced down-regulation could not be observed. As this effect, however, was not specific to both or either of the pathway inhibition settings but present also in the DMSO negative control, this was concluded to be rather due to cytotoxicity rather than a specific pathway effect.

Although the data indicate no difference between solvent control and use of inhibitors of the WNT and TGFβ1 pathways, further studies should address the role of these pathways in the context of OD under visfatin stimulation.

30.1 H19 endogenous micro RNA regulation

Another downstream mechanism of H19 potentially influencing OD could be found its molecular structure and its specific nature as an RNA molecule [114, 133, 134]. One established effector mechanism of lncRNAs in general is the fact that they themselves may contain micro RNA sequences which can be spliced from the originally transcribed lncRNA. micro RNAs, however, can effectively alter gene expression.

H19 consists of five exons. The rtPCR primers used to measure H19 expression in the experiments conducted for this study target a sequence in exon 5/5 of H19. In exon 1/5 of H19, two miRNAs are encoded: miRNA-675-3p and miRNA-675-5p [126, 144–146].

As a continuous down-regulation of lncRNA H19 by visfatin could be established in the present study, it must be noted that this merely proves a down-regulation of the exon 5/5 of H19. Visfatin stimulation could therefore lead to the release of micro RNAs from exon 1/5 of lncRNA H19 by alternative splicing and degradation of the remaining H19 molecule including the marker sequence measured by rtPCR in exon 5/5.

Considering the structure and nature of H19, two hypotheses were established.

A: miRNA is continuously spliced from H19. As H19 is down-regulated, less source material is available for alternative splicing and miRNA expression is down-regulated in parallel with H19.

B: miRNA is actively spliced from H19. As the splicing process is induced, more miRNAs can be found. In contrast, H19 is degraded after splicing and hereby down-regulated over the course of OD.

Evaluating the kinetics of these micro RNAs and comparing them to the established kinetics found in H19 was performed to provide further insight in the downstream pathways of H19. As two miRNAs are encoded in the H19 sequence, this hypothesis was tested for both miRNAs individually.

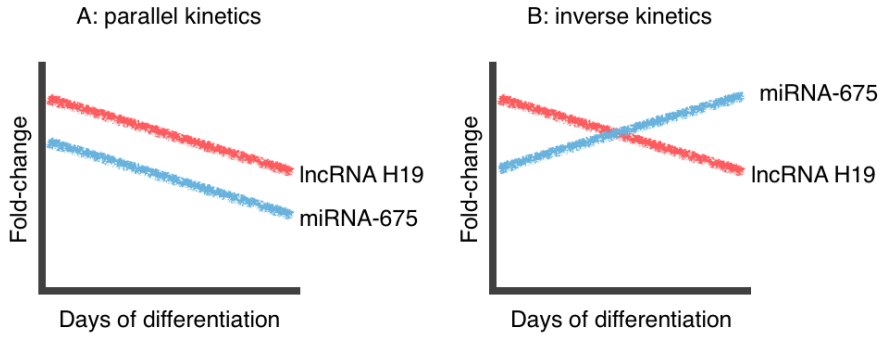

Fig. 33: H19-miRNA-675 hypothesis: The sequence of lncRNA contains two micro RNAs (miRNA-675-3p and miRNA-675-5p). The miRNAs are positioned in the exon 1/5 of H19, whereas the primer to evaluate H19 expressions targets a sequence in exon 5/5 of H19. miRNAs can be released from the lncRNA by alternative splicing. This could result in degradation of the remains of H19 and the observed down-regulation over the course of OD. If lncRNA H19 is down-regulated, this could result in less miRNAs released from H19 over time (A). On the other hand if the release of miRNAs leads to the degradation of H19, the micro RNAs could present an inverse kinetic to H19 (B).

Measuring micro RNAs with their length of ~20 nucleotides inherited methodical challenges. Fortunately, our cooperation partner in Zürich agreed to perform the micro

RNA analysis using TAQMAN MICRORNA ASSAYS. To provide suitable RNA samples for this assay, new samples were prepared using a different kit for RNA isolation. A set of 6 samples with validated H19 kinetics over the course of differentiation were chosen and sent to the collaborators. TaqMan analysis were conducted for all 6 samples provided, targeting miRNA 675-5p and -3p. Results were normalized to two different endogenous control genes, RNU44 and snU6 separately. Subsequent data analyses of the targets fold-changes as well as comparison to the H19 kinetics were conducted by the author.

miRNAs 675-3p and -5p over the course of OD

The regulation of unstimulated samples is illustrated in figure 32 on page 89. As shown in this figure, miRNA 675-5p was regulated in a similar pattern as H19 itself, with an increase from day 2 to day 7 and remaining at similar levels up to day 14. miRNA 675-3p, on the other hand, was regulated in an inverse pattern, with a down-regulation towards day 7 and similar levels until day 14 in this set of experiments.

Notably, TaqMan analysis results were normalized to the two endogenous control genes RNU44 and snU6. miRNA 675-5p showed a continuous up-regulation over the course of OD, consistent in both normalizations. miRNA 675-3p was continuously down-regulated in the snU6 normalized values. No differential regulation was seen in the RNU44 normalized results.

Apart from the miRNAs evaluated in this study, other groups presented findings showing that other miRNAs are also regulated by H19. Li et al. presented a study in mice, where H19 acted as a sponge for miRNA-149, hereby increasing osteogenic differention [186]. Other studies suggest a sponging mechanism of H19 for miRNA-29a or -140 [151, 152], these mechanisms remain to be evaluated in the context of visfatin-altered OD.

30.2 Kinetics of H19 and its endogenous miRNAs over the course of OD

In the synopsis shown in figure 32, a differential regulation of the kinetics of H19 and its endogenous miRNAs over the course of OD could be observed. In unstimulated OD, an up-regulation of lncRNA H19, as well as miRNA 675-5p was observed, whereas miRNA 675-3p was down-regulated or remained as baseline levels. Upon visfatin-stimulation, lncRNA H19 and miRNA 675-5p were instead down-regulated. miRNA 675-3p, however, was up-regulated over the course of OD.

Along with the established hypothesis, miRNA 675-5p was regulated in parallel with lncRNA H19. As H19 is up-regulated in the unstimulated control setting, more source material for miRNA675-5p release is provided. In visfatin-stimulated samples, however, H19 is down-regulated, thus, providing less source material for 5p release. This leads to the assumption of a passive release of miRNA 675-5p from H19 (Hypothesis A).

miRNA 675-3p on the other hand was regulated inversely to lncRNA H19. In unstimulated OD, H19 levels increased over time whereas 3p levels decreased continuosly. The visfatin stimulus, on the other hand, leads to more 3p being released from H19, leading to decreasing levels as H19 is degraded. (Hypothesis B).

The regulatory effect of visfatin on H19 and its endogenous miRNAs is summarized in figure 34.

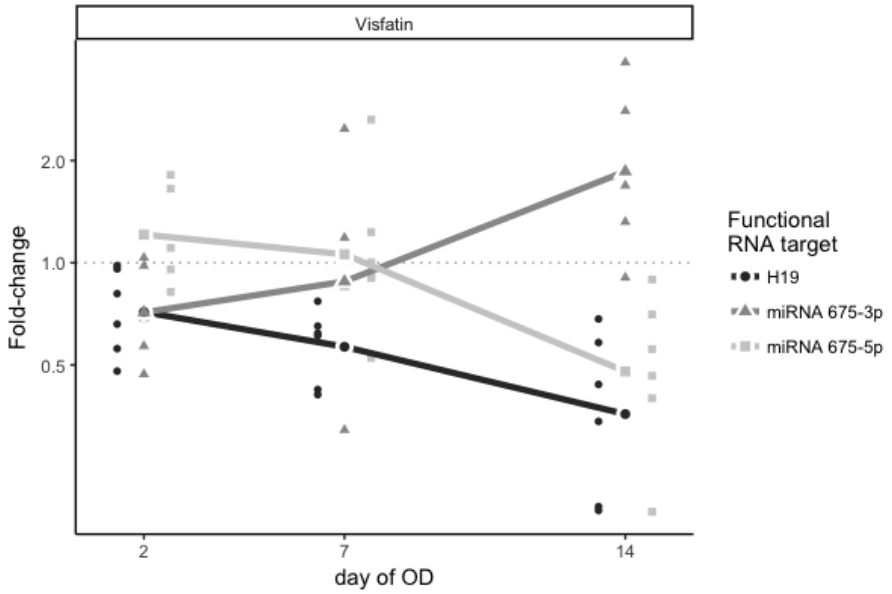

Fig. 34: Differential regulation of H19 and its endogenous miRNAs 675-3p and 675-5p over the course of OD. Fold-changes of H19 (normalized to 18s) and miRNAs in samples of 6 visfatin stimulated phMSC populations (normalized to snU6) were compared to same-day unstimulated controls. H19 (black circles) was continuously down-regulated upon visfatin stimulation over the course of OD. miRNA 675-5p (light grey triangles) was continuously down-regulated in parallel to H19. miRNA 675-3p (grey squares) was inversely regulated with a continuous up-regulation over the course of OD.

This thesis confirmes previously published results on the kinetics of H19 during OD [147, 149]. For the first time it demonstrates the regulation of H19s endogenous miRNAs 675-3p and -5p in differentiating MSCs. It also provides first evidence for the role of visfatin in the regulation of this lncRNA H19/miRNA 675-3p/-5p axis. The relationship between H19 and miRNA 675-3p and -5p respectively have been described in the context of other pathologies in previous studies [187, 188]. This novel pathway helps to further the understanding of the effects of visfatin on OD, as well as provide a model to understanding the H19 and miRNA 675-3p/-5p regulation.

31 Conclusions

In this thesis, the regulation of long non-coding RNA H19 during the osteogenic differentiation of mesenchymal stromal cells has been evalated. Specifically, a novel regulatory effect of visfatin, via alteration of long non-coding RNA H19 expression and processing could be demonstrated. Visfatin stimulation was shown to differentially regulate lncRNA H19 and its endogenous micro RNAs miRNA 675-5p and miRNA 675-3p.

Visfatin stimulation during OD increases osteogenic potential and matrix mineralization. On the other hand, it reduces collagen I production, resulting in a more brittle, fragile, osteoporotic bone structure. H19 is a regulatory lncRNA that is found up-regulated during OD. It could be shown that visfatin stimulation leads to the down-regulation of lncRNA H19. The effect of H19 has not yet been conclusively clarified. This thesis presents a possible effect of H19, which could be mediated by two miRNAs that are excised from its sequence. In basal differentiation of MSCs, miRNA 675-5p is up-regulated along with H19, while miRNA 675-3p is continuously down-regulated. Visfatin stimulation during OD down-regulated miRNA 675-5p as well as lncRNA H19, while miRNA 675-3p was inversely up-regulated.

This study confirms the up-regulation of lncRNA H19 in osteogenic differentiation of MSCs, as has been previously published by other groups [147, 149]. It could not, however, reproduce a down-regulation of H19 in adipogenic differentiation of MSCs [174–176].

In this thesis, a new potential regulatory pathway for the effects of visfatin-stimulation during OD could be demonstrated, via the regulation of lncRNA H19 expression. Previously described pathways for H19 downstream signaling, the WNT and TGFβ1 pathways, could not be substantially evaluated in our experiments [147, 155]. We could, however, demonstrate a novel pathway showing the differential regulation of lncRNA H19 and its endogenous micro RNAs 675-3p and -5p upon visfatin stimulation. These micro RNAs may also represent a novel mechanism influencing OD in in healthy patients and those with diseases associated with an increased visfatin load such as OA and chronic-inflammatory RA.

Taken together, the research questions of this thesis can be answered as follows:

Do adipokines affect the regulation of lncRNA H19 during the course of OD? The results presented in this thesis demonstrate, how the adipokine visfatin affects the regulation of lncRNA H19 during osteogenesis. In unstimulated cells, lncRNA H19 is continuously up-regulated over the course of OD. Upon visfatin-stimulation, however, H19 is down-regulated.

Is lncRNA H19 differentially regulated in adipogenic differentiation of MSCs? In MSCs undergoing adipogenic differentiation, a similar but less prominent reduction of H19 levels could be observed at the late time points of AD.

Is the differential regulation of lncRNA H19 a visfatin-specific effect? The observed effects were compared to both stimulation of differentiating MSCs with two other key immunoregulatory adipokines, leptin and resistin, as well as the pro-inflammatory cytokine TNFα. In neither of these settings, a similar regulation could be observed. The regulation of lncRNA H19 seems therefore to be a specific effect of visfatin that is not caused by other adipokines or other pro-inflammatory stimuli.

What is the mechanism of lncRNA H19 affecting osteogenic differentiation? One known effector mechanism of lncRNA H19 is the release of micro RNAs encoded in the H19 RNA-sequence: miRNAs 675-3p and -5p. A previously unknown effect of visfatin on the regulation of these miRNAs was demonstrated in this thesis. Upon visfatin stimulation, both lncRNA H19 and miRNA 675-5p were down-regulated, whereas miRNA 675-3p was up-regulated. As micro RNAs have been shown to play a role in "fine tuning" gene expression, this regulatory axis could further help to explain the changes in osteoblast phenotype upon visfatin stimulation.

Part VII. Summary / Zusammenfassung

32 Short Summary

In rheumatic diseases, the delicate balance between bone remodeling, formation and degradation is disbalanced by mechanical stress, inflammatory factors and other mediators. Visfatin is expressed as a pro-inflammatory adipocytokine in adipose tissue and influences osteogenic and adipogenic differentiation of mesenchymal stromal cells (MSCs). Dr. Tsiklauri from our research group was able to show, how the altered production of matrix components, matrix metalloproteinases and inflammatory mediators of differentiated osteoblasts leads to the formation of an osteoporotic bone structure.

The aim of this thesis was to investigate the role of long non-coding (lnc-)RNA as a potential pathway in the regulation of osteogenesis and matrix production by visfatin. lncRNAs are RNA molecules over 200 nucleotides in length. They are transcribed and processed analogously to 'classical' messenger RNA, but are not translated into proteins. Instead, as 'RNA molecules', they directly regulate gene expression, RNA-protein interaction and other metabolic processes. In the context of osteogenesis, lncRNA H19 was of particular interest, as it was shown to be up-regulated in healthy bone in the course of osteogenic differentiation.

For this purpose, MSCs from healthy donors and osteoarthritis patients from our biobank were brought to osteogenic differentiation and examined. The increased expression of H19 during differentiation described in the literature could be confirmed. When stimulated simultaneously with visfatin, this up-regulation was suppressed. Other investigated adipokines (leptin and resistin) and inflammatory mediators (TNFα) did not show this effect. H19 itself contains the micro-RNAs 675-3p and -5p in its nucleotide sequence. In the experiment, it could be shown that although 'total' H19 as well as -5p were suppressed by visfatin, whereas miRNA 675-3p was up-regulated.

This demonstration of the down-regulation of lncRNA H19 and miRNA 675-5p as well as the increased expression of miRNA 675-3p can contribute to the understanding of the matrix changes in the inflammatory milieu of rheumatoid diseased bone.

33 Kurzzusammenfassung

In rheumatischen Erkrankungen gerät das diffizile Gleichgewicht zwischen Um-, Auf- und Abbau des Knochens durch mechanischen Stress, Entzündungsfaktoren und andere Mediatoren aus der Waage. Visfatin wird als pro-inflammatorisches Adipo*zyto*kin im Fettgewebe exprimiert und beeinflusst die osteogene und adipogene Differenzierung mesenchymaler Stromazellen (MSCs). Dr. Tsiklauri aus unserer Arbeitsgruppe konnte zeigen, wie die so veränderte Produktion von Matrixbestandteilen, Matrixmetalloproteinasen und Entzündungsmediatoren differenzierter Osteoblasten zum Aufbau einer osteoporotischen Knochenstruktur führt.

Ziel dieser Arbeit war es, die Rolle von Long non-coding (lnc-)RNA als möglichen Faktor dieser Regulation der Differenzierung und Matrixproduktion durch Visfatin zu untersuchen. lncRNAs sind RNA Moleküle mit über 200 Nukleotiden Länge. Sie werden analog zu 'klassischer' messenger-RNA transkribiert und prozessiert, jedoch nicht in Proteine translatiert. Statt dessen regulieren sie als 'RNA-Moleküle' direkt die Genexpression, die RNA-Protein-Interaktion und andere Stoffwechselprozesse. Im Rahmen der Osteogenese war insbesondere lncRNA H19 von besonderem Interesse, die im gesunden Knochen im Laufe der osteogenen Differenzierung vermehrt exprimiert wird.

Hierzu wurden MSCs gesunder Spender sowie von Arthrose-Patienten aus unserer Biobank zur osteogenen Differenzierung gebracht und untersucht. Die in der Literatur beschriebene vermehrte Expression von H19 im Laufe der Differenzierung konnte bestätigt werden. Bei gleichzeitiger Stimulation mit Visfatin war diese Hochregulation unterdrückt. Andere untersuchte Adipokine (Leptin und Resistin) und Entzündungsmediatoren (TNFα) zeigten diesen Effekt nicht.

H19 selbst beinhaltet die micro-RNAs 675-3p und -5p in seiner Nukleotidsequenz. Im Experiment konnte gezeigt werden, dass zwar die 'gesamte' H19 sowie -5p durch Visfatin unterdrückt werden, miRNA 675-3p jedoch vermehrt vorliegt.

Die dargestellte Herabregulation von lncRNA H19 und miRNA 675-5p sowie die vermehrte Expression von 675-3p kann somit zu einem tieferen Verständnis der Matrixveränderung im entzündlichen Milieu des rheumatisch erkrankten Knochens beitragen.

Part VIII. Nomenclature, Lists of Tables and Figures

Nomenclature

ASC	adipose-derived stem cells
HDAC	Histone deacetylase
hMSCs	human MSCs, commertially obtained
ICR	imprinting control region
IGF	Insulin-like growth factor
IL-6	Interleukin 6
lncRNA	long non-coding RNA
M-CSF	macrophage colony-stimulation factor
MMPs	matrix metalloproteases
mRNA	messenger RNA
ncRNA	non(-protein) coding RNA
OAOB	Osteoarthritis Osteoblast
OP	Osteoporosis
phMSCs	primary human MSCs
RAOB	Rheumatoid Arthritis Osteoblast
rRNA	ribosomal RNA
SMAD	Group of signal transducers of TGF-beta-receptors.
SRP RNA	signal recognition particles
TGFβ1	Transforming growth factor β (beta) 1
TNFα	Tumor necrosis factor α (alpha)
tRNA	transfer RNA
β-Catenin	β-(beta)-Catenin, cadherin-associated protein

List of Tables

List of Figures

Part IX. Bibliography

References

1. Neogi T and Zhang Y. Epidemiology of Osteoarthritis. Rheum. Dis. Clin. North Am. 2013;39:1–19.
2. Simard JF, Neovius M, et al. Mortality rates in patients with rheumatoid arthritis treated with tumor necrosis factor inhibitors: Drug-specific comparisons in the Swedish Biologics Register. Arthritis Rheum. 2012;64:3502–10.
3. Chaparro del Moral R, Rillo OL, et al. Work Productivity in Rheumatoid Arthritis: Relationship with Clinical and Radiological Features. Arthritis 2012:1–7.
4. Aigner T, Schmitz N, et al. Pathogenesis and pathology of osteoarthritis. In: *Rheumatol. Sixth Ed.* Ed. by Hochberg MC, Silman AJ, et al. Vol. 2-2. Philadelphia: Elsevier, 2015:1462–76.
5. Junker S, Krumbholz G, et al. Differentiation of osteophyte types in osteoarthritis â proposal of a histological classification. Jt. Bone Spine 2016;83:63–7.
6. Meunier P, Aaron J, et al. Osteoporosis and the replacement of cell populations of the marrow by adipose tissue. A quantitative study of 84 iliac bone biopsies. Clin. Orthop. Relat. Res. 1971;80:147–54.
7. Justesen J, Stenderup K, et al. Adipocyte tissue volume in bone marrow is increased with aging and in patients with osteoporosis. Biogerontology 2001;2:165–71.
8. Moerman EJ, Teng K, et al. Aging activates adipogenic and suppresses osteogenic programs in mesenchymal marrow stroma/stem cells: The role of PPAR-γ2 transcription factor and TGF-β/BMP signaling pathways. Aging Cell 2004;3:379–89.
9. Kay J and Upchurch KS. ACR/EULAR 2010 rheumatoid arthritis classification criteria. Rheumatol. (United Kingdom) 2012;51:vi5–vi9.
10. Neumann E, Frommer K, et al. Rheumatoid arthritis. Z. Rheumatol. 2018;77:769–75.
11. Health Effects of Overweight and Obesity in 195 Countries over 25 Years. N. Engl. J. Med. 2017;377:13–27.
12. Singh GM, Danaei G, et al. The age-specific quantitative effects of metabolic risk factors on cardiovascular diseases and diabetes: A pooled analysis. PLoS One 2013;8. Ed. by Wang G:e65174.
13. Jiang L, Rong J, et al. The relationship between body mass index and hip osteoarthritis: A systematic review and meta-analysis. Jt. Bone Spine 2011;78:150–5.
14. Jiang L, Tian W, et al. Body mass index and susceptibility to knee osteoarthritis: A systematic review and meta-analysis. Jt. Bone Spine 2012;79:291–7.
15. Lauby-Secretan B, Scoccianti C, et al. Body Fatness and Cancer - Viewpoint of the IARC Working Group. N. Engl. J. Med. 2016;375:794–8.
16. Garn H, Bahn S, et al. Current concepts in chronic inflammatory diseases: Interactions between microbes, cellular metabolism, and inflammation. J. Allergy Clin. Immunol. 2016;138:47–56.

17. Trayhurn P, Bing C, et al. Adipose tissue and adipokines - Energy regulation from the human perspective. J. Nutr. 2006;136:1935S–1939S.

18. Arita Y, Kihara S, et al. Paradoxical decrease of an adipose-specific protein, adiponectin, in obesity. Biochem. Biophys. Res. Commun. 1999;257:79–83.

19. Cancello R and Clément K. Is obesity an inflammatory illness? Role of low-grade inflammation and macrophage infiltration in human white adipose tissue. BJOG An Int. J. Obstet. Gynaecol. 2006;113:1141–7.

20. Frommer KW, Zimmermann B, et al. Adiponectin-mediated changes in effector cells involved in the pathophysiology of rheumatoid arthritis. Arthritis Rheum. 2010;62:2886–99.

21. Frommer KW, Schäffler A, et al. Adiponectin isoforms: A potential therapeutic target in rheumatoid arthritis? Ann. Rheum. Dis. 2012;71:1724–32.

22. Meier FM, Frommer KW, et al. Visfatin/pre-B-cell colony-enhancing factor (PBEF), a proinflammatory and cell motility-changing factor in rheumatoid arthritis. J. Biol. Chem. 2012;287:28378–85.

23. Frommer KW, Schäffler A, et al. Free fatty acids: Potential proinflammatory mediators in rheumatic diseases. Ann. Rheum. Dis. 2015;74:303–10.

24. Junker S, Frommer KW, et al. Expression of adipokines in osteoarthritis osteophytes and their effect on osteoblasts. Matrix Biol. 2017;62:75–91.

25. Krumbholz G, Junker S, et al. Response of human rheumatoid arthritis osteoblasts and osteoclasts to adiponectin. Clin. Exp. Rheumatol. 2017;35:406–414.

26. Carrión M, Frommer KW, et al. The adipokine network in rheumatic joint diseases. Int. J. Mol. Sci. 2019;20.

27. Byers Kraus V and Doherty M. Chapter 9: Osteoarthritis. In: *ABC Rheumatol.* Ed. by Dunkley L and Adebajo A. 2018.

28. McAlindon T, Formica M, et al. Changes in Barometric Pressure and Ambient Temperature Influence Osteoarthritis Pain. Am. J. Med. 2007;120:429–34.

29. Altman RD. Clinical features of osteoarthritis. In: *Rheumatol. Sixth Ed.* Ed. by Hochberg MC, Silman AJ, et al. Vol. 2. 2015:1447–53.

30. Sakellariou G, Conaghan PG, et al. EULAR recommendations for the use of imaging in the clinical management of peripheral joint osteoarthritis. Ann. Rheum. Dis. 2017;76:1484–94.

31. Sulzbacher I. Osteoarthritis: Histology and pathogenesis. Wiener Medizinische Wochenschrift 2013;163:212–9.

32. Rausch Osthoff AK, Niedermann K, et al. 2018 EULAR recommendations for physical activity in people with inflammatory arthritis and osteoarthritis. Ann. Rheum. Dis. 2018;77:1251–60.

33. Geenen R, Overman CL, et al. EULAR recommendations for the health professional's approach to pain management in inflammatory arthritis and osteoarthritis. Ann. Rheum. Dis. 2018;77:797–807.

34. Hochberg MC and Dougados M. Pharmacological therapy of osteoarthritis. Best Pract. Res. Clin. Rheumatol. 2001;15:583–93.

35. Pritzker KP, Gay S, et al. Osteoarthritis cartilage histopathology: Grading and staging. Osteoarthr. Cartil. 2006;14:13–29.

36. Al-Suhaimi EA and Shehzad A. Leptin, resistin and visfatin: The missing link between endocrine metabolic disorders and immunity. Eur. J. Med. Res. 2013;18.

37. Long F. Building strong bones: Molecular regulation of the osteoblast lineage. Nat. Rev. Mol. Cell Biol. 2012;13:27–38.

38. Meczekalski B, Podfigurna-Stopa A, et al. Hypoestrogenism in young women and its influence on bone mass density. Gynecol. Endocrinol. 2010;26:652–7.

39. Bianco P, Robey PG, et al. Mesenchymal Stem Cells: Revisiting History, Concepts, and Assays. Cell Stem Cell 2008;2:313–9.

40. Friedenstein AJ, Chailakhyan RK, et al. Bone marrow osteogenic stem cells: in vitro cultivation and transplantation in diffusion chambers. Cell Prolif. 1987;20:263–72.

41. D'Ippolito G, Diabira S, et al. Low oxygen tension inhibits osteogenic differentiation and enhances stemness of human MIAMI cells. Bone 2006;39:513–22.

42. Pittenger MF, Mackay AM, et al. Multilineage potential of adult human mesenchymal stem cells. Science (80-.). 1999;284:143–7.

43. Bobis S, Jarocha D, et al. Mesenchymal stem cells: Characteristics and clinical applications. Folia Histochem. Cytobiol. 2006;44:215–30.

44. Kern S, Eichler H, et al. Comparative Analysis of Mesenchymal Stem Cells from Bone Marrow, Umbilical Cord Blood, or Adipose Tissue. Stem Cells 2006;24:1294–301.

45. Digirolamo CM, Stokes D, et al. Propagation and senescence of human marrow stromal cells in culture: A simple colony-forming assay identifies samples with the greatest potential to propagate and differentiate. Br. J. Haematol. 1999;107:275–81.

46. Vacanti V, Kong E, et al. Phenotypic changes of adult porcine mesenchymal stem cells induced by prolonged passaging in culture. J. Cell. Physiol. 2005;205:194–201.

47. Heino T and Hentunen T. Differentiation of Osteoblasts and Osteocytes from Mesenchymal Stem Cells. Curr. Stem Cell Res. Ther. 2008;3:131–45.

48. Funahashi T, Nakamura T, et al. Role of adipocytokines on the pathogenesis of atherosclerosis in visceral obesity. Intern. Med. 1999;38:202–6.

49. Trayhurn P and Wood IS. Adipokines: inflammation and the pleiotropic role of white adipose tissue. Br. J. Nutr. 2004;92:347–55.

50. Zhang Y, Proenca R, et al. Positional cloning of the mouse obese gene and its human homologue. Nature 1994;372:425–32.

51. Conde J, Scotece M, et al. Adipokines: Biofactors from white adipose tissue. A complex hub among inflammation, metabolism, and immunity. BioFactors 2011;37:413–20.

52. Seven A, Güzel S, et al. Serum and synovial fluid leptin levels and markers of inflammation in rheumatoid arthritis. Rheumatol. Int. 2009;29:743–7.

53. Otero M, Logo R, et al. Changes in plasma levels of fat-derived hormones adiponectin, leptin, resistin and visfatin in patients with rheumatoid arthritis. Ann. Rheum. Dis. 2006;65:1198–201.

54. Otero M, Lago R, et al. Signalling pathway involved in nitric oxide synthase type II activation in chondrocytes: synergistic effect of leptin with interleukin-1. Arthritis Res. Ther. 2005;7.

55. Hotamisligil GS, Shargill NS, et al. Adipose Expression of Tumor Necrosis Factor-α: Direct Role in Obesity-Linked Insulin Resistance. Science (80-.). 1993;259:87–91.

56. Mohamed-Ali V, Goodrick S, et al. Subcutaneous adipose tissue releases interleukin-6, but not tumor necrosis factor-α, in vivo. J. Clin. Endocrinol. Metab. 1997;82:4196–200.

57. Wellen KE and Hotamisligil GS. Inflammation, stress, and diabetes. J. Clin. Invest. 2005;115:1111–9.

58. Fried SK, Bunkin DA, et al. Omental and subcutaneous adipose tissues of obese subjects release interleukin-6: Depot difference and regulation by glucocorticoid. J. Clin. Endocrinol. Metab. 1998;83:847–50.

59. Poitou C, Viguerie N, et al. Serum amyloid A: Production by human white adipocyte and regulation by obesity and nutrition. Diabetologia 2005;48:519–28.

60. Chiellini C, Bertacca A, et al. Obesity modulates the expression of haptoglobin in the white adipose tissue via TNFα. J. Cell. Physiol. 2002;190:251–8.

61. Coleman DL. Effects of parabiosis of obese with diabetes and normal mice. Diabetologia 1973;9:294–8.

62. Muoio DM and Dohm GL. Peripheral metabolic actions of leptin. Best Pract. Res. Clin. Endocrinol. Metab. 2002;16:653–66.

63. Koerner A, Kratzsch J, et al. Adipocytokines: Leptin - The classical, resistin - The controversical, adiponectin - The promising, and more to come. Best Pract. Res. Clin. Endocrinol. Metab. 2005;19:525–46.

64. Dalamaga M, Chou SH, et al. Leptin at the intersection of neuroendocrinology and metabolism: Current evidence and therapeutic perspectives. Cell Metab. 2013;18:29–42.

65. Juge-Aubry CE and Meier CA. Immunomodulatory actions of leptin. Mol. Cell. Endocrinol. 2002;194:1–7.

66. Toussirot É, Michel F, et al. The role of leptin in the pathophysiology of rheumatoid arthritis. Life Sci. 2015;140:29–36.

67. Yan M, Zhang J, et al. The role of leptin in osteoarthritis. Med. (United States) 2018;97:e0257.

68. Steppan CM, Bailey ST, et al. The hormone resistin links obesity to diabetes. Nature 2001;409:307–12.

69. Thommesen L, Stunes AK, et al. Expression and regulation of resistin in osteoblasts and osteoclasts indicate a role in bone metabolism. J. Cell. Biochem. 2006;99:824–34.

70. Silswal N, Singh AK, et al. Human resistin stimulates the pro-inflammatory cytokines TNF-α and IL-12 in macrophages by NF-κB-dependent pathway. Biochem. Biophys. Res. Commun. 2005;334:1092–101.

71. Plotkin SA. Natural vs vaccine-acquired immunity to cytomegalovirus. JAMA 2003;290:1709, author reply 1709.

72. Neumann E, Frommer KW, et al. Adipocytokines as driving forces in rheumatoid arthritis and related inflammatory diseases? Arthritis Rheum. 2011;63:1159–69.

73. Schwartz DR and Lazar MA. Human resistin: Found in translation from mouse to man. 2011.

74. Samal B, Sun Y, et al. Cloning and characterization of the cDNA encoding a novel human pre-B-cell colony-enhancing factor. Mol. Cell. Biol. 1994;14:1431–7.

75. Ying W. NAD+/NADH and NADP+/NADPH in cellular functions and cell death: Regulation and biological consequences. Antioxidants Redox Signal. 2008;10:179–206.

76. Kim MK, Lee JH, et al. Crystal Structure of Visfatin/Pre-B Cell Colony-enhancing Factor 1/Nicotinamide Phosphoribosyltransferase, Free and in Complex with the Anti-cancer Agent FK-866. J. Mol. Biol. 2006;362:66–77.

77. Haider DG, Schindler K, et al. Increased plasma visfatin concentrations in morbidly obese subjects are reduced after gastric banding. J. Clin. Endocrinol. Metab. 2006;91:1578–81.

78. Chen MP, Chung FM, et al. Elevated plasma level of visfatin/pre-B cell colony-enhancing factor in patients with type 2 diabetes mellitus. J. Clin. Endocrinol. Metab. 2006;91:295–9.

79. Sandeep S, Velmurugan K, et al. Serum visfatin in relation to visceral fat, obesity, and type 2 diabetes mellitus in Asian Indians. Metabolism. 2007;56:565–70.

80. Krzysik-Walker SM, Ocón-Grove OM, et al. Is visfatin an adipokine or myokine? Evidence for greater visfatin expression in skeletal muscle than visceral fat in chickens. Endocrinology 2008;149:1543–50.

81. Revollo JR, Körner A, et al. Nampt/PBEF/Visfatin Regulates Insulin Secretion in β Cells as a Systemic NAD Biosynthetic Enzyme. Cell Metab. 2007;6:363–75.

82. Garten A, Petzold S, et al. Nicotinamide phosphoribosyltransferase (NAMPT / PBEF / visfatin) is constitutively released from human hepatocytes. Biochem. Biophys. Res. Commun. 2010;391:376–81.

83. Costford SR, Bajpeyi S, et al. Skeletal muscle NAMPT is induced by exercise in humans. Am. J. Physiol. - Endocrinol. Metab. 2010;298:E117–E126.

84. Škop V, Kontrová K, et al. Autocrine effects of visfatin on hepatocyte sensitivity to insulin action. Physiol. Res. 2010;59:615–8.

85. Rongvaux A, She RJ, et al. Pre-B-cell colony-enhancing factor, whose expression is up-regulated in activated lymphocytes, is a nicotinamide phosphoribosyltransferase, a cytosolic enzyme involved in NAF biosynthesis. Eur. J. Immunol. 2002;32:3225–34.

86. Song TY, Yeh SL, et al. A Nampt inhibitor FK866 mimics vitamin B3 deficiency by causing senescence of human fibroblastic Hs68 cells via attenuation of NAD+-SIRT1 signaling. Biogerontology 2015;16:789–800.

87. Teixeira da Silva JA and Dobránszki J. Highly cited retracted papers. Scientometrics 2017;110:1653–61.

88. Chen H, Jiang GX, et al. Retraction: Post-operative neuropathy after total hip arthroplasty. Bone Joint J. 2017;99-B:702–4.

89. Sethi JK and Vidal-Puig A. Visfatin: The missing link between intra-abdominal obesity and diabetes? Trends Mol. Med. 2005;11:344–7.

90. Xie H, Tang SY, et al. Insulin-like effects of visfatin on human osteoblasts. Calcif. Tissue Int. 2007;80:201–10.

91. Moschen AR, Kaser A, et al. Visfatin, an Adipocytokine with Proinflammatory and Immunomodulating Properties. J. Immunol. 2007;178:1748–58.

92. Kishimoto T. The biology of interleukin-6. Blood 1989;74:1–10.

93. Wang GJ, Shen NJ, et al. Visfatin triggers the in vitro migration of osteosarcoma cells via activation of NF-κB/IL-6 signals. Eur. J. Pharmacol. 2016;791:322–30.

94. Wu MH, Tsai CH, et al. Visfatin promotes IL-6 and TNF-α production in human synovial fibroblasts by repressing miR-199a-5p through ERK, p38 and JNK signaling pathways. Int. J. Mol. Sci. 2018;19.

95. Kristiansen OP and Mandrup-Poulsen T. Interleukin-6 and diabetes: The good, the bad, or the indifferent? Diabetes 2005;54:S114–S124.

96. Dubiński A and Zdrojewicz Z. The role of interleukin-6 in development and progression of atherosclerosis. Pol. Merkur. Lek. 2007;22:291–4.

97. Tackey E, Lipsky PE, et al. Rationale for interleukin-6 blockade in systemic lupus erythematosus. Lupus 2004;13:339–43.

98. Hirohata S and Kikuchi H. Changes in Biomarkers Focused on Differences in Disease Course or Treatment in Patients with Neuro-Behçet's Disease. Intern. Med. 2012;51:3359–65.

99. Nishimoto N. Interleukin-6 in rheumatoid arthritis. Curr. Opin. Rheumatol. 2006;18:277–81.

100. Dowlati Y, Herrmann N, et al. A Meta-Analysis of Cytokines in Major Depression. Biol. Psychiatry 2010;67:446–57.

101. Swardfager W, Lanctt K, et al. A meta-analysis of cytokines in Alzheimer's disease. Biol. Psychiatry 2010;68:930–41.

102. Gadó K, Domján G, et al. Role of interleukin-6 in the pathogenesis of multiple myeloma. Cell Biol. Int. 2000;24:195–209.

103. Smith PC, Hobisch A, et al. Interleukin-6 and prostate cancer progression. Cytokine Growth Factor Rev. 2001;12:33–40.

104. Chen WP, Bao JP, et al. Increased serum concentrations of visfatin and its production by different joint tissues in patients with osteoarthritis. Clin. Chem. Lab. Med. 2010;48:1141–5.

105. Laiguillon MC, Houard X, et al. Expression and function of visfatin (Nampt), an adipokine-enzyme involved in inflammatory pathways of osteoarthritis. Arthritis Res. Ther. 2014;16.

106. Duan Y, Hao D, et al. Increased synovial fluid visfatin is positively linked to cartilage degradation biomarkers in osteoarthritis. Rheumatol. Int. 2012;32:985–90.

107. Calvet J, Orellana C, et al. Synovial fluid adipokines are associated with clinical severity in knee osteoarthritis: A cross-sectional study in female patients with joint effusion. Arthritis Res. Ther. 2016;18.

108. Fioravanti A, Giannitti C, et al. Circulating levels of adiponectin, resistin, and visfatin after mud-bath therapy in patients with bilateral knee osteoarthritis. Int. J. Biometeorol. 2015;59:1691–700.

109. Tsiklauri L, Werner J, et al. Visfatin alters the cytokine and matrix-degrading enzyme profile during osteogenic and adipogenic MSC differentiation. Osteoarthr. Cartil. 2018;26:1225–35.

110. McNulty AL, Miller MR, et al. The effects of adipokines on cartilage and meniscus catabolism. Connect. Tissue Res. 2011;52:523–33.

111. He X, He J, et al. Nicotinamide phosphoribosyltransferase (Nampt) may serve as the marker for osteoblast differentiation of bone marrow-derived mesenchymal stem cells. Exp. Cell Res. 2017;352:45–52.

112. Li Y, He X, et al. Nicotinamide phosphoribosyltransferase (Nampt) affects the lineage fate determination of mesenchymal stem cells: A possible cause for reduced osteogenesis and increased adipogenesis in older individuals. J. Bone Miner. Res. 2011;26:2656–64.

113. Martin L and Chang HY. Uncovering the role of genomic "dark matter" in human disease. J. Clin. Invest. 2012;122:1589–95.

114. Brannan CI, Dees EC, et al. The product of the H19 gene may function as an RNA. Mol. Cell. Biol. 1990;10:28–36.

115. Rinn JL and Chang HY. Genome regulation by long noncoding RNAs. Annu. Rev. Biochem. 2012;81:145–66.

116. Monticelli S, Ansel KM, et al. Regulation of gene expression in mast cells: MicroRNA expression and chromatin structural analysis of cytokine genes. In: *Novartis Found. Symp.* Vol. 271. 2005:179–87.

117. Kishore S and Stamm S. Regulation of alternative splicing by snoRNAs. In: *Cold Spring Harb. Symp. Quant. Biol.* Vol. 71. 2006:329–34.

118. St.Laurent G, Wahlestedt C, et al. The Landscape of long noncoding RNA classification. Trends Genet. 2015;31:239–51.

119. Ma L, Bajic VB, et al. On the classification of long non-coding RNAs. RNA Biol. 2013;10:924–33.

120. Smith CM, Catchpoole D, et al. Non-Coding RNAs in Pediatric Solid Tumors. Front. Genet. 2019;10.

121. Li Z, Hassan MQ, et al. Biological functions of miR-29b contribute to positive regulation of osteoblast differentiation. J. Biol. Chem. 2009;284:15676–84.

122. Chen L, HolmstrØm K, et al. MicroRNA-34a inhibits osteoblast differentiation and in vivo bone formation of human stromal stem cells. Stem Cells 2014;32:902–12.

123. Eskildsen T, Taipaleenmäki H, et al. MicroRNA-138 regulates osteogenic differentiation of human stromal (mesenchymal) stem cells in vivo. Proc. Natl. Acad. Sci. U. S. A. 2011;108:6139–44.

124. Hwang S, Park SK, et al. MiR-140-5p suppresses BMP2-mediated osteogenesis in undifferentiated human mesenchymal stem cells. FEBS Lett. 2014;588:2957–63.

125. Kureel J, Dixit M, et al. MiR-542-3p suppresses osteoblast cell proliferation and differentiation, targets BMP-7 signaling and inhibits bone formation. Cell Death Dis. 2014;5.

126. Cai X and Cullen BR. The imprinted H19 noncoding RNA is a primary microRNA precursor. Rna 2007;13:313–6.

127. Frankish A, Diekhans M, et al. Gencode 2021. Nucleic Acids Res. 2021;49:D916–D923.

128. Ma L, Cao J, et al. Lncbook: A curated knowledgebase of human long non-coding rnas. Nucleic Acids Res. 2019;47:D128–D134.

129. Guttman M, Amit I, et al. Chromatin signature reveals over a thousand highly conserved large non-coding RNAs in mammals. Nature 2009;458:223–7.

130. Wilusz JE, Freier SM, et al. 3' end processing of a long nuclear-retained noncoding RNA yields a tRNA-like cytoplasmic RNA. Cell 2008;135:919–32.

131. Huynh NP, Anderson BA, et al. Emerging roles for long noncoding RNAs in skeletal biology and disease. Connect. Tissue Res. 2017;58:116–41.

132. Zhang Y, Zhang XO, et al. Circular Intronic Long Noncoding RNAs. Mol. Cell 2013;51:792–806.

133. Wang KC and Chang HY. Molecular Mechanisms of Long Noncoding RNAs. Mol. Cell 2011;43:904–14.

134. Hurst LD and Smith NG. Molecular evolutionary evidence that H19 mRNA is functional. Trends Genet. 1999;15:134–5.

135. Poirier F, Chan CT, et al. The murine H19 gene is activated during embryonic stem cell differentiation in vitro and at the time of implantation in the developing embryo. Development 1991;113:1105–14.

136. Gabory A, Jammes H, et al. The H19 locus: Role of an imprinted non-coding RNA in growth and development. BioEssays 2010;32:473–80.

137. Gabory A, Ripoche MA, et al. H19 acts as a trans regulator of the imprinted gene network controlling growth in mice. Development 2009;136:3413–21.

138. Wu K feng, Liang WC, et al. H19 mediates methotrexate resistance in colorectal cancer through activating Wnt/β-catenin pathway. Exp. Cell Res. 2017;350:312–7.

139. Rafiee A, Riazi-Rad F, et al. Long noncoding RNAs: regulation, function and cancer. Biotechnol. Genet. Eng. Rev. 2018;34:153–80.

140. O'Brien SJ, Scheurlen K, et al. Increased Expression of Long Non-coding RNA H19 is Associated With Colon Cancer Recurrence. J. Surg. Res. 2022;269:59–68.

141. Chen S, Sun Z, et al. Whole transcriptome analysis of long noncoding RNA in beryllium sulfate-treated 16HBE cells. Toxicol. Appl. Pharmacol. 2022;449:116097.

142. Stuhlmüller B, Kunisch E, et al. Detection of oncofetal H19 RNA in rheumatoid arthritis synovial tissue. Am. J. Pathol. 2003;163:901–11.

143. Zhang Y and Tycko B. Monoallelic expression of the human H19 gene. Nat. Genet. 1992;1:40–4.

144. Keniry A, Oxley D, et al. The H19 lincRNA is a developmental reservoir of miR-675 that suppresses growth and Igf1r. Nat. Cell Biol. 2012;14:659–65.

145. Dey BK, Pfeifer K, et al. The H19 long noncoding RNA gives rise to microRNAs miR-675-3p and miR-675-5p to promote skeletal muscle differentiation and regeneration. Genes Dev. 2014;28:491–501.

146. Zhou YW, Zhang H, et al. miR-675-5p enhances tumorigenesis and metastasis of esophageal squamous cell carcinoma by targeting REPS2. Oncotarget 2016;7:30730–47.

147. Liang WC, Fu WM, et al. H19 activates Wnt signaling and promotes osteoblast differentiation by functioning as a competing endogenous RNA. Sci. Rep. 2016;6:20121.

148. Vennin C, Spruyt N, et al. The long non-coding RNA 91H increases aggressive phenotype of breast cancer cells and up-regulates H19/IGF2 expression through epigenetic modifications. Cancer Lett. 2017;385:198–206.

149. Wang L, Wang Y, et al. Differential expression of long noncoding ribonucleic acids during osteogenic differentiation of human bone marrow mesenchymal stem cells. Int. Orthop. 2015;39:1013–9.

150. Li Z, Hong Z, et al. An emerging potential therapeutic target for osteoporosis: LncRNA H19/miR-29a-3p axis. Eur. J. Histochem. 2020;64:279–84.

151. Wang Z, Feng C, et al. lncRNA-H19/miR-29a axis affected the viability and apoptosis of keloid fibroblasts through acting upon COL1A1 signaling. J. Cell. Biochem. 2020;121:4364–76.

152. Yang B, Xu L, et al. Regulation of lncrna-h19/mir-140-5p in cartilage matrix degradation and calcification in osteoarthritis. Ann. Palliat. Med. 2020;9:1896–904.

153. Huang G, Kang Y, et al. Identification and Characterization of Long Non-Coding RNAs in Osteogenic Differentiation of Human Adipose-Derived Stem Cells. Cell. Physiol. Biochem. 2017;42:1037–50.

154. Zhu Y, Gui W, et al. Knock-down of circular RNA H19 induces human adipose-derived stem cells adipogenic differentiation via a mechanism involving the polypyrimidine tract-binding protein 1. Exp. Cell Res. 2020;387:111753.

155. Huang Y, Zheng Y, et al. Long Noncoding RNA H19 Promotes Osteoblast Differentiation Via TGF-β1/Smad3/HDAC Signaling Pathway by Deriving miR-675. Stem Cells 2015;33:3481–92.

156. Lu YF, Liu Y, et al. Long noncoding RNA H19 accelerates tenogenic differentiation & promotes tendon healing through targeting miR-29b-3p & activating TGF-β1 signaling. FASEB J. 2017;31:954–64.

157. Zhu M, Chen Q, et al. LncRNA H19/miR-675 axis represses prostate cancer metastasis by targeting TGFBI. FEBS J. 2014;281:3766–75.

158. Alliston T, Choy L, et al. TGF-β-induced repression of CBFA1 by Smad3 decreases cbfa1 and osteocalcin expression and inhibits osteoblast differentiation. EMBO J. 2001;20:2254–72.

159. Kang JS, Alliston T, et al. Repression of Runx2 function by TGF-β through recruitment of class II histone deacetylases by Smad3. EMBO J. 2005;24:2543–55.

160. Westendorf JJ, Kahler RA, et al. Wnt signaling in osteoblasts and bone diseases. Gene 2004;341:19–39.

161. Monaghan H, Bubb VJ, et al. Adenomatous polyposis coli (APC), β-catenin, and cadherin are expressed in human bone and cartilage. Histopathology 2001;39:611–9.

162. Cheng SU, Lecanda F, et al. Human osteoblasts express a repertoire of cadherins, which are critical for BMP-2-induced osteogenic differentiation. J. Bone Miner. Res. 1998;13:633–44.

163. Nishisho I, Nakamura Y, et al. Mutations of chromosome 5q21 genes in FAP and colorectal cancer patients. Science (80-.). 1991;253:665–9.

164. Kinzler KW, Nilbert MC, et al. Identification of FAP locus genes from chromosome 5q21. Science 1991;253:661–5.

165. Luo M, Li Z, et al. Long non-coding RNA H19 increases bladder cancer metastasis by associating with EZH2 and inhibiting E-cadherin expression. Cancer Lett. 2013;333:213–21.

166. Kallen AN, Zhou XB, et al. The Imprinted H19 LncRNA Antagonizes Let-7 MicroRNAs. Mol. Cell 2013;52:101–12.

167. Liang WC, Fu WM, et al. The LncRNA H19 promotes epithelial to mesenchymal transition by functioning as MiRNA sponges in colorectal cancer. Oncotarget 2015;6:22513–25.

168. Bach DH and Lee SK. Long noncoding RNAs in cancer cells. Cancer Lett. 2018;419:152–66.

169. Delás MJ and Hannon GJ. lncRNAs in development and disease: From functions to mechanisms. Open Biol. 2017;7.

170. Zhang M, Guo JM, et al. Research progress on the effect of long non-coding RNA H19 on osteogenic differentiation and bone diseases. Sheng Li Xue Bao 2018;70:531–8.

171. Wu J, Zhang TP, et al. Decreased h19, gas5, and linc0597 expression and association analysis of related gene polymorphisms in rheumatoid arthritis. Biomolecules 2020;10:55.

172. Ju C, Liu R, et al. Mesenchymal stem cell-associated lncRNA in osteogenic differentiation. Biomed. Pharmacother. 2019;115.

173. Liu XY, Zhang TQ, et al. Differential Long Non-Coding RNA Expression Analysis in Chronic Non-Atrophic Gastritis, Gastric Mucosal Intraepithelial Neoplasia, and Gastric Cancer Tissues. Front. Genet. 2022;13:833857.

174. Huang Y, Zheng Y, et al. Long Non-coding RNA H19 Inhibits Adipocyte Differentiation of Bone Marrow Mesenchymal Stem Cells through Epigenetic Modulation of Histone Deacetylases. Sci. Rep. 2016;6.

175. Wang Y, Liu W, et al. Long noncoding RNA H19 mediates LCoR to impact the osteogenic and adipogenic differentiation of mBMSCs in mice through sponging miR-188. J. Cell. Physiol. 2018;233:7435–46.

176. Zhu Y, Gui W, et al. Knock-down of circular RNA H19 induces human adipose-derived stem cells adipogenic differentiation via a mechanism involving the poly-pyrimidine tract-binding protein 1. Exp. Cell Res. 2020;387:111753.

177. Wang Y, Meng F, et al. Associations between adipokines gene polymorphisms and knee osteoarthritis: a meta-analysis. BMC Musculoskelet. Disord. 2022;23:166.

178. Liao Z, Jin Y, et al. Single-cell transcriptome analysis reveals aberrant stromal cells and heterogeneous endothelial cells in alcohol-induced osteonecrosis of the femoral head. Commun. Biol. 2022;5:324.

179. Shintani N and Hunziker EB. Differential effects of dexamethasone on the chondrogenesis of mesenchymal stromal cells: Influence of microenvironment, tissue origin and growth factor. Eur. Cells Mater. 2011;22:302–20.

180. Raicevic G, Najar M, et al. Inflammation and toll-like receptor ligation differentially affect the osteogenic potential of human mesenchymal stromal cells depending on their tissue origin. Tissue Eng. - Part A 2012;18:1410–8.

181. Li X, Bai J, et al. Comprehensive characterization of four different populations of human mesenchymal stem cells as regards their immune properties, proliferation and differentiation. Int. J. Mol. Med. 2014;34:695–704.

182. Barter M, Ajekigbe B, et al. Identification and characterisation of long non-coding RNAS expressed and dysregulated in knee and hip osteoarthritic cartilage. Osteoarthr. Cartil. 2018;26:S28.

183. Lv D, Su C, et al. Expression of long non-coding RNAs in chondrocytes from proximal interphalangeal joints. Mol. Med. Rep. 2017;16:5175–80.

184. Wang WT, Ye H, et al. LncRNAs H19 and HULC, activated by oxidative stress, promote cell migration and invasion in cholangiocarcinoma through a ceRNA manner. J. Hematol. Oncol. 2016;9:1–12.

185. Yang J, Li Y, et al. LncRNA H19 aggravates TNF-α-induced inflammatory injury via TAK1 pathway in MH7A cells. BioFactors 2020;46:813–20.

186. Zhu Z, Cui Y, et al. Long non-coding RNA H19 promotes osteogenic differentiation of renal interstitial fibroblasts through Wnt-β-catenin pathway. Mol. Cell. Biochem. 2020;470:145–55.

187. Müller V, Oliveira-Ferrer L, et al. Interplay of lncRNA H19/miR-675 and lncRNA NEAT1/miR-204 in breast cancer. Mol. Oncol. 2019;13:1137–49.

188. Zhang T, Lei F, et al. H19/miR-675-5p Targeting SFN Enhances the Invasion and Metastasis of Nasalpharyngeal Cancer Cells. Curr. Mol. Pharmacol. 2019;12:324–33.

Part X. List of Publications

Citeable Abstracts

1. Küppers, D. M. et al. Visfatin down-regulates growth promoting lncrna h19 in osteogenic differentiation of mesenchymal stromal cells. Ann. Rheum. Dis. 2018: 880.3-881
2. Küppers, D. M. et al. Visfatin down-regulates growth promoting lncrna H19 during osteogenic differentiation of mesenchymal stromal cells. Ann. Rheum. Dis. 2019: in Abstracts A52.1-A52
3. Küppers, D. M. et al. Wirkung von Visfatin auf das osteogene Potential mesenchymaler Stromazellen. Internist 2019: 60, 32
4. Küppers, D. M. et al. Visfatin effects on MSCs during OD via differential regulation of lncRNA H19 and micro RNA 675-3p. Ann. Rheum. Dis. 2020: 79, 784 LP – 784
5. Küppers, D. M. et al. lncRNA H19 and Micro RNA 675-3p Are Altered by Visfatin During Osteogenesis. Arthritis Rheumatol. 2020: 72 (suppl 10)

Posters & Presentations

1. - 9. May 2015: **22nd European Conference on Obesity** Prague, Czech Republic
"Barriers to healthy eating among medical students at university hospital and medical school canteens in Germany: results from a cross-sectional study"

3. - 6. June 2015: **Annual Meeting of the Int. Society for Behavioural Nutrition and Physical Activity** Edinburgh, Scotland
"The food environment and choice architecture of German medical faculty and university hospital cafeterias: a multi-method cross-sectional study"

13. - 16. June 2018: **Annual European Congress of Rheumatology 2018** Wiesbaden, Germany
"Visfatin down-regulates growth promoting lncrna h19 in osteogenic differentiation of mesenchymal stromal cells."

4. - 7. May 2019: **125. Kongress der Deutschen Gesellschaft für Innere Medizin** Amsterdam, Netherlands
"Wirkung von Visfatin auf das osteogene Potential mesenchymaler Stromazellen."

28. Feb. - 2. March 2019 **39th European Workshop for Rheumatology Research** Lyon, France
"Visfatin down-regulates growth promoting lncrna H19 during osteogenic differentiation of mesenchymal stromal cells."

9. - 12. Sept. 2020 **Deutscher Rheumatologie-eKongress**
48. Kongress der Deutschen Gesellschaft für Rheumatologie
34. Jahrestagung der Deutschen Gesellschaft für Orthopädische Rheumatologie
"Visfatin alters lncRNA H19 and micro RNA 675-3p during osteogenesis."

From 3. June 2020 **EULAR European e-Congress of Rheumatology**
Poster presentation: "Visfatin effects on MSCs during OD via differential regulation of lncRNA H19 and micro RNA 675-3p."

5. - 9. Nov. 2020 **ACR Convergence 2020**
"lncRNA H19 and Micro RNA 675-3p Are Altered by Visfatin During Osteogenesis."

Part XI. Ehrenwörtliche Erklärung

„Hiermit erkläre ich, dass ich die vorliegende Arbeit selbständig und ohne unzulässige Hilfe oder Benutzung anderer als der angegebenen Hilfsmittel angefertigt habe. Alle Textstellen, die wörtlich oder sinngemäß aus veröffentlichten oder nichtveröffentlichten Schriften entnommen sind, und alle Angaben, die auf mündlichen Auskünften beruhen, sind als solche kenntlich gemacht. Bei den von mir durchgeführten und in der Dissertation erwähnten Untersuchungen habe ich die Grundsätze guter wissenschaftlicher Praxis, wie sie in der „Satzung der Justus-Liebig-Universität Gießen zur Sicherung guter wissenschaftlicher Praxis“ niedergelegt sind, eingehalten. Ich versichere, dass Dritte von mir weder unmittelbar noch mittelbar geldwerte Leistungen für Arbeiten erhalten haben, die im Zusammenhang mit dem Inhalt der vorgelegten Dissertation stehen, und dass die vorgelegte Arbeit weder im Inland noch im Ausland in gleicher oder ähnlicher Form einer anderen Prüfungsbehörde zum Zweck einer Promotion oder eines anderen Prüfungsverfahrens vorgelegt wurde. Alles aus anderen Quellen und von anderen Personen übernommene Material, das in der Arbeit verwendet wurde oder auf das direkt Bezug genommen wird, wurde als solches kenntlich gemacht. Insbesondere wurden alle Personen genannt, die direkt an der Entstehung der vorliegenden Arbeit beteiligt waren. Mit der Überprüfung meiner Arbeit durch eine Plagiatserkennungssoftware bzw. ein internetbasiertes Softwareprogramm erkläre ich mich einverstanden.“

Datum: Gießen, den _____

Unterschrift: _____

Part XII. Danksagung

Diese Dissertation entstand am Institut für Rheumatologie und klinische Immunologie des Lehrstuhls für Innere Medizin mit Schwerpunkt Rheumatologie der Justus-Liebig-Universität Giessen. Ich möchte an dieser Stelle von Herzen all den Menschen danken, die seit Beginn dieser Arbeit zu ihrem Gelingen beigetragen haben.

Prof. Dr. Ulf Müller Ladner und sein Team in Klinik und Labor haben diese Arbeit erst ermöglicht. Ich danke ihm für die Einblicke in die klinische Arbeit und die Ermutigung zu Veröffentlichungen und der Teilnahme an Kongressen. Prof. Dr. Uwe Lange hat freundlicherweise klinische Fallbeispiele und Bilder für diese Arbeit zur Verfügung gestellt. Ich danke dem großartigen Labor-Team, Dr. Klaus Frommer, zu dem ich jederzeit mit Fragen und Modellen, Graphiken und Zahlen kommen durfte. Dr. Marie Hülser, die mich angeleitet und unterstützt hat und die mir eine Freundin geworden ist. Ich danke Dr. Lari Tsiklauri und Christane Schönfeld, auf deren Vorarbeiten ich aufbauen durfte, Carina Schreiyäck, die mich in der praktischen Laborarbeit angeleitet und unterstützt hat sowie Mona Theresa Arnold, die mich in der letzten Phase meiner Arbeit unterstützt hat und diese weiter fortführt. Ich danke auch Prof. Dr. Caroline Ospelt, die freundlicherweise die Micro-RNA Taq-Man Analysen durchgeführt und damit einen letzten Baustein zu dieser Arbeit beigetragen hat.

Ganz besonders möchte ich mich bei PD Dr. Elena Neumann bedanken. Sie hat mich in schweren Zeiten motiviert, eigene Überlegungen zu entwickeln. Ich danke für deine Geduld, das Vertrauen und die unermüdlichen Gespräche, die mir und dieser Arbeit die Richtung gewiesen haben.

Ich danke dem Prägraduiertenkolleg der Universität Gießen, durch das ich mich ein Semester voll auf diese Arbeit konzentrieren konnte, sowie der Kerckhoff- und Pickenpack Stiftung, die diese Arbeit ermöglicht haben.

Abschließend möchte ich meiner Familie, Freunden und meiner Partnerin danken, die mich in meinem Studium und meiner Doktorarbeit unterstützt und abgelenkt, hinterfragt und vorangebracht haben.